Chloride transport and chloride thresholdvalues-Studies on concretes and mortars with Portland cement and limestone blended cement

Boubitsas, Dimitrios

2015

Chloride transport and chloride threshold values

Studies on concretes and mortars with Portland cement and limestone blended cement

Chloride transport and chloride threshold values

Studies on concretes and mortars with Portland cement and limestone blended cement

Dimitrios Boubitsas

LUND
UNIVERSITY

DOCTORAL DISSERTATION
by due permission of the Faculty of Engineering, Lund University, Sweden.
To be defended at Stora Hörsalen, Ingvar Kamprads Designcentrum, Sölvegatan 26, Lund, Sweden, 18 March 2016 at 10.15.

Faculty opponent
Prof.dr. R.B. Polder
Delft University of Technology
The Netherlands

LUND UNIVERSITY, Faculty of Engineering, Building Materials	DOCTORAL DISSERTATION
	2016-01-21
Author: Dimitrios Boubitsas	Lund University

Chloride transport and chloride threshold values. Studies on concrete and mortars with Portland cement and limestone.

Reinforced concrete is one of the most widely used building materials and if it is properly designed and produced, it is an extremely durable material with a service life up to 100 years. However, under certain environmental conditions the service life of reinforced concrete structures is more limited. Deterioration of concrete structure is in most cases caused by the penetration of aggressive media from the surrounding environment. Chloride initiated reinforcement corrosion is one of the major causes of deterioration of concrete structures. One conflicting issue is how replacing Portland cement with mineral additions influences chloride initiated reinforcement corrosion. This issue is of immediate interest, as there is a steady growth in the use of cement blended with mineral additions, such as blast-furnace slag, fly ash and limestone filler. This is done by the cement and concrete industry to reduce the CO_2 emissions linked to Portland cement manufacturing, by limiting the use of clinker in the cement.

The main objective of this work has been to further clarify the role of limestone filler as partial substitute to Portland cement on the two main decisive parameters for chloride induced reinforcement corrosion: chloride ingress rate and chloride threshold values. In the first part of this work the chloride ingress was studied both with accelerated laboratory methods and also after field exposure. The initial focus for the second part of the study was to determine the chloride threshold values for the binders investigated in the first part, so a comprehensive view of the effect of limestone addition on chloride initiated corrosion could be presented. However, during the work the need for the development of a practice-related method for determining the chloride threshold values was identified and the focus of the research was redirected to meet that need.

The efficiency of limestone filler concerning chloride ingress showed to be dependent on replacement ratio, time (age) and on the test method. It was not possible to draw any rigid conclusion of the limestone filler's efficiency regarding chloride ingress. But part of the inconsistency in the results was identified to be that limestone filler has two opposite effects on chloride ingress, on one hand contribute to a refinement of microstructure and on the other hand diminishing the chloride binding.

The steel surface condition was shown to have a strong effect on the corrosion initiation, and can likely be one of the most decisive parameters attributing to the variability in the reported chloride threshold values obtained in laboratory experiments. The chloride threshold value for the sulphate resistant Portland cement from the laboratory experiments was estimated to be about 1% by weight of binder. For the concrete with limestone blended cement (CEM II/A-LL 42.5R) tested in this work the chloride threshold value was at the same level as for the sulphate resistant Portland cement. From the field study but with a somewhat different definition of chloride threshold value, a chloride threshold value of about 1% by weight of binder was also estimated for ordinary Portland cement and sulphate resistance Portland with 5% silica fume exposed to marine environment.

Key words: Cement, Mortar, Concrete, Corrosion, Reinforcement, Chloride ions

Classification system and/or index terms (if any)

Supplementary bibliographical information	Language: English
ISSN 03487911	ISBN 978-91-7623-653-6
Recipient's notes	Number of pages: 86 / Price
	Security classification

Signature  Date 20160121

Chloride transport and chloride threshold values

Studies on concrete and mortars with Portland cement and limestone blended cement

Dimitrios Boubitsas

Cover photo by Per Malmback.

Division of Building Materials, Faculty of Engineering, Lund University

ISBN 978-91-7623-653-6 (print)
ISBN 978-91-7623-654-3 (pdf)
ISSN 03487911
ISRN LUTVDG/TVBM--00/1034--SE (1-86)

Printed in Sweden by Media-Tryck, Lund University
Lund 2016

PREFACE

This thesis is submitted to Lund Institute of Technology as a partial fulfilment of the requirements for a Doctor of Philosophy degree. It is based on papers published in and submitted to scientific journals.

The work has been carried out at the Division of Building Materials, Lund Institute of Technology and CBI Cement and Concrete Research Institute. Main supervisors have been Professor Lars-Olof Nilsson (Lund Institute of Technology) and Professor Tang Luping (Chalmers University of Technology/CBI).

The initial work started in 2001 and through a bumpy ride ended 2015. Through the years many people have contributed to the achievement of this work, thank you all.

A special thanks for giving me this opportunity to Professor Per-Erik Peterson, Professor Göran Fagerlund and Professor Lars-Olof Nilsson.

I am very grateful to Professor Lars Wadsö, Professor Tang Luping and Doctor Peter Utgenannt for their patient and encouragement during this work.

I want also to express my love and appreciation to my family, and especially to my beloved daughter.

ABSTRACT

Reinforced concrete is one of the most widely used building materials and if it is properly designed and produced, it is an extremely durable material with a service life up to 100 years. However, under certain environmental conditions the service life of reinforced concrete structures is more limited. Deterioration of concrete structure is in most cases caused by the penetration of aggressive media from the surrounding environment. Chloride initiated reinforcement corrosion is one of the major causes of deterioration of concrete structures. One conflicting issue is how replacing Portland cement with mineral additions influences chloride initiated reinforcement corrosion. This issue is of immediate interest, as there is a steady growth in the use of cement blended with mineral additions, such as blast-furnace slag, fly ash and limestone filler. This is done by the cement and concrete industry to reduce the CO_2 emissions linked to Portland cement manufacturing, by limiting the use of clinker in the cement.

The main objective of this work has been to further clarify the role of limestone filler as partial substitute to Portland cement on the two main decisive parameters for chloride induced reinforcement corrosion: chloride ingress rate and chloride threshold values. In the first part of this work the chloride ingress was studied both with accelerated laboratory methods and also after field exposure. The initial focus for the second part of the study was to determine the chloride threshold values for the binders investigated in the first part, so a comprehensive view of the effect of limestone addition on chloride initiated corrosion could be presented. However, during the work the need for the development of a practice-related method for determining the chloride threshold values was identified and the focus of the research was redirected to meet that need.

The efficiency of limestone filler concerning chloride ingress showed to be dependent on replacement ratio, time (age) and on the test method. It was not possible to draw any rigid conclusion of the limestone filler's efficiency regarding chloride ingress. But part of the inconsistency in the results was identified to be that limestone filler has two opposite effects on chloride ingress, on one hand contribute to a refinement of microstructure and on the other hand diminishing the chloride binding.

The steel surface condition was shown to have a strong effect on the corrosion initiation, and can likely be one of the most decisive parameters attributing to the variability in the reported chloride threshold values obtained in laboratory experiments. The chloride threshold value for the sulphate resistant Portland cement from the laboratory experiments was estimated to be about 1% by weight of binder. For the concrete with limestone blended cement (CEM II/A-LL 42.5R) tested in this work the chloride threshold value was at the same level as for the sulphate resistant Portland cement. From the field study but with a somewhat different definition of chloride threshold value, a chloride threshold value of about 1% by weight of binder was also estimated for ordinary Portland cement and sulphate resistance Portland with 5% silica fume exposed to marine environment.

THE PAPERS INCLUDED

This thesis is based on the following papers, which are appended at the end of the thesis. The papers will be referred to in the thesis by their Roman numerals.

I. **Use of limestone in cement: the effect on strength and chloride transport in mortars**
D. Boubitsas
Nordic Concrete Research, No. 47, 61-80, (2013)

II. **Replacement of cement by limestone filler or ground granulated blast furnace slag: the effect on chloride penetration in cement mortars**
D. Boubitsas
Nordic Concrete Research, No. 36, 65-77, (2007)

III. **Replacement of Cement by Limestone Filler: the Effect on Chloride Diffusion in Cement Mortars**
D. Boubitsas, L-O. Nilsson and L. Tang
Submitted (2015) to Cement, Concrete and Composites.

IV. **An approach for measurement of chloride threshold values**
D. Boubitsas and L. Tang
Int. Journal of Structural Engineering, Vol. 4, 24-34, (2013)

V. **The influence of reinforcement steel surface condition on initiation of chloride induced corrosion**
D. Boubitsas and L. Tang
Materials and Structures, DOI: 10.1617/s11527-014-0343-2, (2014)

VI. **Determining the Chloride Threshold Value for Corrosion of Reinforcement Steel in Concrete: Influence of the Electrochemical Method and the Chloride Exposure**
D. Boubitsas and L. Tang
Nordic Concrete Research, No. 49, 145-161, (2013)

VII. **Chloride Threshold Value for Corrosion Initiation of "As-Received" Rebars in Concrete**
D. Boubitsas and L. Tang
To be submitted (2016)

VIII. **Estimation of chloride threshold values in concrete exposed to Swedish marine environment over 20 years**
D. Boubitsas, L. Tang and P. Utgenannt (2015)
Accepted in Nordic Concrete Research (2015)

MY CONTRIBUTIONS

Paper III I planned the study and did all the experimental work. Professor Lars-Olof Nilsson helped me evaluate the results and write the paper. Professor Luping Tang helped me evaluate the results.

Paper IV I performed most of the experimental work. Together with Professor Luping Tang I planned the study, evaluated the results and wrote the paper.

Paper V I performed most of the experimental work and wrote the paper. Professor Luping Tang helped me plan the study and evaluate the results.

Paper VI I performed most of the experimental work and wrote the paper. Professor Luping Tang helped me plan the study.

Paper VII I performed the experimental work and wrote the paper. Professor Luping Tang helped me evaluate the results.

Paper VIII I performed the experimental work and wrote the paper. Professor Luping Tang and Peter Utgenannt helped me evaluating the results.

CONTENTS

1 INTRODUCTION

Reinforced concrete is one of the most used building materials worldwide, and in most of its applications it is difficult to be replace it with any other material. Because of its versatility, reinforced concrete is used in a vast range of environments, and if it is properly designed and produced, reinforced concrete is an extremely durable material with a service life up to 100 years. However, under certain environmental conditions the service life of reinforced concrete structures is more limited. Deterioration of concrete structure is in most cases caused by the penetration of aggressive media from the surrounding environment. Chloride initiated reinforcement corrosion is one of the major causes of deterioration of concrete structures [1]. Usually chloride ions penetrate into the concrete from de-icing salts or marine environments.

Steel embedded in concrete is normally protected from corrosion due to the high alkalinity of the concrete pore solution and the physical barrier that the concrete cover provides. When chloride ions are present they can penetrate through the concrete cover and after reaching a certain critical level at the depth of the steel, the protective action of concrete against corrosion can be compromised.

Both the chloride ingress rate and the critical chloride level depend beside the surrounding environment also to a large extent on the concrete composition. One conflicting issue is how replacing cement with mineral additions influences chloride initiated reinforcement corrosion. This issue is of immediate interest, as there is a steady growth in the use of cement blended with mineral additions, such as blast-furnace slag, fly ash and limestone filler. This is done by the cement and concrete industry to reduce the CO_2 emissions linked to Portland cement manufacturing, by limiting the use of clinker in the cement.

The objective of this work is to further clarify the role of limestone filler as partial substitute to Portland cement on the two main decisive parameters for chloride induced reinforcement corrosion: chloride ingress rate and critical chloride level.

1.1 Objectives and limitations

The aim was to study the effect on chloride induced reinforcement corrosion when a certain amount of cement is replaced by limestone filler. The two major influencing factors; chloride ingress rate and the critical chloride levels (chloride threshold values) were studied. The approach in this thesis can be divided in two parts:

1. **Chloride ingress**
   Chloride ingress was studied both with accelerated laboratory methods and also after field exposure. The tested specimens in this first part of the work were mortar mixtures.

2. **Chloride threshold values**
   The focus of this second part of the work was towards the development of an applied method for the measurements of chloride threshold values. The effect of parameters such as the initial surface condition of the embedded steel, the corrosion monitoring method, the pre-conditioning and the chloride concentration of the exposure solution was investigated. The impact from limestone filler and other mineral additions was also included as a minor part in the investigations.

As a natural continuation of the first part of the study, the initial focus for the second part of the study was to determine the chloride threshold values for the mixtures investigated in the first part, so a comprehensive view of the effect of limestone addition on chloride initiated corrosion could be presented. However, during the work the need for the development of a practice-related method for determining the chloride threshold values was identified and the focus of the research was redirected to meet that need.

1.2 Organisation of the thesis

First, the background to the work is summarized in chapter 2. Then all the experimental methods being used are described in chapter 3. In chapter 4 the main results from papers I-VIII are presented and discussed. Finally, conclusions are drawn and some future work is proposed.

2 BACKGROUND

In this chapter the background to the work is briefly given and a number of concepts being dealt with in the next chapters are defined.

2.1 Cement-based materials

Cement is a fine mineral powder with the principle constituents being silicate and aluminate compounds of lime. When cement is mixed with water it reacts (hydrates) and gains strength so that it can bond aggregates (sand, rock) together to a strong material. Depending on the size of the incorporated aggregates this hardened state is referred to as concrete (large aggregate) or mortar (smaller size aggregate). Both concrete and mortar can be regarded as composite materials consisting of two main phases (at least to the naked eye): aggregates and cement paste. Cement paste is the adhesive product of the hydration and its structure and composition determine much of the properties of concretes and mortars. In this chapter an overview of the structure of cement paste and its influence on properties vital to chloride induced reinforcement corrosion will be given.

Portland cement has traditionally been the most commonly used cement throughout the world. According to the European standard EN 197-1 [2] a Portland cement shall consist of at least 95% of Portland cement clinker, and Portland cement clinker shall consist of at least two-thirds by mass of calcium silicates ($3CaO{\cdot}SiO_2$ and $2CaO{\cdot}SiO_2$), the remainder consisting of aluminate and iron containing clinker phases and other compounds. Table 1 shows the variety in content range of the main components that can be found in Portland cements (mass per cent), the notations used in cement chemical nomenclature for those components are also included [3].

Table 1. Main components of Portland cement in mass per cent [3]-[4].

Compound		Notation	Content range
Tricalcium silicate	$3CaO{\cdot}SiO_2$	C_3S	40 – 70 %
Dicalcium silicate	$2CaO{\cdot}SiO_2$	C_2S	10 – 35 %
Tricalcium aluminate	$3CaO{\cdot}Al_2O_3$	C_3A	5 – 13 %
Tetracalcium ferroaluminate	$4CaO{\cdot}Al_2O_3{\cdot}Fe_2O_3$	C_4AF	5 – 15 %
Gypsum	$CaSO_4{\cdot}2H_2O$	C$	3 – 5 %

Other minor components are also present in Portland cement, and despite being present at low concentrations, some of them have a major effect on the durability properties of concrete. Typically, these minor compounds can be (from reference [3], given in order of descending concentrations), MgO, K_2O, SO_3, Na_2O, TiO_2, Mn_2O_3, P_2O_5, SrO, fluorides, chlorides and Cr_2O_3 [3].

Besides Portland cement, a large number of other cements are produced. In most cases, a certain fraction of the Portland cement clinker has been replaced with mineral additions such as ground

granulated blast furnace slag (GGBS), fly ash (FA), silica fume (SF), natural puzzolana (NP) or limestone filler (LSF) [2][3]. The European standard EN 197-1 [2] groups with regard to composition the most common cements into five types:

- CEM I (Portland cement), at least 95% of the total cement mass consist of clinker
- CEM II (Portland-composite cement), up to 35% of the cement mass can be replaced with another mineral addition
- CEM III (Blast furnace cement), 36% - 95% of the cement mass can consist of GGBS
- CEM IV (Pozzolanic cement), 11% - 55% of the cement mass can consist of pozzolanic materials (FA,SF or NP)
- CEM V (Composite cement), 18% - 49% of the cement mass can consist both of GGBS and pozzolanic material (FA or NP)

The term 'blended cements' is often used as a generic term for cements where a certain amount of Portland cement clinker has been replaced with a mineral addition. Portland cement is being increasingly replaced by blended cements [5] as blended cements have environmental, economic, and/or technical benefits.

Mineral additions may broadly be categorized as latent hydraulic, pozzolanic or filler. Neither type reacts significantly with water by itself, but together with Portland cement they are reactive to a varying degree [3] GGBS is latent hydraulic and can be considered as the most reactive of the mineral additions. If a minimal amount of a suitable activator is present, GGBS shows hydraulic properties similar to Portland cement. Fly ash, silica fume and natural pozzolan are pozzolanic materials, they are reactive if for example Portland cement is present, but not to the same extend as slag. Limestone is widely described as filler and is sometimes regarded as inert; however, some chemical reactions do occur in the presence of Portland cement [3].

2.1.1 Cement hydration

This section is not intended to cover the complex and extensive topic of cement hydration as a whole; instead, its purpose is to provide some background on the subject, which will make the experimental work and results in this thesis more comprehensible. In this section the hydration of Portland cement will be dealt with; the influence on hydration when incorporating limestone filler in the cement will be treated in section 2.5.2.

Hydration denotes the reaction of cement with water, and is associated with both chemical and physical changes of the system, in particular with setting and hardening [3]. Since Portland cement is composed of a heterogeneous mixture of several compounds (see Table 1), the hydration process consists of several reactions occurring simultaneous and successively. The silicates (C_3S and C_2S), which are the main constituents in Portland cement, play a dominant role for the hardening (strength development) of the cement paste. The hydration products of C_3S and C_2S consist of nearly amorphous calcium silicate hydrate, called C-S-H, and calcium hydroxide (CH) [3]. Because C-S-H has the properties of a rigid gel the term cement gel is sometimes used. The dashes in C-S-H indicate that there is a range of possible compositions. Its stoichiometry depends on the cement composition, water-cement ratio, hydration temperature, age of hydration and the method employed for its determination [3][6]. The composition of the C-S-H product is reported to be similar for the two silicates, the difference is that C_2S has both a much lower reaction rate and production of CH compared with C_3S.

The aluminates (C_3A and C_4AF) hydrate much faster than the silicates, and unless the rapid hydration was slowed down it would not been possible to use Portland cement for construction applications [7]. The needed retardation is accomplished by the addition of gypsum, which therefore is an important component of cements (see Table 1). Despite the addition of gypsum the aluminates still react faster than the silicates, and are responsible to a large extend for the early stiffening (loss of consistency) of a Portland cement paste. Initially and in the presence of gypsum the hydration of aluminates gives a group of products referred to as AFt. The term AFt denotes the phases related to ettringite-calcium aluminium trisulfat ($C_3A{\cdot}3CS{\cdot}32H_2O$) with the F indicating the possible substitution of iron for aluminium in the structure [8]. When the available gypsum is consumed the initially formed AFt, further reacts with aluminates, yielding a group of products referred to as AFm. The AFm phases are isostructural with calcium aluminium monosulfate ($C_3A{\cdot}CS{\cdot}12H_2O$), with the possible substation of aluminium by iron, where also, hydroxide, carbonate, or chloride ions may replace the sulphate (S) [8]. Figure 1 shows diagrammatically the progress of hydration of the individual clinker phases and the products formed in Portland cement pastes, as given by Odler [6].

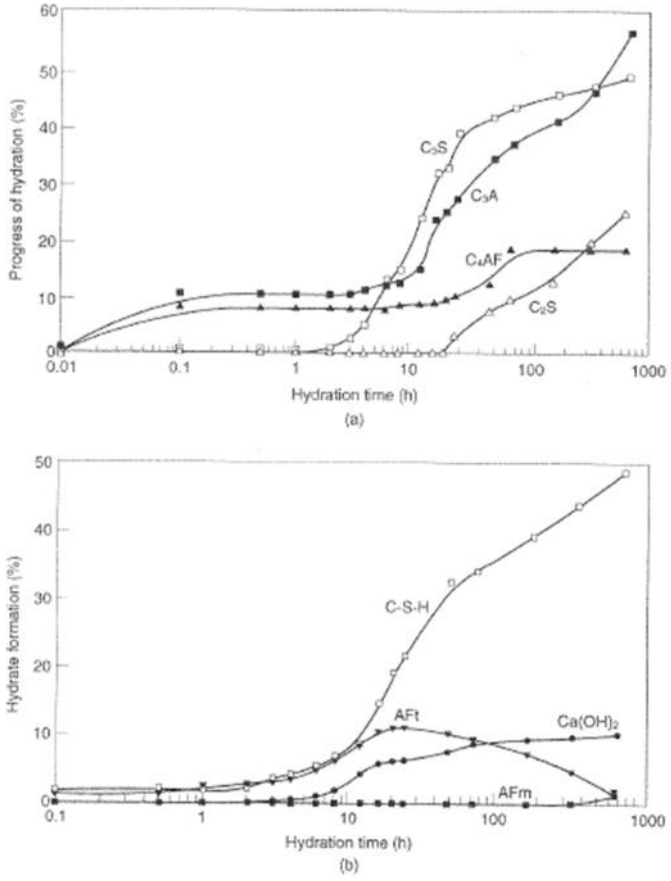

Figure 1. Hydration progress of a Portland cement [6]. (a) Consumption of clinker phases, (b) formation of hydration products.

The hardened cement paste (hcp), which incorporates all hydration products and to a certain extent unhydrated reactants, is a relatively rigid and strong solid of high porosity and very high internal surface area. The resulting microstructure for a given cement paste will depend primarily on the extent of reaction (the degree of hydration; a function of age, moisture state, and temperature) and the water-cement ratio. These two parameters will be discussed further in section 2.1.2.

Another important product of the cement hydration is the pore solution, whose chemical composition plays an important role for concrete durability, and especially so for reinforced concrete structures. For pastes of Portland cement the only ions present in concentrations above a few mmol/l are K^+, Na^+ and OH^- [3]. Accordingly, the pore solution has a high pH; typical pH values for low alkali cements are about 13.5, while high alkali cement can have a pH as high as 13.8 [3][9].

2.1.2 Structure of cement-based materials

In most cases when it comes to actual structures the primary focus is on the behaviour of concrete. However, many of the properties of concrete that determine how it will perform in the field are investigated on cement pastes and mortars. This is done for several reasons, viz. sample size restrictions for the investigation methods, simplified experimental conditions, need to reduce test costs and a wish to separate the influencing parameters. Because the investigations in the cited literature and some of the experiments described in this thesis are performed either on mortars or concretes, a short review of the structures of these cement-based materials is given in this section. This short review will hopefully make it easier for the reader to see the differences and similarities between the performances of these cement-based materials.

Cement paste

Most investigations dealing with the hydration process and the reaction products have been related to pastes because the presence of aggregate complicates these studies in mortars and concretes [3].

After a certain hydration time four principal solid phases can be detected in the hcp microstructure. Those are the hydration products stated earlier (see Fig. 1b) plus unhydrated clinker grains. C-S-H is the main phase determining the properties of the paste [7]. In addition to solids, the hcp contains several types of voids, which also have an important influence on its properties. Depending on the environmental humidity and the water-cement ratio, the hcp is also capable of holding different amounts of water.

A classical model describing the structure of hcp and allowing quantitative calculations of the volumetric composition of the different phases was proposed by Powers and Brownyard [10] and was later slightly modified by Powers [11]. A simplified picture of this model has been given among others by Hansen [12], Fagerlund [13] and Taylor [3]. It must be pointed out that this model is valid only for hardened Portland cement pastes cured at room temperature. In this model the hcp was assumed to contain unreacted cement, hydration product (referred to as cement gel) and capillary pores. The model is based on the volume fractions of these three components and the individual solid phases are not considered.

Several other models have been proposed to describe the structure of hcp. Their peculiarities are briefly reviewed Taylor [3], who concluded that the models principally differ in whether, to what extent or on what scale the gel is regarded as being composed of separate particles. The Powers-Brownyard model is adopted in the following discussion for describing the structure of hcp, because the capability of this model to predict the volumetric composition of the different phases simplifies the bridging between structure and the properties of interest in this thesis.

Cement gel (hydration product) is mostly a rigid colloidal matter that occupies about 2.2 times as much space as the cement it was derived from. Its porosity was estimated to be around 28% with an average width of its pores of about 2 nm, which is about five times the diameter of a water molecule. This volume change is partially caused by the cement gel porosity and partially due to that water is chemically bound to cement during hydration. Powers [11] also estimated that the volume of the chemically bound water (the non-evaporable water) is about 75 % of the volume off "free water".

The different volumetric quantities are primarily determined by the ratio of mixing water to cement and the degree of hydration. This water-cement ratio is defined as:

$$\mathrm{w/c} = \frac{W_0}{C}, \tag{1}$$

where W_0 and C are the masses of mixing water and cement. The degree of hydration, which denotes how close the hydration of the cement is to completion, is defined as:

$$\sim = \frac{C_n}{C}, \tag{2}$$

where C_n denotes the mass of hydrated cement and C is the original mass of cement. Powers and Brownyard [10] stated that 1 gram of cement binds roughly 0.25 gram water, which implies that Eq. (2) can also be expressed as:

$$\sim = \frac{W_n}{0.25 \cdot C}, \tag{3}$$

where W_n is the mass of chemically bound water and C is the original mass of cement.

Because the cement gel occupies more space than the cement it is formed from, and since the total volume of the paste scarcely changes on hydration, complete hydration cannot occur if w/c is below a certain value due to lack of space. This value is about 0.38 if the paste is kept in contact with an excess of water during curing. If excess of water is not accessible during curing the hydration will be very slow or stop already at w/c < 0.44 due to lack of available water.

Capillary pores are the remains of originally water-filled spaces that have not become filled with gel. These pores are larger than the gel pores. No dimensions was confirmed at the time of development of the model [11] other than that capillary spaces were much larger than gel pores, but later investigations have shown typical pore size distributions ranging from 50 nm up to 1000 nm [7]. The capillary porosity of the hcp, which is a major factor for characteristics such as strength and permeability of cement-based materials, can according to this model be calculated as:

$$P_{cap} = \frac{w/c - 0.38\sim}{0.32 + w/c}, \tag{4}$$

where P_{cap} is expressed as a fractional volume of the total volume of the cement paste. It is also assumed in Eq. (4) that the critical value of w/c for complete hydration is 0.38, and that the density of cement is 3150 kg/m^3. Fig. 2 shows the total capillary porosity in hcp related to w/c

for different degrees of hydration, calculated with Eq. (4). A low *w*/*c* and high degree of hydration give a low capillary porosity and vice versa.

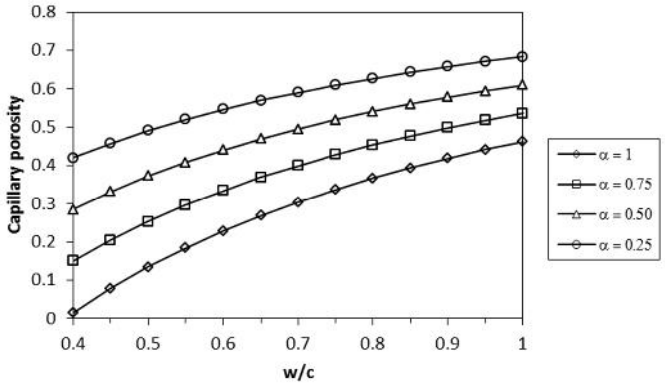

Figure 2. Capillary porosity in hydrated cement paste related to w/c for different degrees of hydration (α), calculated by Eq. (4).

It has been suggested that the pore size distribution, not the total capillary porosity is a better criterion for evaluating characteristics such as strength and permeability of hcp [7]. Typical pore size distribution plots of hydrated cement pastes from mercury intrusion porosimetry measurements are shown in Fig. 3.

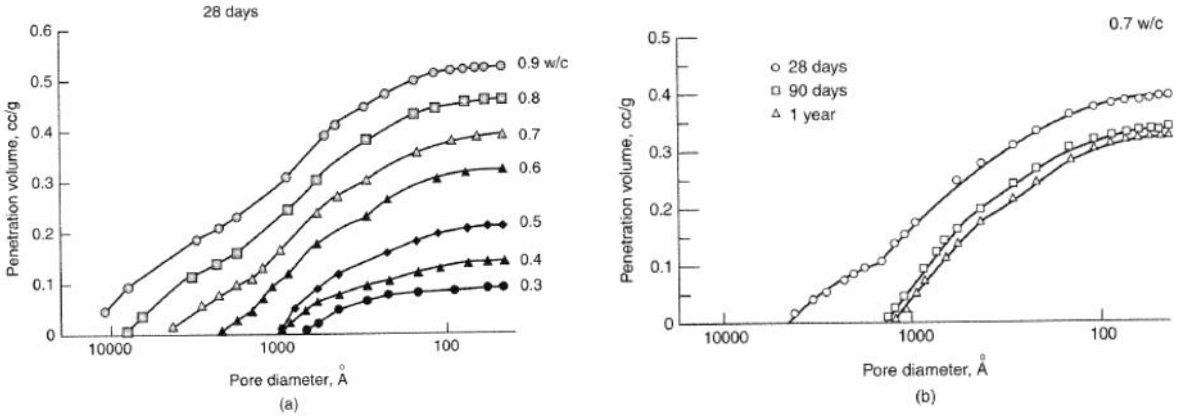

Figure 3. Pore size distribution in hydrated cement pastes [7].(a) Influence of w/c ratio. (b) Influence of degree of hydration (age).

Figure 3 shows that the pore size distribution is to a large extent determined by the *w*/*c* and the degree of hydration. It has been suggested that the amount of capillary pores larger than 50 nm is more influential in determining strength and permeability [7].

Mortars and concretes

While cement paste is made from only water and cement, mortar and concrete also contain aggregate. The difference between mortars and concrete lies in the size of the incorporated aggregates. An important consequence of the size of the incorporated aggregates is that the amount of cement paste is generally higher for mortars than for concretes. The following discussion is mainly focused on concretes but to a large extent it is valid also for mortars.

Concrete can at a first sight be assumed to be a two phase composite material of cement paste plus aggregate, but investigations have shown that a more correct assumption is to consider these materials as three phase composite [8][14][15]. This is because the cement paste around aggregate particles is perturbed by the presence of the aggregate, this region is referred to as the interfacial transition zone (ITZ). Its origin has been suggested to lie in the so called "wall effect" [14][15]. Cement grains range in size from less than a micrometre to up to 100 micrometre; aggregate particles are several orders of magnitudes larger. This difference in size means that each aggregate particle acts as a "wall" disturbing the packing of the cement grains. The result is that in the vicinity of an aggregate particle a zone predominantly containing small cement grains arises, while larger grains are found further out. This uneven packing of the cement grains leaves a more porous zone of 15 to 20 μm around the aggregate. An increased amount of calcium hydroxide precipitates around the aggregate compared to the bulk paste has also been reported [14][15][16]. Although ITZ primary manifest itself at the surface of coarse aggregate particles, such a zone can also be found around the fine aggregate particles [18].

Another feature reported about the ITZ is that investigations have shown the existence of very fine cracks at the interface between coarse aggregate and cement paste. Because those cracks have been noted also prior to any load application on the concrete, these findings have been coupled to differences in shrinkage and thermal movement of aggregate and hcp [18]. Despite the difference of the ITZ from a bulk paste it is very difficult to quantify the overall effect on properties of concrete. Scrivener et al [15] pointed out two reasons to this complexity, firstly because ITZ is not a discrete zone but a region of gradually changing microstructure, and secondly, the preparation of specimens for studies of the properties of ITZ tends to produce different ITZs than those in "real" concrete. It should be noted that the general view of the ITZ has been challenged by Diamond et al. [19] who came to the conclusion that ITZ shows only modestly higher porosity than the bulk and therefore can have a marginal effect, if any, on the properties of concrete.

Other common occurring phenomena that alter the microstructure of concrete are bleeding (water separation) and the presence of entrapped air and entrained air bubbles. The first two phenomena can be seen as artefacts while the last one is added purposely for increasing the frost resistance.

2.2 Structure-property relationship

Cement-based materials and especially concrete have as previous discussed a highly heterogeneous and complex microstructure. It is therefore very difficult to make realistic models of its microstructure from which the behaviour of the material can be reliably predicted [7]. However, knowledge of the relationship between microstructure and properties is essential to be able to control the properties. Strength and penetration of aggressive media and their relation to microstructure are discussed in this section.

2.2.1 Strength

The most valuable property of concrete is often considered to be its strength, although, in many cases, properties like permeability and diffusivity, may in fact be more important, especially when it comes to durability aspects. Nevertheless, strength often gives a good indication of the overall quality of concrete. In this section compressive strength will be considered unless otherwise stated.

Numerous factors have been identified to influence the strength of cement-based materials [7][17][18], but porosity (which depends of *w*/*c* and degree of hydration) can be considered to be the major factor [7][18]. In the literature several equations have been reported to express the strength-porosity relationship for different porous material, including cement-based materials. A review on this subject is given by Fagerlund [20]. In general, there exists a fundamental inverse relationship between porosity and strength. Commonly referred empirical relationships between the strength of hcp (originally found to hold for other porous materials) and porosity can be found in [17][20]. A relatively good fit of those equations with experimental data when cement based materials (mostly cement pastes) were tested has been reported [17][20]. This is also illustrated in Fig. 4 [21]. However, Fig. 4 indicates that only one function cannot fit the experimental data throughout the whole porosity range; something that was also concluded by Fagerlund [20].

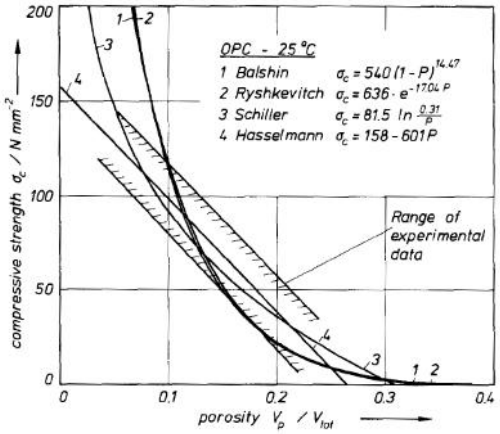

Figure 4 Experimental data showing the relation between porosity in hcp and compressive strength [21].

Even though equations in which the strength is expressed as a function of total porosity agree fairly well with experimental data, it has been suggested that pores of different sizes (and shapes) influence strength to a varying degree [3][17][20][24]. Taylor [3] suggests by referring to several investigations that the capillary pores, or the volume of pores above a certain size, are more appropriate than total porosity to relate to strength.

The hcp strength cannot easily be related to mortar and concrete strength. The incorporation of aggregates has a strength reducing effect [20][22]. This difference can be attributed to a somewhat different mechanism of failure under compressive stress of cement based materials with and without aggregates [23].

Because a direct determination of the porosity of concrete, and even of mortar, is complicated by the presence of the aggregate, empirical relations between concrete strength and water-cement ratio have been developed. The basis of the strength versus water-cement ratio relation is that an increase in the water-cement ratio produces more capillary pores in the matrix portion of mortar and concrete, resulting in decreased strength. It must be pointed out that the degree of hydration also influences the capillary porosity, as illustrated in Fig. 2. At a given storage conditions the degree of hydration is time dependent and so is strength [24].

Figure 5 shows the relationship between compressive strength of concrete and water-cement ratio for different Swedish Portland cements with aggregate from different deposits. Well

known empirical equations predicting the relationship between concrete strength and *w*/*c* are [7][18][17]:

Abrams´ equation

$$f_c = \frac{k_1}{k_2^{w/c}}; \tag{5}$$

Bolomey´s equation

$$f_c = k_1\left(\frac{1}{w/c} - a\right); \tag{6}$$

where f_c is the strength, w is the amount of mixing water, c is the amount of cement, and k_1, k_2 and a are empirical constants depending on parameters such as cement quality, test method, test conditions and degree of hydration.

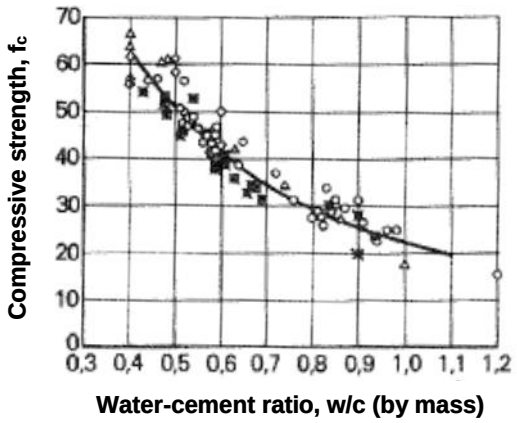

Figure 5. Relation between compressive strength of concrete and water-cement ratio for different Portland cements and with aggregates from different deposits [25].

The relationship between concrete strength and water-cement ratio is only approximate because it may be affected by secondary factors, such as type of cement, hydration temperature, maximum aggregate size and certainly by the consolidation and air entrainment [7][18][24].

2.2.2 Mass transport

It is generally accepted that durability of cement-based materials to a large extent is governed by their resistance to penetration of aggressive media [3][7][18][26]. The aggressive media may be present in a liquid or gaseous state, and transported by various mechanisms: in particular; permeation, diffusion, convection and capillary suction, and combinations of these modes of transport [26]. Permeation is the flow of liquids or gases due to pressure differences. Diffusion is the flow of species by random motion due to concentration differences. Convective flow is the transport of substance due to the movement of a fluid that contains the substance, for instance the flow of water vapour due to air movement, and the flow of ions dissolved in moving water. Capillary suction is the transport of liquid in porous materials due to surface tension acting in the pores. Most of the mechanisms are treated in references [27] and [28]. Different

transport mechanisms have been used in the literature when discussing investigations of transport properties of cement-based materials and their relation to the durability of concrete [29]. These transport mechanisms are to some extent interrelated [30]. In section 2.3 a closer look will be devoted to the transport mechanisms that normally are responsible for chloride ingress into concrete.

2.2.3 Parameters influencing mass transport in cement-based materials

Mass transport in cement-based materials, like that of other porous materials, is mainly a function of the pore characteristics, where size distribution and the connectivity of the pores have been found to play a dominant role [7][31]. As discussed previously (section 2.1.2), pore size distribution and the connectivity depends mainly on the water-cement ratio and the degree of hydration. Other parameters that have been identified to be influencing the transport characteristics are mineral additions and to some extent aggregate amount and characteristics [31]. The effect of mineral additions and particularly that of less reactive ones such as limestone filler will be discussed in a subsequent section.

Many of the studies on the relationship between pore structure and mass transport have been investigating the permeability of hydrated cement pastes with water as fluid medium [32][34] [35]. Although, this particular transport mechanism is not treated in this work, results from such investigations are presented here because they increase the understanding of the influencing parameters for mass transport mechanism.

Powers et al. [33] stated that the permeability of hardened cement paste mainly depends on its capillary porosity; the relationship between permeability and capillary porosity of matured pastes with different cements is shown in Fig. 6(a) [33]. For one of the cements in the same investigation the permeability versus water-cement ratio is shown in Fig. 6(b) [32]. When comparing Figs. 6(a) and 6(b) it is obvious that a decrease in w/c is associated with a decrease in capillary porosity and, consequently, a decrease in the permeability coefficient.

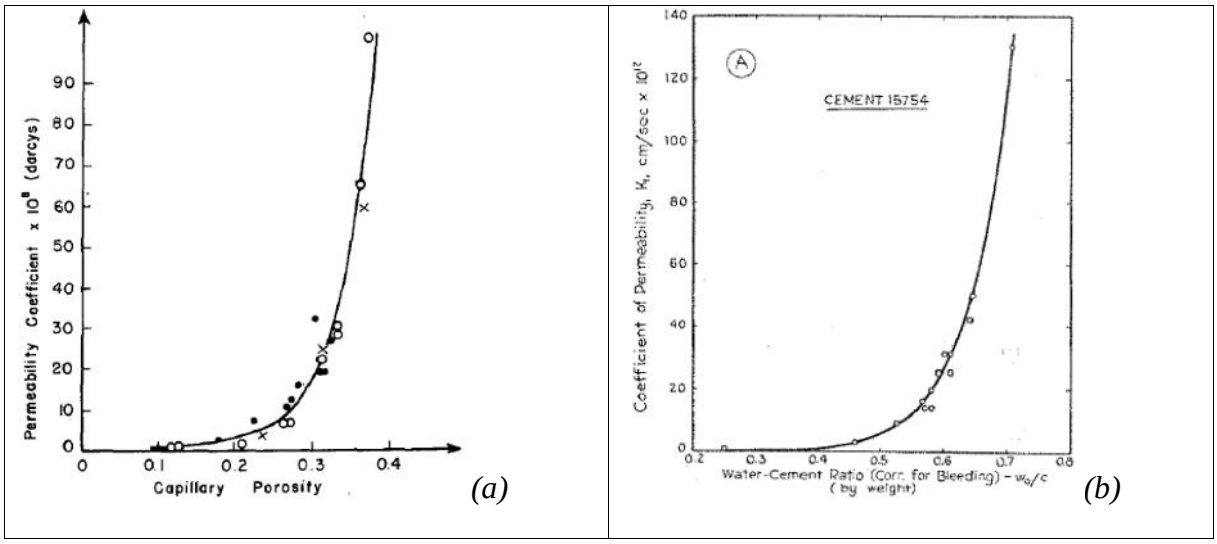

Figure 6. (a) Relationship between water permeability and capillary porosity [33], (b) Relationship between water permeability and w/c ratio [32]

Permeability coefficients presented by Mehta and Manmohan [34] were in general agreement with those of Powers et al. [32]. However, these authors [34] conclude from the pore size distribution measurements that were included in their investigation, that the larger pores (>132

nm) played a more important role in determining permeability than the smaller pores. That there is no unique relationship between total porosity and permeability, since specimens of similar porosity may have totally different pore size distributions, was also stated by Nyame and Illstone [35] (see Fig.7).

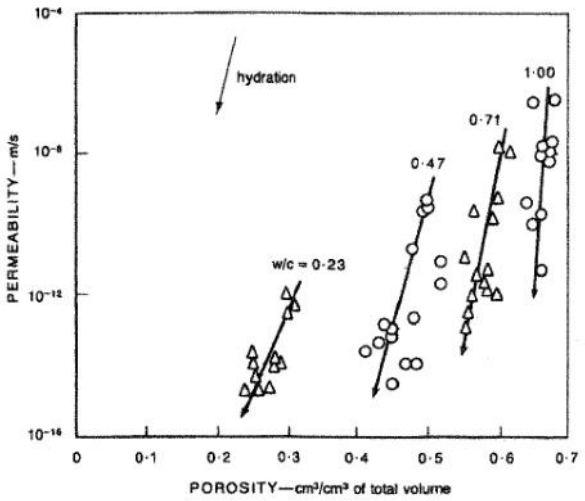

Figure 7. Relationship between permeability and porosity for various w/c ratios [35].

Gas permeability, such as that of oxygen, has also often been used for relating pore structure of cement-based materials to durability aspects, although diffusivity is believed to be theoretically a more useful parameter [29]. Lawrence [36], when studying transport of oxygen through concrete, found a linear relationship between oxygen diffusivity and permeability. Further, this author [36] showed that water-cement ratio provided the best representation of the diffusivity by a single variable. The effect of initial curing conditions for concretes prepared with different water-cement ratios was studied by Dhir et al. [37]. The air permeability coefficient increased with *w*/*c* and decreased with the initial water curing period, the influence of curing condition was most pronounced as *w*/*c* was increased [37].

In their review on the influence of paste/aggregate interface on ionic transport mechanisms Marchand and Delagrave [38] found that the presence of aggregate in an hcp matrix has two opposite effects on transport properties. Firstly, the addition of solid particles (aggregates) leads to an increase in the tortuosity of the matrix. This implies an interruption of the capillary pore continuity where ions have to move around the solid inclusions, and hence, slowing down the transport. Secondly, the presence of ITZ will contribute to facilitate the movement of ions. Another feature that must be accounted for in this context is the dilution effect of solid particles, i.e. the reduction of the volume fraction of the conductive phase (paste) due to the presence of the non-conducting aggregate. Marchand and Delagrave [38] concluded that the increased tortuosity has a higher influence on the transport properties than the presence of ITZ. This conclusion is also in agreement with that of Wong et al. [39], who found that transport properties are governed by the overall pore structure and that the net effect of ITZ porosity is small.

Except for pure material properties, parameters such as internal relative humidity, carbonation and temperature also influence the transport characteristics of cement-based materials [31]. Ollivier et al [31], reviewed numerous publications showing that gas permeability and diffusivity of concrete increases significantly as moisture is dried out. The influence of moisture on ion transport is the opposite of that gas permeability.

2.3 Chloride transport in concrete

Chloride transport in concrete is a complex process, involving transport mechanisms such as diffusion, capillary suction and convective flow with flowing water, accompanied by physical and chemical binding [40]. Depending on the exposure conditions as well as on the moisture content of the concrete, the transport mechanisms may act simultaneously or in sequence during consecutive periods, or one of them may be the exclusive mechanism [41]. Even if concrete is assumed to be homogeneous, crack-free and with water saturated pore system, two major characteristics makes it difficult to theoretically describe chloride transport in cement-based materials, viz. interaction with other ions in the pore solution and interaction between chloride ions and the matrix of the cement-based materials [40].

Interaction with other ions in the pore solution

As chloride ions are charged particles and the pore solution is a strong electrolyte, various ions will interact with each other to maintain electric neutrality. Consequently, the flux of one type of ion will affect the flux of other types of ions because of the electrical field created between them. A theoretically accurate description of the chloride flux in pore solution of cement-based materials will have to be based on the Nernst-Planck equation, which incorporates the interaction with other ions [42]:

$$q_i = -D_i \frac{\partial c_i}{\partial x}\left(1 + \frac{\partial \ln ¥_i}{\partial \ln c_i}\right) + c_i D_i \frac{z_i F}{RT}\frac{\partial ¨}{\partial x}, \qquad (7)$$

where q_i is the flux of ions, D denotes the diffusion coefficient, c is the molar concentration, R is the gas constant, T is the absolute temperature, x is distance, γ is the activity coefficient, z is the valence of ions, F is the Faraday constant and φ is the counter-electrical potential. Convection is neglected in eq. (7).

Conceptually Eq. (7) can be broken down to:

$$Flux = diffusion + migration$$

It has been found that cations (Na^+, K^+, Li^+ etc.) have lower diffusion rates than chloride ions in cement paste. Since chloride ions cannot exist alone some cations must be around to keep the solution electrical neutral [42]. Consequently, when chloride ions move forward, a counter-electrical field ($\partial\varphi/\partial x$) between them and the surrounding slower cations will be formed, which will slow down the chloride ions. Tang et al. [40] pointed out that the main difficulty in applying Eq. (7) for modelling chloride ingress is to quantify the potential gradient $\partial\varphi/\partial x$, because it is a function of the fluxes of all ions and consequently, changes with time.

In migration tests, simplified versions of Eq. 7 are used because the applied external electrical field may dominate over the potential field due to various ion interactions. For example, if assuming a constant gradient of the electrical potential, $\partial\varphi/\partial x$ is replaced by E (V/m), the electrical field, and Eq. 15 can be expressed as [42]:

$$q_m = -D\frac{\partial c}{\partial x} + D\frac{zFE}{RT}c. \qquad (8)$$

Others have, by assuming that the pure diffusion part is negligible compared to a high applied *E*, further simplified Eq. (8) by omitting the diffusion part [43].

Even if Eq. (7) is close to a description of the chloride transport in cement-based materials the situation becomes even more complex due to ionic interaction also with the hydration products (pore walls) [42].

Interaction between chloride ions and the matrix of cement-based materials

When chloride ions from environmental solutions penetrate into concrete, some of them are captured by the cement hydration products. This is called 'chloride binding' [40]. The mechanism of chloride binding is yet not well understood but it is in general believed that both physical adsorption and chemical reactions are involved [44][45]. The binding of chloride ions delays the chloride ingress into concrete since binding reduces the concentration of mobile chloride ions in the pore solution.

Chloride ingress into concrete is usually shown as a 'chloride profile', a curve showing the total amount of chlorides as a function of the penetration depth at a certain time. Figure 8 shows such chloride profiles (hypothetical), highlighting the importance of chloride binding on chloride ingress. The concrete composition is one of the parameters influencing chloride binding, which in turn will influence the shape of the chloride profile [44], as can be seen in Fig. 8(b). The concrete with the higher binding capacity will have higher total chloride content at the exposed surface, since the amount of bound chlorides is larger. On the other hand the penetration depth in that concrete will be smaller because a part of the chlorides that penetrate are bound. This means that chlorides occur in different forms in concrete, where some of the chlorides are free ions dissolved in the pore solution and others are chemically or physically bound to the cement hydration products. However, the definition of what ions that are free and what ions that are bound is not clear, because chloride binding seems to vary in strength over a wide range [44].

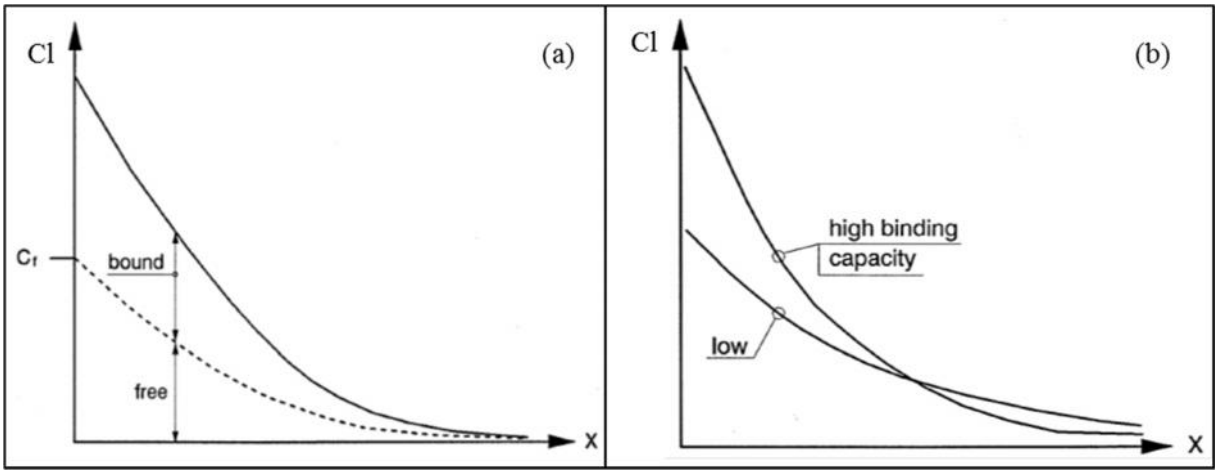

Figure 8 a) and b). Hypothetical chloride profiles in concrete highlighting the importance of chloride binding [44].

Chloride binding is influenced by many factors such as chloride concentration, binder content and composition, hydroxyl concentration and other ions present, temperature, carbonation etc. [44][45]. The chloride concentration has been pointed out to be one of the most decisive parameters for chloride binding [44][45]. Therefore, the relationship between the free and the bound chlorides is often presented as a 'binding isotherm', see Fig. 9 revised from [46]. The

higher the availability of chlorides the more chlorides are bound. Binding isotherms are used even when other influencing parameters are investigated, such as pH as shown in Fig. 9.

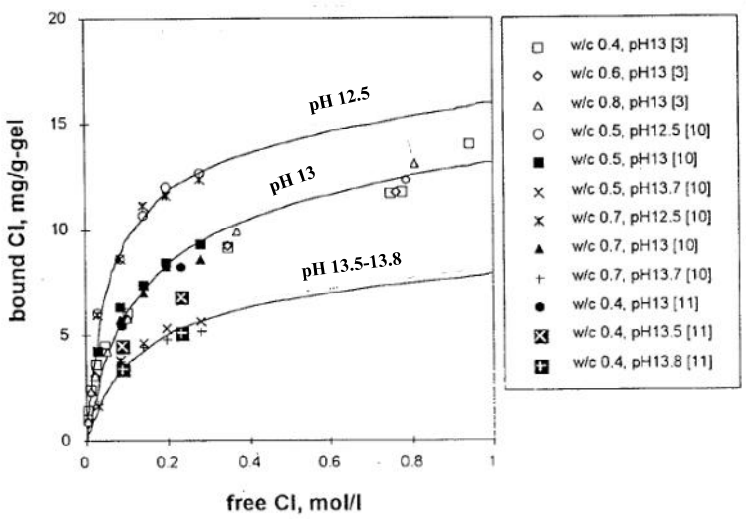

Figure 9. Examples of chloride binding isotherms at different pH-levels, revised from [46].

Except that the amount of bound chloride increases with chloride concentration, it is also obvious in Fig. 9 that the capacity of a material to bind chlorides changes when the ion concentration changes. The capacity of a material to bind chlorides when the ion concentration change is called 'binding capacity' [44], and is defined as:

$$\text{Binding capacity} = \frac{\partial c_b}{\partial c_f}, \tag{9}$$

where c_b is the concentration of bound chloride and c_f is the concentration of free chloride. This means that the binding capacity is the slope of a binding isotherm, and that it is concentration dependent as shown in Fig. 9.

In summary, this means that to theoretical describe chloride transport in cement-based materials the interaction with other ions in the pore solution and interaction between chloride ions and the matrix of the cement-based materials must be combined in physical models. As such physical models require a huge amount of input data, which are not readily available at present [40], it is necessary to make a number of assumptions and simplifications to be able to study particular variables that influence chloride ingress.

Simplifications

With the current state of knowledge, diffusion is assumed to be the transport mechanism describing in a satisfactory way the chloride ingress in water-saturated cement-based materials [40]. Diffusion is the transfer of mass by random motion of particles resulting in a net flow from regions of higher concentration to regions of lower concentration of the diffusing substance [47]. This net flow is assumed to be proportional to the concentration gradient, neglecting the other terms in equation (7), and can be expressed as:

$$q_D = -D_{F1}\frac{\partial c}{\partial x}, \tag{10}$$

where q_D is the mass flux (kg/m^{2}s), D_{F1} is the diffusion coefficient (m^2/s), c is the concentration of ions (kg/m^3 solution) and $\partial c/\partial x$ is the concentration gradient. Equation (10) is often referred to as Fick's first law of diffusion. For transient conditions, where the chloride concentration changes with time (t), Fick's first law has to be used in the mass balance equation, which then can be expressed as:

$$\frac{\partial c}{\partial t} = \frac{\partial q_D}{\partial x} = D_{F1}\frac{\partial^2 c}{\partial x^2} \tag{11}$$

Equation 11 is only applicable for ions ("free movable") in solutions. When modelling chloride ingress in cement-based materials (porous materials with binding), c is replaced with C (kg/m^3 material), this is the total amount of chlorides (free and bound). Eq 11 is then expressed as:

$$\frac{\partial C}{\partial t} = D_{F2}\frac{\partial^2 C}{\partial x^2} \tag{12}$$

Equation 12 is referred to as Fick's second law of diffusion, a more detailed interpretation of this simplification can be found in [44]. However, by comparing Eq. (11) with Eq. (12), it is obvious that the two diffusion coefficients, despite having the same unit are different; in Eq. (11) D_{F1} describes the diffusion of free ions, while in Eq. (12) D_{F2} includes also binding. The suggested relationship in cement-based materials is [48]:

$$D_{F2} = \frac{D_{F1}}{\frac{\partial C}{\partial c}} = \frac{D_{F1}}{p_{sol}\left(1+\frac{\partial c_b}{\partial c_f}\right)}, \tag{13}$$

where p_{sol} is the porosity containing pore solution that acts as a solvent for chloride ions. This term must be included because the concentration is expressed different in the two terms; in c as kg/m^3 solution and in C as kg/m^3 material. The diffusion coefficients in Eqs. (11) and (12) will be discussed further in chapter 3.

2.4 Corrosion of steel in concrete

Reinforcement steel is an alloy that essential consists of iron, small amount of carbon and other so called trace elements. In nature, most of the iron exists in a stable form as iron ore mainly in oxides such as magnetite (Fe_3O_4) and hematite (Fe_2O_3). When steel is manufactured a lot of energy is added to the iron ore to transform it to steel; metallic corrosion can simple be regarded as the tendency for the steel to transform back to its original thermodynamically stable state [49]. Corrosion of metals is an electrochemical process, which means that it occurs not by direct chemical reaction of the metal with its environment but rather through coupled electrochemical half-cells reactions involving the passage of electrical charge. For steel in neutral and in alkaline solutions such as the pore solution of concrete, the following electrochemical reactions are usually relevant [50]:

Anodic reaction (dissolution of iron):

$$Fe \rightarrow Fe^{2+} + 2e^- \tag{14}$$

Cathodic reaction (electron consuming reaction):

$$O_2 + 2H_2O + 4e^- \rightarrow 4OH^- \quad (15)$$

On a corroding metal surface, anodic and cathodic reactions occur in a coupled manner with the same rate at different places on the metal surface. The overall balanced reaction can be written as:

$$2Fe + O_2 + H_2O + 4e^- \rightarrow 2Fe(OH)_2 \quad (16)$$

where the product of the last reaction is hydrated ferric oxide (rust).

In the following section the fundamentals of chloride induced corrosion of embedded steel in concrete will be discussed with the support of the theory of aqueous corrosion.

2.4.1 Thermodynamical aspects

Electrode potentials

Immersion of a metal (electrode) into a solution creates a metal/solution interface; positively charged metal ions dissolve into solution, leaving behind electrons in the metal. This is like an electrical capacitor, bringing about a charge separation [49]. The charge of the metal side of the interface is balanced by a distribution of ions at the solution side of the interface; this is called the electrical double layer, an electric potential difference is created across the metal/solution interface.

This potential difference across a metal/solution interface is commonly referred to as an electrode potential. The electrode potential is a measure of the ease of electrons to transfer from the metal/solution interface, i.e. the tendency of the metal to dissolve. As it is not possible to measure the electrode potential absolutely, but only the potential difference against another interface, a standard reference electrode is defined against which the 'relative' electrode potential is measured. The standard hydrogen electrode (SHE) is universally accepted as the primary standard against which all electrode potentials are compared (arbitrarily defined as 0 V). Another common reference electrode is the saturated calomel electrode (SCE). The potential of the SCE is + 245 mV vs. SHE.

The magnitude of electrode potentials is affected by several variables where some are included in Table 2 [50].

Table 2. Effect of various factors on the electrode potential. After [50].

Effect	**Order of magnitude**
Nature of the metal	1 V
Chemical nature of the solution	0.1-1 V
Surface state (oxide film)	0.1 V
Absorbed gases	0.01-0.1 V
Mechanical stress	0.001-0.01 V

As previously mentioned, corrosion of metals is an electrochemical process including a chemical reaction accompanied by the passage of an electric current. For this to occur a potential difference must exist between one part of the metal and another. A large number of factors can give rise to variation in potential on a metal; these variations (heterogeneities) may vary in size from the sub-microscopic or atomic scale to the macroscopic when the separate anodic and cathodic areas may be seen with the naked eye [51].

Figure 10 shows some of these heterogeneities. The heterogeneities 1 to 6 in Fig. 10 will promote substantial potential difference in the case in which the solutions has direct access to the metal surface. However, the conditions will generally differ from this, and will be complicated by the presence of an oxide film or a layer of corrosion product on the metal surface [51]. Case 7 shows the breakdown of a protective film (passive layer, see next section), and case 8 shows discontinuous mill-scale. These discontinuities in the oxide films will render the part not covered by the oxide film anodic.

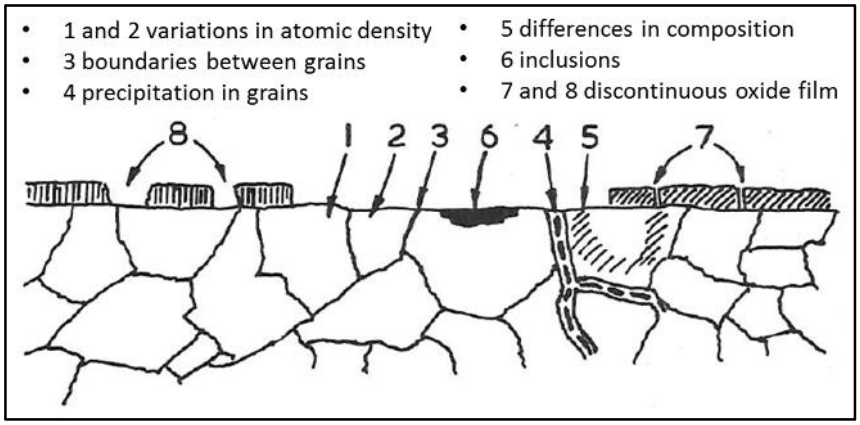

Figure 10. Heterogeneities that can form micro-cells on typical metal surface [51]

Further, potential difference can arise due to variations (in the solution in contact with the metal surface) in the concentration of e.g. chloride ions, pH-value and oxygen [51].

Potential-pH diagram

The potential-pH diagram (Fig. 11), usually called 'Pourbaix diagram', gives a guide to the stability (thermodynamically) of a metal in a specific environment [52]. Figure 13 shows a potential-pH diagram of iron in pure water at 25°C. The chemical environment is characterized by the pH of the aqueous solution (x-axis), and the electrode potential E (y-axis), is a measure of the electrochemical environment.

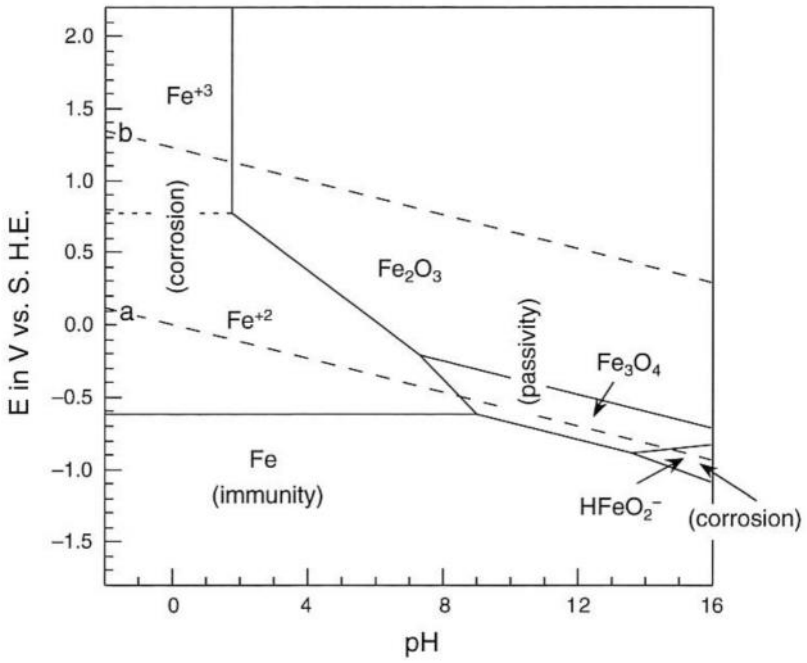

Figure 11. Pourbaix diagram for iron at 25îC. After [50]; data from [52].

The different regions in the diagram specify which species are stable under a certain pH and E. When the stable species is a dissolved ion, the region is in the diagram labelled 'corrosion'. When the stable species is a solid oxide or a solid hydroxide, the region is labelled as 'passivity, this means that the metal is protected by a surface film of an oxide or a hydroxide. Finally, when the stable species is the metal itself, the region is labelled as 'immunity'. In Fig. 11 also two dashed lines are plotted, labelled 'a' and 'b'. Between the 'a' and 'b' lines, water is stable, below 'a' line, H_2 evolution is possible, and above the 'b' line, O_2 evolution is possible.

The pore solution in concrete has usually a pH above 13, where the oxides Fe_3O and Fe_2O are stable for a wide range of potentials (in the passive region) [53].

Although the potential-pH diagram gives a first guide of metals corrosion behaviour it is still subjected to several limitations [50]. Some of them are: (1) the regions have been calculated using thermodynamic data assuming equilibrium, where in practice conditions may be far from equilibrium, (2) the diagram gives no information about kinetics, i.e. corrosion rates, (3) the diagram do not consider localized corrosion by chlorides ions, and special experimental diagrams must be constructed.

Passivity

Passivity can be defined as the reduction in chemical or electrochemical activity of a metal due to the reaction of the metal with its environment so as to form a protective film on the metal surface [50]. Note that the oxides (Fe_2O_3 and Fe_3O_4) plotted in Fig. 11 are in fact corrosion products, but are insoluble thereby preventing the electrolyte from coming in contact with iron and greatly reduces the corrosion rate. The exact nature of the passive film on iron remains elusive, part of the reason is that it is very thin (1.5-5 nm) [50].

In the absence of aggressive substance Hansson [53] summarised the following sequence of events that can be expected when fresh concrete is poured around steel reinforcement:

- A rapid development of a passive surface film, due to the high pH of the pore solution and the availability of oxygen. The potential of the steel will lie anywhere between +175 and -594 mV vs. SCE (approximate -70 and -840 mV vs SHE). The corrosion current (rate) will be negligible, around 0.01 to 0.1 µA/cm^2, corresponding to a corrosion penetration rate of 0.1 to 1.0 µm/year.
- The maintenance of the passive film requires both a high pH and access of oxygen. The greater the availability of oxygen, the thicker will be the passive film and the more positive will be the potential. In aerated concrete, steel normally exhibits a potential in the range +100 to -200 mV vs. SCE [55].
- If the concrete is buried under moist ground or deep water, eventually all the oxygen in the concrete will be reduced and the passive film cannot be maintained; the potential will then drop and the embedded steel will be in an 'active state'. However, because of the lack of oxygen, the corrosion rate will still be negligibly low, and in the same order of magnitude as in the passive state.

Localized corrosion

It is well known that the ability of the passive films to protect the metal can be compromised in the presence of chlorides or other halides [49][50][56][57]. These aggressive ions can give rise to a local breakdown of the passive film, resulting in accelerated dissolution of the underlying metal. If this attack initiates on an open surface, it is called pitting corrosion, at an occluded site it is called crevice corrosion [49][57]. Once initiated, the attack takes a very similar geometrical characteristics (a pit), and the propagation electrochemistry of pitting and crevice corrosion converge [49].

The mechanism of the very initiation of the breakdown of the otherwise protective passive film is not clearly understood. Different theories for the passive film breakdown and pit initiation have been proposed [57][58]. The pit propagation is illustrated in Fig. 12 for steel in concrete when chloride ions are present.

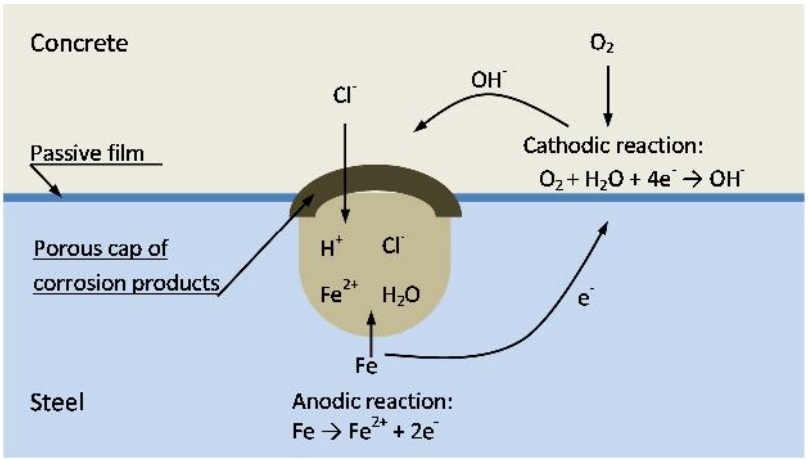

Figure 12. Schematic representation of the propagation stage of pitting of steel embedded in concrete.

When pitting corrosion has been initiated on steel embedded in concrete, areas no longer protected by the passive film will act as anodes (active zones) while large areas in the

surrounding still passive will act as cathodes, i.e. a site of oxygen reduction [59]. As the pit grows (anode), the dissolved metal ions are confined within the pit due to the restricted geometry and of a cap of porous corrosion products, which may exist [50]. As a result, accumulated metal ions undergo hydrolysis, and a local acidity develops within the pit creating a very aggressive environment. Finally chloride ions migrate from the bulk electrolyte to the pit electrolyte to maintain charge neutrality. When the corrosive pit electrolyte has been formed, pitting is considered to be autocatalytic [50]. The average potential is between that of the passive steel and that of the local anode, typically -200 to -500 mV (SCE) [55].

2.4.2 Kinetics

In order for the corrosion to proceed, there must be a complete electrical circuit between the anodic and cathodic areas. In Fig. 12 four partial processes can be identified for maintaining the current in the corrosion cell, i.e. the corrosion rate, those are:

- Oxidation of iron liberating electrons (anod).
- Reduction of oxygen consuming electrons (cathode).
- Transport of electrons within the metal.
- Current flow inside the concrete, transported by ions in the pore solution.

The slowest of the four partial processes will determine the corrosion rate. In reality the transport of electrons within the metal will never be the slowest process. Therefore, one of the other three processes will control the corrosion rate, i.e. be the kinetically controlling one. Which one it actually will be depends on the prevailing condition inside the concrete [59]:

- Slow anodic process because the reinforcement is passive, as in the absence of carbonation and chloride ions.
- Slow cathodic process because the rate at which oxygen reaches the reinforcement surface is low, as in water-saturated concrete.
- Slow current flow inside the concrete, as when the concrete has a low relative humidity.

From the above, the moisture content of the concrete can be pointed out as one the most decisive parameter controlling the corrosion rate. The moisture content can have two opposite effect on corrosion rate, too high it will restrict the diffusion of oxygen, and too low it will restrict the diffusion of the charge bearing ions [60].

Polarization resistance (R_p) is the only electrochemical technique to measure instantaneous (actual) corrosion rate [61]. It is based on the observation of linearity of the polarization curve around the corrosion potential (E_{corr}). If an external current (Δi) is applied for instance on a rebar it will move the potential away from E_{corr} (by ΔE), this is known as polarization. If the polarization is within several mV of E_{corr}, the potential change is almost always linear proportional to the current applied [54]. This linear proportionality is known as the Stern-Geary equation and can be expressed as:

$$R_p = \left(\frac{\Delta E}{\Delta i} \right)_{\Delta E \to 0} . \tag{17}$$

The R_p (Ω m^2) is related to the instantaneous corrosion rate through Eq. 18.

$$i_{corr} = \frac{B}{R_p}, \tag{18}$$

where i_{corr} is the corrosion current density, A/m^2, B is a constant, with suggested values of around 26 mV for active corroding reinforcement and 52 mV if the reinforcement is passive [61].

With the assumption of a homogeneous corrosion attack i_{corr} can be converted to corrosion penetration depth through Faraday's law:

$$X_{corr} = i_{corr} \cdot \frac{M}{Fz\circ} \tag{19}$$

Where X_{corr} has the unit m/s (but it is commonly instead expressed in units of mm/year), M is the molar mass of the metal (kg/mole), F is the Faraday's constant (96500 coulombs/mole electrons), z is the valence number of ions (2 for iron), and ρ is the metal density (kg/m^3).

2.4.3 Chloride threshold value

As previously mentioned the exact mechanism of the breakdown (corrosion initiation) of the passive film by chloride ions, is not clearly understood. For simplicity it has been suggested, for steel corrosion in concrete, that it can be considered as a function of the net balance between two competing processes; stabilization and repair of the film by OH^- ions, and disruption of the film by Cl^- ions [54]. It is generally accepted that depassivation occurs when the chloride ion concentration reaches a certain critical concentration, often referred as the chloride threshold value (CTV) [59][54]**[**62**]**. The chloride threshold value depends on many parameters; comprehensive literature reviews on the subject are found in references [62][63].

Both Angst et al. [62] and Alonso et al [63] reported large scatter in the reported chloride threshold values found in the literature. Figure 13 shows the scatter in data reported from field and laboratory tests [63].

One of the decisive parameters for CTV has been identified to be pH of the pore solution (which mainly depends on the binder type) [54][62]. This is reasonable as the maintainance of the passive film is strongly dependent on the level of pH (content of OH^- ions), see Fig. 11. Two common references in the literature linking the chloride threshold value to the concentration of OH^- is Hausmann [64] and Diamond [65], which both suggested a concentration ratio of Cl^-/OH^-. Hausmann [64] suggested a Cl^-/OH^- to be 0.6 while Diamond [65] proposed 0.3. In both cases this quantitative data are based on experiments in solutions. For reinforcement bars embedded in concrete additional effects may influence the CTV. This is shown in Fig. 14 where Andrade [61] summarised results found in the literature expressed as Cl^-/OH^- in alkaline solutions, mortars and concretes.

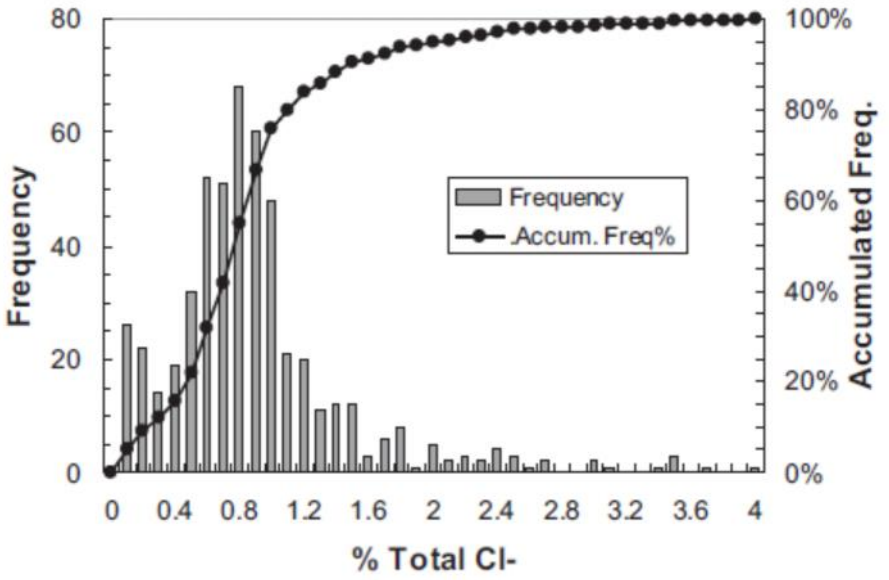

Figure 13. Frequency distribution and accumulated frequency of CTV found in the literature expressed as per cent chloride by cement weight [63].

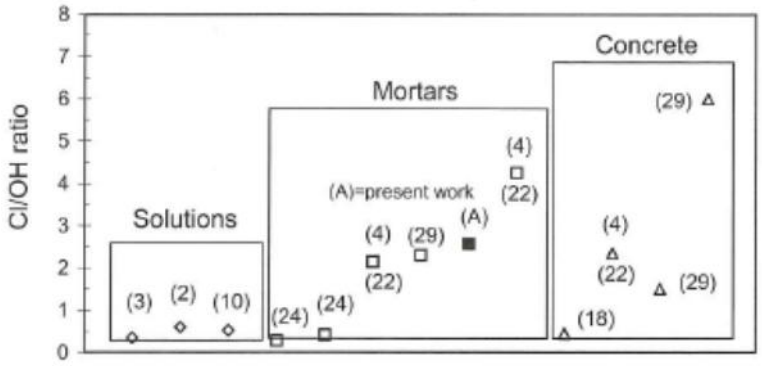

Figure 14. Chloride threshold values expressed as Cl^-/OH^- reported in the literature for alkaline solutions, mortars and concretes [61].

Another decisive parameter affecting the CTV is the quality of the steel-concrete interface [66][67]. For example, it has been suggested that when concrete is cast against a steel bar a dense cement rich layer containing a significant quantity of precipitated $Ca(OH)_2$ is formed at the interface. This restricts the mobility of the available chloride ions to reach incipient anodic sites (see Fig. 12), and the tendency for the pH to decrease there. This is suggested to be one of the reasons for higher chloride threshold values of steel embedded in concrete and mortars as compared with steel immersed in alkaline solutions (see Fig.14). In addition, the presence of hydration products on the steel surface restricts both the cathodic and anodic reactions.

The large scatter in the reported data has partially be attributed to the variability in the testing methods [62][63]. The need of laboratory tests under conditions that are as realistic as possible to predict threshold chloride values for embedded reinforcement steel has been identified [62][63][67].

Expression of chloride threshold values

The chloride threshold value can be expressed in different forms [62], such as:

1. Total chloride content relative to the weight of concrete (C_T/Con)
2. Total chloride content relative to the weight of binder (C_T/B)
3. Free chloride content relative to the weight of binder (C_F/B)
4. Free chloride relative to the hydroxyl concentration in the pore solution (C_F/OH^-)

There are various advantages and disadvantages of the different forms of expression. The various forms differ in the way they reflect the aggressive ion (Cl^-) and the inhibitive properties of the cement matrix [68].

The simplest form of expression is as C_T/Con. In this form the determined amount of chloride content at the depth of interest can sometimes be misleading, if a part of a concrete sample consists of large aggregates, the C_T/Con will be lower than that in an adjacent sample at the same depth with a higher amount of cement paste. This can in particular cause erroneous results if the chloride content is determined at a single point without performing a chloride profile. With relatively little additional effort, the CTV can be expressed as C_T/B [69]. This form eliminates the above risk of misleading results, but has been criticized for including also the bound chlorides, that do not take part in the corrosion process. This is taken into consideration in the last two forms of expression (3 and 4), in which only the free chlorides are counted as harmful. The difference between these two forms is the assumption that in the last one only the OH^- concentration (pH) reflects the inhibitive properties of the cement matrix.

By analysis of literature data and theoretical considerations, the authors in reference [68] concluded that the CTV is best presented as C_T/B. It is also important to bear in mind that practically it is very difficult to measure the C_F or the pH of the concrete pore solution. This was experienced in the experimental work in paper VIII, where pore solution extraction for chemical analysis was attempted on several concrete mixes (with low w/c) without any success. Also from the data presented in [62], the expression forms C_F/B and C_F/OH^- did not reduce the large scatter in the reported CTVs, on the contrary in many cases even higher scatter was reported.

In real structures one additional complication arises in expressing the CTV as C_F/OH. The chloride binding is temperature depended [40], and C_F will vary with temperature variations. On the contrary C_T/B is stable at temperature variations. The CTV is most commonly presented as total chloride content relative to the weight of binder (expression form 2); this was also adopted in this work.

2.5 Mineral additions

The incorporation of mineral additions in cement-based materials can lead to favourable influences on many properties, some by physical effects and others by physical-chemically effects [70][71]. The physical effects depend mainly on the particle size of the mineral addition and affects properties such as the rheological behaviour and early hydration. Limestone filler can be considered as a mineral addition mainly contributing by physical effects. Though, some chemical reactions occur as will be discussed later. Slag, fly ash and silica fume are more associated to physical-chemical effects such as pozzolanic reactions affecting to a larger extent properties like strength and permeability.

Mehta [70][72] stated, referring to mineral additions with physical-chemical effects, that any improvements of strength and durability of concrete associated with the use of these materials are possible only through pore refinement of its paste and reduction of microcracking at the

ITZ. Beneficial effects on concrete durability, because of paste pore refinement when incorporating mineral additions, have also been supported by many others [71][73][74][75]. However, when it comes to the controversial subject of ITZ, Leemann et al. [76] did not detect any major differences of the pore volume of the ITZ when comparing cement types with and without mineral additions. Further, the authors in reference [76] concluded that the pore characteristics of the bulk paste have a stronger impact on permeability than the pore volume in the ITZ. This conclusion is in agreement with previous cited references [38] and [39].

Also mineral additions without pozzolanic properties can influence the hydration and microstructure of cement-based materials [77][78]. The influence of these additions can be assigned mainly to physical effects. Examples of these kinds of mineral additions are quartz filler and the widely used limestone filler. In the literature quartz filler is often regarded as chemically inert [77][78], whereas the action of limestone filler is considered to lie somewhere in between that of an inert filler and a reactive one [3]. Three main physical effects are reported to be observed on cement hydration when so called inert additions are used. These three effects are: cement dilution, modification of the particle size distribution and heterogeneous nucleation [77][78]. The dilution effect is connected with the replacement level of cement clinker with mineral addition, and equivalent to an increase in water-cement ratio. The effect of particle size distribution depends on the fineness and amount of the mineral addition, and is related to the modification of the initial porosity of the mix.

The heterogeneous nucleation is a physical process enhancing the cement hydration by providing nucleation sites (on the mineral addition) to the cement hydrates. Lawrence et al. [78] cited Stumm [79] giving a qualitative explanation for this process: "*Qualitatively, if the surface of the solid substrate matches well with the crystal, the interfacial energy between the solids is smaller than the interfacial energy between the crystal and the solution, and nucleation may take place at a lower saturation ratio on a solid substrate surface than in pore solution*". Decrease of particle size and increase of the amount of mineral addition favours this process. Further, nucleation depends also on the affinity of the mineral addition for cement hydrates, which is related to the nature of the mineral addition used. The physical effects described above are to various extents also valid for the reactive additions before their potential chemical reaction starts [80]. In the literature the effects of modification of the particle size distribution and heterogeneous nucleation are seldom separated; the term "filler effect" is often used as a collective term. However, the term filler effect is sometimes used for either one of the effects [77][81].

2.5.1 Efficiency coefficient for mineral additions

The water-cement ratio is as previously discussed one of the dominant factors defining the properties of cement-based materials. When mineral additions are used as cement replacement the interdependency between water-cement ratio and properties such as strength and permeability are altered from what had been the case if pure Portland cement had been used. A rational methodology for using the *w*/*c* concept in predicting concrete properties when mineral additions are used was to the author's knowledge first proposed by Smith [82]. In Smiths methodology when pozzolans (in his case fly ash) are used the water-cement ratio is substituted with the equivalent water-cement ratio $(w/c)_{eq}$ and an efficiency factor, called the *k-value* is introduced. The equivalent water-cement ratio can then be expressed as:

$$(w/c)_{eq} = \frac{w}{(c + kR)}, \tag{20}$$

where the *k*-value, also referred to as the coefficient of efficiency, defines how many per cent by mass of a specified mineral addition can be regarded as equivalent to Portland cement. *R*, *c* and *w* are the masses of the mineral addition, Portland cement and mixing water. The *k*-value can be determined by taking the following steps:

1. Determine the relationship between the property to be studied (strength, permeability, etc.) and *w/c* for the Portland cement used, see Fig. 15.
2. Determine the value of the property to be studied for a given concrete mixture containing the mineral addition to be investigated.
3. By using the results from Fig. 15 and the result from step 2, $(w/c)_{eq}$ can be determined.
4. By using the known values of *c*, *R* and *w* and the value of $(w/c)_{eq}$ determined in step 3, the *k*-value can be calculated using Eq. (20).

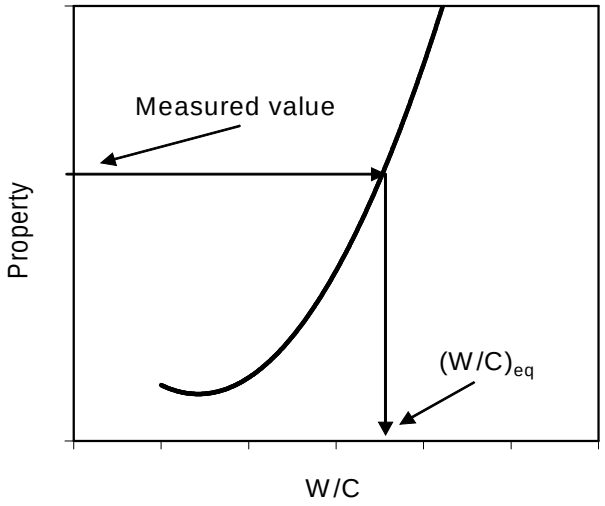

Figure 15. Graphical illustration of the steps to be taken for determining the coefficient of efficiency for a mineral addition with regards to a certain property.

The *k*-value summarises both the physical and chemical effects of the mineral addition and, hence, is influenced by a large array of parameters. The efficiency of a mineral addition depends, apart from the particular type used, on its fineness, the type of Portland cement it is combined with, and also by the replacement ratio [72]. The concept of equivalent water-cement ratio has been adopted by national standards; e.g., the European Standard [83] gives *k*-values for type II additions, i.e. reactive additions. The values are 0.2-0.4 for fly ash and 1.0-2.0 for silica fume. No values are given for slag, but in the documents for application of EN 206-1 in Sweden [84] a *k*-value of 0.6 is given for ground granulated blast-furnace slag. Exactly how the *k*-values in European Standard [83] are to be determined is not specified.

2.5.2 Limestone

The European standard EN 197-1 [2] permits use of limestone as an ingredient in Portland composite cements (CEM II) in two ranges: CEM II/A cements containing between 6% and 20% limestone (by mass) and CEM II/B cements containing between 21% and 35% limestone. From the data presented in [85] it can be concluded that Portland composite cement was the single largest type of cement used in 2010 in Europe, where Portland limestone cement was the most common alternative.

The reactivity of limestone filler in blended cements has been debated [86], and for a long time ground limestone was considered as inert filler [3]. Nowadays, it is generally accepted that limestone participates to some extent in the hydration reactions. It has been reported that $CaCO_3$ reacts with C_3A to form carboaluminates, and a transformation of the ettringite-monosulphate system occurs [87][88][89]. Further, interaction between calcium silicate (C_3S) and calcium carbonate, resulting in acceleration of the hydration of C_3S and modification of the Ca/Si ratio of C-S-H have also been reported [90][91]. Investigations on cements have also shown that the overall hydration rate of cement is accelerated with the incorporation of limestone filler [92].

From mercury intrusion studies Pipilikaki et al. [93] reported that an increased limestone addition gave an increased intruded mercury volume indicating an increasing porosity. However, in the same study [93] a decreased threshold diameter (d_{th}) with increased limestone addition was also reported. The threshold diameter corresponds to the narrowest path in the interconnected pore, and it has been found that permeability of cement paste is more sensitive to the d_{th} than the total porosity [94]. Also from mercury intrusion studies Sellevold et al. [95] reported, when they compared mature pastes with and without 12% limestone (very fine filler), that the specimens containing limestone filler had a finer pore structure. Bonavetti et al. [89] stated that the final hydration product of C_3A in limestone blended cements is an unstable compound in sulphate and chloride environment, and presumably can introduce durability problems. Ranc et al. [96] reported that, compared with quartz filler, the 28-day strength contribution of calcareous filler may be more than 5 MPa, and this could be due to the formation of carboaluminates. There is a general agreement in the literature [97] that at levels of replacement of clinker up to 5% by limestone has little impact on the properties of concrete.

Strength

The higher degree of hydration at an early age due to limestone as previously mentioned is also reflected by higher early age strength. It has been shown that the use of limestone filler as a replacement for cement may improve or at least not affect significantly the strength of both mortars and concretes at early ages, but this improvement has been found to disappear at a later age [99][100][101][102][103].

Chloride ion ingress

The literature is found to be conflicting about limestone addition with respect to the resistance of chloride ion ingress. In cell diffusion tests on mortar specimens, in which cement had been replaced (20%) by limestone filler but in which the water/clinker-ratio had been kept constant, the measured steady-state chloride diffusion coefficient was found to be lower for limestone blended mortars, but the time required to establish steady-state was longer for neat PC mortars [104]. With the same method of testing cement pastes, Tezuka et al. [105] reported somehow contradictory results; the chloride diffusion coefficient decreased in the following order of filler replacement: 25, 15, 35, 10, 0 and 5%.

Dhir et al. [106] tested the resistance to chloride penetration in a two-compartment cell applying a potential difference across the assembly. The result showed minor decrease of the resistance to chloride ingress for a limestone replacement ratio of 15% compared with pure Portland cement. For replacement rates beyond this level, there was a more progressive decrease in the resistance to chloride ingress. When the chloride penetration resistance was determined with a migration test (acceleration of ion transport by applying an electric voltage), the concretes with

blended binder of Portland cement and limestone showed a somewhat higher migration than those with neat Portland cement; the binders had comparable 28 days compressive strength [107]. Ghrici et al. [108] also tested concretes with a migration test, with different water/binder-ratios with and without 15% replacement of cement with limestone filler. In all cases the concretes with limestone blended cements showed larger chloride ingress.

In laboratory trials of mortars immersed in artificial seawater [109] an addition of 20% limestone filler by weight of cement to a reference mix led to a much higher chloride penetration than in the reference mortars. Bonavetti et. al. [110] exposed concrete specimens to a 3% sodium chloride solution in an immersion test (natural diffusion). Portland cement and two limestone-blended cements with a limestone content of 9.3% and 18.1% were tested. The chloride ingress increased with the increase of limestone filler content for wet cured specimens, but for air cured specimens the concrete with plain Portland cement showed the highest chloride ingress. For chloride ingress measurements made on concrete specimens exposed to a tidal zone in a marine exposure site, only relatively small systematic differences between cements with 0%, 5% and 25% limestone were revealed, the 5% cements being slightly better and the 25% cements somewhat worse than ordinary Portland cements [111].

One durability aspect that must be mentioned when limestone filler is used as Portland cement replacement is the resistance to sulphate attack and formation of thaumasite. Irassar [98] concluded in his review in the subject, that for external sulphate attack the effective *w*/*c* is the main variable. A low replacement ratio (<10%) causes no significant change in sulphate resistance, as the increase of the effective *w*/*c* is limited, while a larger proportion (>15%) may worsen performance when exposed to sulphate. Also the C_3A content of the parent Portland cement influences sulphate performance as for ordinary Portland cement.

3 EXPERIMENTAL METHODS

In the following, the most important experimental techniques used in the present work are briefly summarised.

3.1 Compressive strength

In principle, strength testing was carried out in accordance with European Standard test method EN 196-1 [2], but with a variety of mortar compositions instead of the standard mortar prescribed in the standard. The method specifies that prismatic mortar specimens, of size 40 mm x 40 mm x 160 mm, are to be used. The mortar is prepared by mechanical mixing and is compacted in a mould using a vibrating table for compacting. Each mould contains three specimens. During the first 24 hours the specimens are stored in the mould tightly covered with a lid to prevent evaporation. After the specimens are de-moulded they are stored under lime-saturated water at a temperature of +20 ± 2 ºC. At the required age, the specimens are taken from their wet storage, broken in flexure into two halves and each half is tested for compressive strength. In the experiments described in this paper, three prisms, i.e. six specimens, were used for determining the compressive strength for each mortar quality.

3.2 Chloride transport

As have been pointed out previously, the chloride ingress in concrete is a complex process influenced by a set of parameters that also in some cases are interrelated. Page et al. [112] pointed out that no single test method can provide adequate information to allow accurate predictions of diffusion rates for a variety of conditions of exposure. This point of view was also supported by Nilsson et al. [44]. However, owing to the important role of chloride ingress in concrete with regard to the durability of concrete structures many methods have been proposed for testing [40]. To be able to study particular variables that influence chloride ingress it is necessary to make a number of assumptions and simplifications. In the following the test methods and models of chloride ingress used in this work are discussed and the significance of the made simplifications is addressed.

3.2.1 Diffusion cell test

The test method that is considered to be the conventional way to determine the ion transport through cement-based materials is the diffusion cell (Fig. 16) [40]. Its underlying assumption is that the relationship between measured values of steady state flux and concentration are as a reasonable approximation described by Fick's first law of diffusion (Eq. 10). Whilst the values of the diffusion coefficient obtained by this method cannot be regarded as material properties, it has been shown that they provide a useful mean of comparison, which allows the major factors that affect chloride 'diffusion' (transport) rates to be evaluated [112][113].

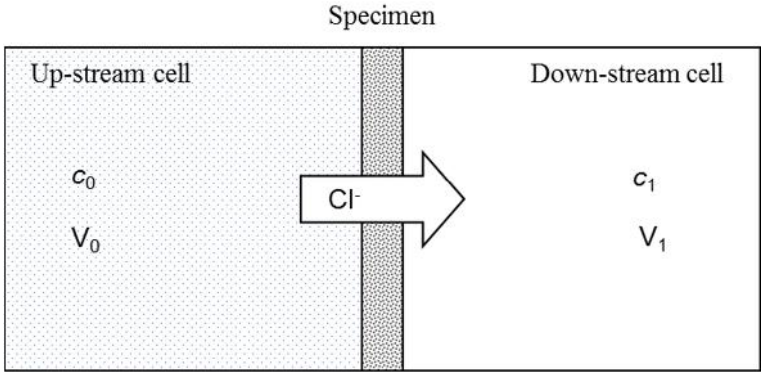

Figure 16. Experimental arrangement for a diffusion cell test.

A diffusion cell test normally involves the following procedures:

- The up-stream cell contains a chloride solution and the down-stream cell initially does not contain any chloride ions; a thin specimen separates the two compartments.
- The concentration of chloride ions in the down-stream cell solution is monitored at a certain time interval.
- A constant increase in chloride concentration of the solution of the down-stream cell implies a steady-state chloride flow and the diffusion coefficient according to Fick's first law can be calculated.

Usually an equation similar to Eq. (10) is used to calculate the steady-state diffusion coefficient (D_{ss}),. That gives:

$$D_{ss} = q_D \cdot \frac{L}{c_0 - c_1} = \frac{V_1}{A} \cdot \frac{\Delta c_1}{\Delta t} \cdot \frac{L}{c_0 - c_1}, \tag{21}$$

where $\Delta c_1/\Delta t$ is the linear slope of the concentration-time curve (see Fig. 17), V_1 is the solution volume of cell 2, L is the thickness of the specimen, A is the area of the specimen exposed to the solution, c_0 is the chloride ion concentration of cell 1, c_1 is the concentration of chloride ions in cell 2. If $c_0 >> c_1$, the latter is negligible. Alternatively, if the increase in c_1 is significant compared to c_0, integrating Eq. 21 in the range from τ to t yields [40]:

$$D_{ss} = \frac{V_1}{A_{specimen}} \cdot \frac{L}{t - \tau} \cdot \left[\ln c_0 - \ln(c_0 - c_1)\right], \tag{22}$$

where τ is the intersection of the linear regression line (see Fig. 17) with the time axis; it is called the 'time lag'. With the given assumptions D_{ss} (Eq. 21) is equal with D_{F1} (Eq. 10).

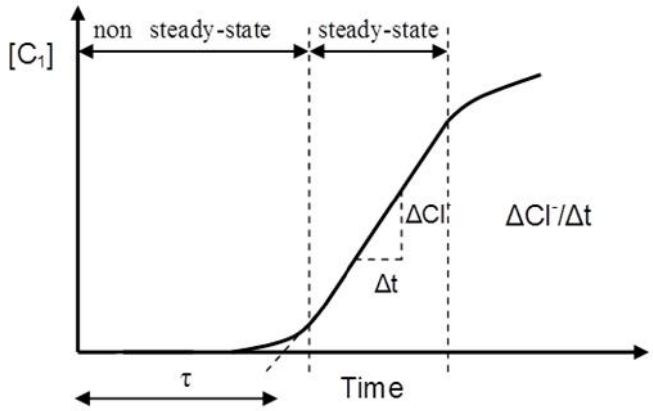

Figure 17. Evaluation of the test results from the diffusion cell test.

With the same experimental arrangement also the diffusion coefficient for transient conditions, where the chloride concentration changes with time (t) can determined. This non-steady state diffusion coefficient D_{nss} can be calculated from the time lag with Eq. (23):

$$D_{nss} = \frac{L^2}{6^2}. \tag{23}$$

Equation (23) is derived from the analytical solution of Fick's second law (Eq. 12) for the conditions in a diffusion cell with the assumption of a constant D_{nss} [114], this mean that D_{nss} is equal with D_{F2}. In cement-based materials, due to chloride binding, the D_{nss} will depend on the concentration in the up-stream cell. When a steady-state chloride flow has been achieved it can be assumed that the chloride binding capacity has been exhausted. That means that D_{ss} is not dependent on chloride binding. Still Arsenault et al. [115] reported a slight decrease of D_{ss} with a chloride concentration increase in the solution of the up-stream cell. During the test other ions then chloride will also be dissolved, diffuse, and participate. The effect of these processes on the test results is yet not clarified. A variation of the diffusion cell test was employed in paper III.

3.2.2 Immersion test (field exposure)

The immersion test can also be regarded as a conventional way to determine the chloride transport through cement-based materials. By immersion of specimens in sodium chloride solutions or submersion in the sea, as was done in paper I and paper II for a certain time (see Fig. 18), and followed by measuring the chloride profile, the non-steady state diffusion coefficient can be determined.

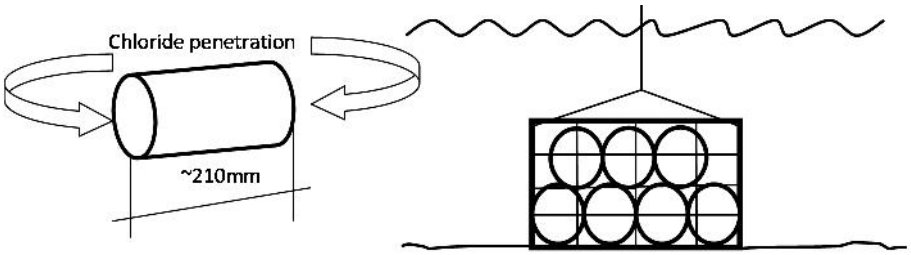

Figure 18. Specimens and submersion arrangement for the field chloride ingress test.

This method involved the following procedures:

- Prevention of multi-directional penetration by sealing all surfaces of the specimen except two. This was done by not removing the plastic moulds and by using a large enough specimen where one-directional penetration can be assumed at the sampling points.
- After one and three years of exposure in the sea the chloride content was determined at certain depths from the exposed surface. This is done by grinding the specimen successively from the exposed surface and then analysing the chloride content of each powder sample.

By modelling the chloride ingress as a diffusion process and assuming that there is no chloride binding, or that a simple linear relationship exist between the bound and free chlorides ions, the diffusion coefficient was obtained by curve-fitting the chloride profile to the so-called 'error function solution' [40] (see Fig. 19). The error function solution is the mathematical solution to Fick's second law (Eq. (12)) for a semi-infinite medium:

$$C_{(x,t)} = C_i + (C_s - C_i) \cdot \left(1 - \mathrm{erf}\left(\frac{x}{2\sqrt{D_{nss} t}} \right) \right), \tag{24}$$

where C(x,t) is the chloride concentration at depth x after exposure period t, C_i is the initial concentration, C_s is the chloride concentration at the exposure surface, D_{nss} is the chloride diffusion coefficient, and erf is the error function. For mortars with high w/c, chloride had penetrated through the centre of the specimens after three years of exposure, as the chloride ingress took place from two sides (see Fig. 18). Then Eq. 24 cannot be used, because the boundary condition is no longer semi-infinite. In these cases, Eq. 25 was used, which also is a solution to Eq. 12, but for double-sided chloride ingress [114].

$$\frac{C(x,t) - C_i}{(C_s - C_i)} = 1 - \frac{4}{®} \sum_{n=0}^{\infty} \frac{(-1)^n}{2n+1} \exp\left(-(2n+1)^2 \cdot \frac{® \cdot F_0}{4} \right) \cos\left(\frac{(2n+1)®}{2} \left(1 - \frac{x}{L} \right) \right), \tag{25}$$

where the Fourier number, F_0, is equal to:

$$F_0 = \frac{D_{nss} t}{L^2}. \tag{26}$$

The rest of the parameters in Eq. 25 correspond to the parameters in Eq. 24, with the addition of parameter L, which is the half-thickness of the specimen.

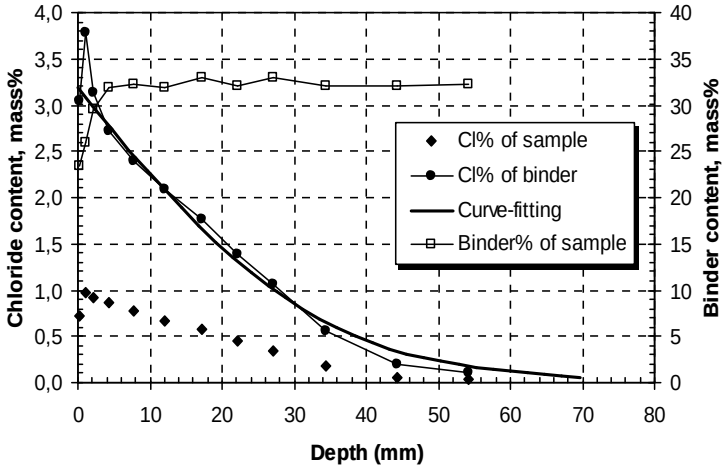

Figure 19. Measured chloride profiles and curve-fitted to the error-function.

The curve-fitting of the measured chloride profile reproduces the regression parameters D_{nss} and C_s. These two parameters should not be seen as direct material properties, but as regression parameters, describing the chloride ingress under a specific exposure condition and after a specific exposure time; the reason for this will be discussed in the following.

A clarification of the difference between the diffusion coefficients obtained from the two conventional methods is given in Eq. (13) as described by Massat et al. [48]. In Eq. (13) it can be seen that the relationship depends on the porosity and the chloride binding capacity. The two non-steady state diffusion coefficients obtained from Eq. (23) and Eqs. (24) and (25) should theoretically be the same if the exposure conditions are the same.

The D_{nss} obtained when curve-fitting data with Eqs. (24) and (25), is a kind of average diffusion coefficient under the time of exposure, and is also referred to as the 'apparent' diffusion coefficient (D_a) [40]. Correspondingly the chloride concentration at the exposed surface C_s obtained from the same curve-fitting is referred to as the 'apparent surface chloride content' C_{sa}. In this case the boundary conditions are assumed to be constant during the exposure time. Contrary to this assumption, data from different exposure times have shown that both D_a and C_{sa} are time dependent [116]. An equation commonly used to describe the time dependency for D_a is [40]:

$$D_a(t) = D_0\left(\frac{t_0}{t}\right)^{\alpha}, \tag{27}$$

where t is the age of the concrete, D_0 is the diffusion coefficient at a reference age t_0 and α is the age exponent. Part of this time dependency has been attributed to normal densification of cement-based materials, where the densification being different for different binders. However, Tang et al. [40] pointed out that the time dependency of D_a has not yet been fully explained.

What is even more intricate than a time dependent D_a is that observations from field data show that also C_{sa} is time dependent [116]. These observations cannot be explained with the current knowledge [40]; time-dependent binding could be a reason [40]. An important consequence of C_{sa} time dependency is that the error function is no longer the correct mathematical solution to Fick's second law (Eq. (12)). Therefore models based on the error function solution must be

considered as strictly empirical, and chloride ingress predictions with those models can be valid only as long as empirical data are available for the particular environment and exposure time.

3.2.3 Chloride migration test

Chloride ingress by diffusion is a slow process, especially for high quality concrete. A number of accelerated methods have been developed. The acceleration in those methods is often achieved by applying an external electrical field over the specimen, driving the chloride ions to migrate from the cathode to the anode. This reduces the test durations from weeks or months to hours or days, depending on the test [40]. Like the conventional methods the accelerated methods can also be under steady-state or non-steady-state conditions.

The accelerated method used in paper I is the widely used Rapid Chloride Migration test (NT-BUILD 492) [117], which is a non-steady-state migration test (Fig. 20) developed by Tang and Nilsson [118]. In this method, an external electrical field with a DC potential of 10-60 V, depending on the quality of concrete, is applied across the specimen. In most cases the specimen is split after 24 h and a silver nitrate solution is sprayed on one of the freshly split sections. The chloride penetration depth can then be measured from the visible white silver chloride precipitation, and the chloride migration coefficient D_m, can be calculated from this penetration depth according to Eq. (28).

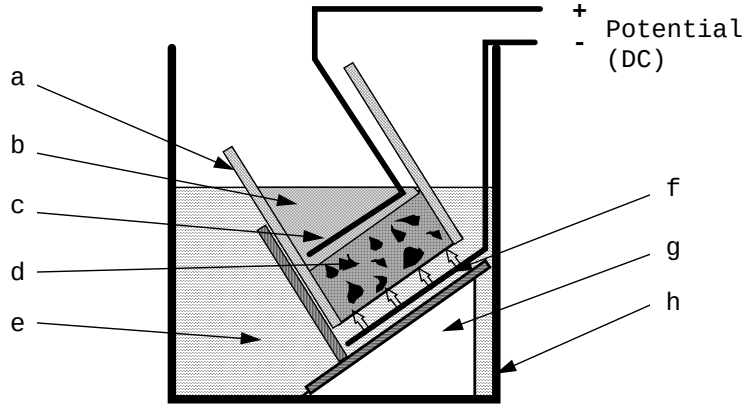

a. Rubber sleeve
b. Anolyte
c. Anode
d. Specimen
e. Catholyte
f. Cathode
g. Plastic support
h. Plastic box

Figure 20. Test set-up for NT-BUILD 492 [117].

$$D_m = \frac{RTL}{zFE} \cdot \frac{x_d - a\sqrt{x_d}}{t}, \tag{28}$$

where R is the gas constant, T is the absolute temperature, L is the specimen thickness, z is the valence of ions, F is the Faraday constant, E is the applied electrical potential minus 2 V (because of the potential drop at the interface between the electrode and the electrolyte [40]), x_d is the average value of the chloride penetration depth, t is test duration time and α is:

$$a = 2\sqrt{\frac{RTL}{zFE}} \cdot \text{erf}^{-1}\left(1 - \frac{2c_d}{c_0}\right), \tag{29}$$

where erf $^{-1}$ is the inverse of the error function, c_d is the chloride concentration at which the colour changes (~ 0.07 mol/L) and c_0 is the chloride concentration in the catholyte solution. The expression for calculating D_m was derived by Tang [119], by inserting the simplified Nernst-Planck expression, Eq. (9), which describes the flux under an external potential, into to the mass balance equation, Eq. (11).

3.3 Chloride threshold values

The initial design of the test specimen in the work for the development of a test method for determining CTVs (papers IV-VI) is shown in Fig. 21. The initial test procedure is similar to that proposed by Nygaard and Geiker [120]. Concrete specimens containing two sets of four embedded steel bars (i.e. a total of eight bars for each surface condition) were cast and cured at least for a couple of weeks, and then preconditioned (dried). The preconditioning was done to achieve an accelerated chloride penetration (resulting from a combination of capillary suction and diffusion) as it would have been very time consuming if saturated specimens had been exposed to the chloride solution for ingress simply by diffusion. After the preconditioning the specimens were exposed to sodium chloride solution.

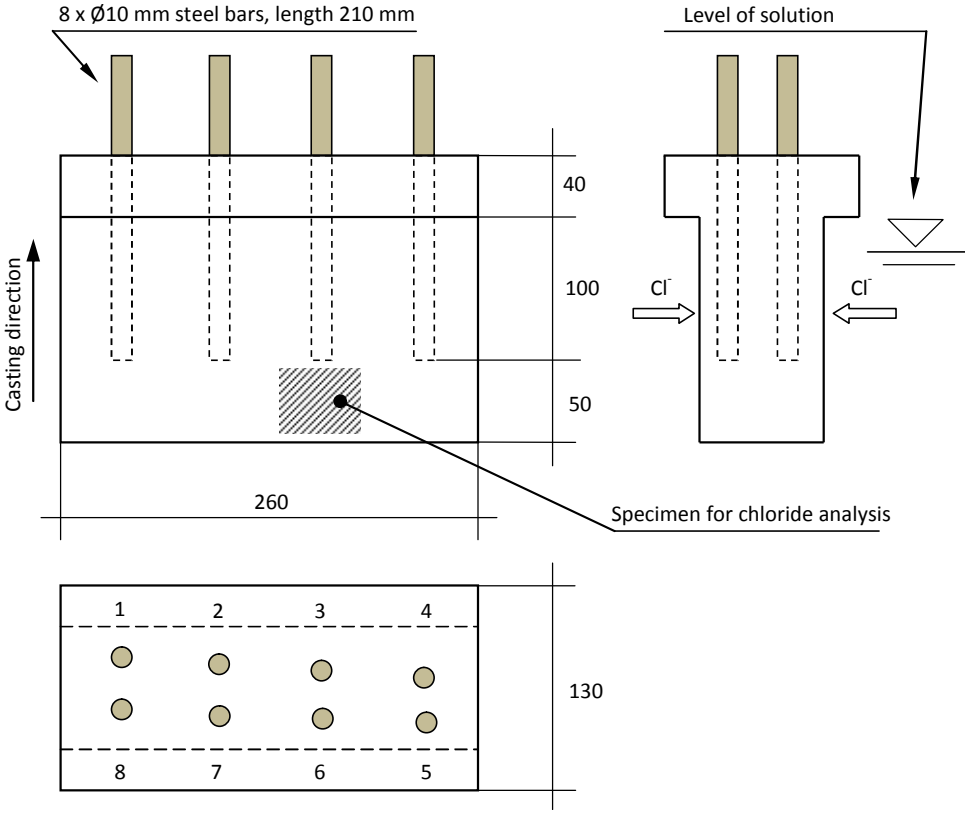

Figure 21. Concrete specimen embedded with steel bars, the dimensions are given in mm.

From the experiences in papers IV-VI and with consideration to the work within RILEM TC 235 CTC, both specimen design (see Fig. 22) and test procedure were further improved, as

discussed in paper VII. In short: a more controlled preconditioning and only one rebar in each specimen for easier handling.

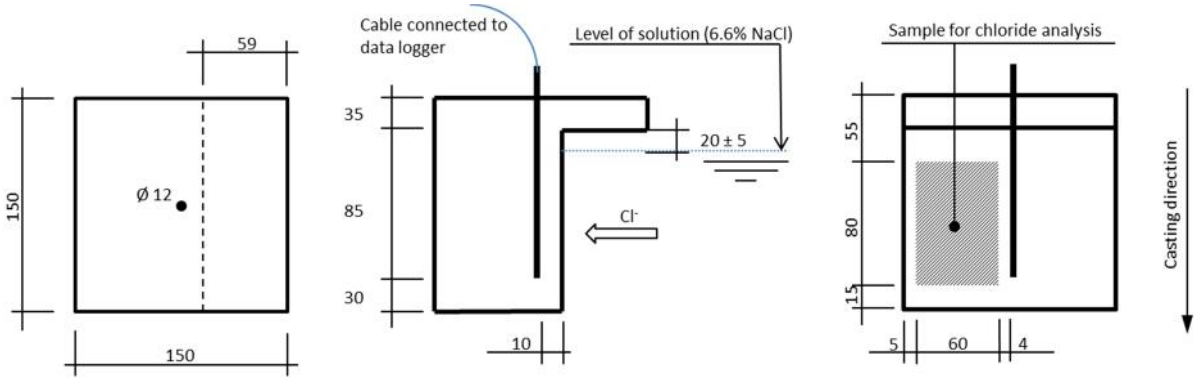

Figure 22. Concrete specimen with embedded steel bar (paper VII).The dimensions are given in mm.

In the field study (paper VIII) concrete slabs of 1000×700×100 mm (see Fig. 23) were cast at the SP Swedish Technical Research Institute in 1992. In most of the exposed slabs three rebars were embedded, one stainless steel and two regular carbon-steel rebars. Apart from different binders and water-binder ratios, different steel dimensions and concrete covers were also included. More details on specimen design, the field-test site and all tested mixture proportions can be found in Boubitsas et al. [121]. The mix proportions for the concretes discussed in Paper VII can be found in Appendix 2. After moisture curing for about two weeks, the slabs were transported to the field site (located in southwest Sweden) and mounted on the sides of pontoons for exposure in seawater (see Fig. 24). The chloride concentration in the seawater varies from 10 to 18 g Cl per litre, with an average value of about 14 g Cl per litre. The water temperature has an annual average of +11°C.

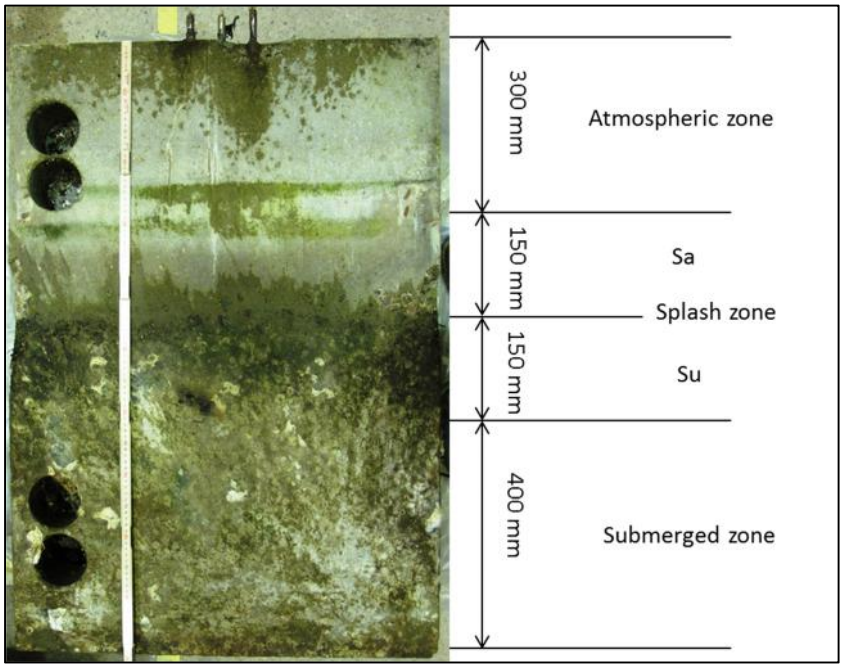

Figure 23. Concrete slab after 20 years of exposure (Paper VIII).

Figure 24. Overview of the field site (Paper VIII).

3.3.1 Corrosion monitoring with a data acquisition system

For one concrete specimen in paper V and for all concrete specimens in paper VI**,** the corrosion process was monitored with a data acquisition system. For one set of bars (bars 1-4, see Fig. 21) the corrosion potential (E_{corr}) was monitored, and for the other set of bars (bars 5-8, see Fig. 21) the polarising current (I_p) was monitored. In both cases a potentiostat developed by Arup et al. [122] was used; the measuring principle is illustrated in Fig. 25. The E_{corr} for bar 1 to 4 (W2) was measured against the reference electrode (R). A commercial available manganese oxide electrode (ERE 20, made by FORCE Technology in Denmark) was employed as reference electrode. For bar 5 to 8 (W1) the I_p was measured against the counter electrode (C) as the voltage drop through a 100 Ω build-in resistor in the potentiostat. A mixed metal oxide titanium mesh placed in the exposure solution was used as a counter electrode. In this work the controlled potential was set at 0 mV vs. SCE.

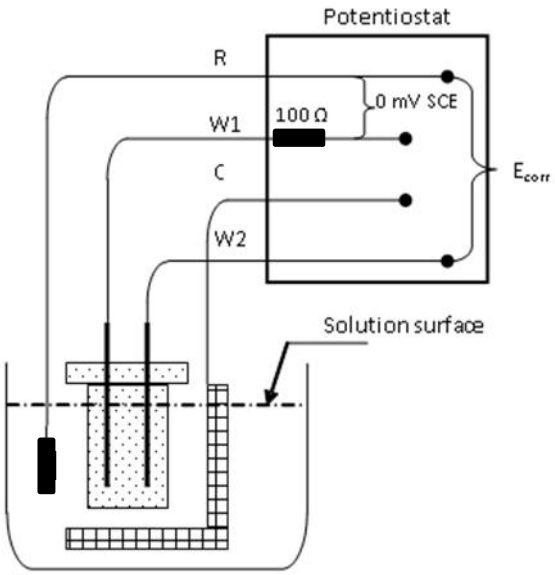

Figure 25. Measurement principle for Ecorr and Ip with potentiastat and data acquisition system.

3.3.2 Corrosion monitoring manually

For all specimens in paper IV and paper VIII and for some of the specimens in paper V the corrosion process was monitored manually; galvanostatic pulse and macro-cell measurements (only paper IV) were used.

The commercially available galvanostatic pulse technique RapiCor was used to monitor the corrosion process. The measuring principle is illustrated in Fig. 26. A wet sponge in placed on the concrete surface over the steel to be measured for improving the contact between the concrete and the electrodes unit. Then the rectangular shaped electrodes unit consisting of two counter electrodes (CE); two guard electrodes (GE) and a reference electrode (RE) are placed on the wet sponge. The instrument measures the E_{corr} by the RE (silver/silver chloride) placed in the centre of the unit. A galvanostatic current is applied to the CE and another current is applied to the GE, after imposing these currents the potential response is recorded. Modelling the system as a single Randles circuit, from the recorded potential-time curve the polarisation resistance (R_p) is obtained. The R_p is used to calculate the corrosion current density (i_{corr}) using the Stern-Geary equation (Eq. 18), where B is assumed to be 26 mV. The instrument gives the corrosion rate in µm/year through Faraday´s law (Eq. 19) and assuming uniform corrosion. Further, the instrument gives the E_{corr} versus the copper/copper sulphate reference electrode. A more detailed description about this technique can be found in reference [123].

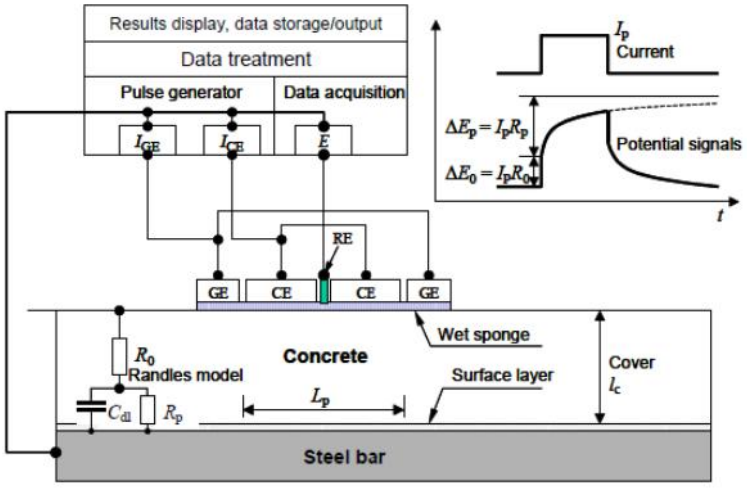

Figure 26 Measurement principle for the galvanostatic pulse technique [123].

The macro-cell current was measured between two neighbouring bars using a zero-resistance ammeter (made by FORCE Technology in Denmark). At every measuring occasion two bars were connected and the current going through the zero-resistance ammeter was noted. The bars were connected in the following scheme; bar 1 with bar 8, bar 2 with bar 7, bar 3 with bar 6, and bar 4 with bar 5 (see Fig. 21).

3.3.3 Determination of chloride threshold values

In this work the chloride content in the determination of CTVs was measured by chloride profiling. A simple empirical model that considers the time dependence both of the surface chloride content and of the chloride diffusion coefficient was used for predicting the chloride ingress [40]. The principle of the model is to obtain the 'apparent diffusion coefficient' $D_a(t)$ and the 'apparent surface chloride content' $C_{sa}(t)$ by curve fitting using the error function (Eq.

24), after different exposure times t_1 and t_2. The time-depended diffusivity $D_a(t)$ is given by Eq. 27, from which the age factor n can be calculated based on two measured chloride profiles. The apparent diffusion coefficient $D_a(t_{corr})$ at the time of corrosion initiation (t_{corr}) can then be estimated with Eq. 27.

The time-dependency of C_{sa} was assumed to be linear between the two curve-fitting occasions. The chloride content, i.e. the chloride threshold value, at the time of corrosion initiation is calculated using again Eq. 24, with the parameters, $D_a(t_{corr})$ and $C_{sa}(t_{corr})$. It must be emphasized that the model must be considered as purely empirical for interpolation between the exposure periods or for extrapolation (slightly) outside the measurement range.

4 MAIN RESULTS AND DISCUSSION

4.1 Cementitious efficiency of limestone

In papers I to III the influence of replacement ratio and *w*/*b* on chloride ingress was studied, also the influence of three different types of limestone filler was included in the studies. The chloride ingress was the main property investigated but also the influence on compressive strength was examined.

Before a further discussion of the main results some corrections must be made in the given mortar mix propositions in paper I and II (same batch). The correct mix proportions are given in Table 3, those given in the papers where the target mix proportions without correction for various air contents. For the mortars with limestone, when referring to *w*/*b*, it includes the all limestone filler (*w*/*b* = water/(cement + filler)) and when referring to water/cement ratio (*w*/*c*) it stands for water/cement clinker. For the PC mortars *w*/*b* and *w*/*c* are equal. In the following discussion the mortars with only Portland cement will be referred to as PC-mortars and the mortars with limestone filler as PLC-mortars. The letters L, C and M denote different types of limestone filler and 12 or 24 stand for the replacement ratios in per cent by weight of binder.

Table 3. Mix proportions in paper I and II.

Mortar	w/b	w/c	Cement	Limestone filler	Aggregate	Air	Consistency	28 days compressive strength
			(kg/m^3)	(kg/m^3)	(kg/m^3)	(%)	(mm)	(MPa)
Portland cement mortars (PC)								
PC-0.4	0.4	0.4	696		1251	2.9	169	82.4
PC-0.5	0.5	0.5	488		1465	4.9	170	66.7
PC-0.6	0.6	0.6	406		1565	3.8	176	48.5
PC-0.7	0.7	0.7	327		1580	7.5	168	42.2
PC-0.8	0.8	0.8	305		1582	6.5	172	33.2
Cement and limestone filler (PLC)								
L12-0.5	0.5	0.57	428	58	1459	5	175	62.3
L24-0.5	0.5	0.66	370	117	1459	4.7	180	48.6
L24-0.7	0.7	0.92	252	80	1604	5.4	164	31.1
M24-0.5	0.5	0.66	365	115	1441	6	178	47.3
C24-0.5	0.5	0.66	369	117	1458	4.8	173	49.8

4.1.1 Strength

The compressive strength was tested for all mortar mixes mostly as an indicator for the overall quality and also as indicator of microstructure development. Results after 28 days [124], 1 year

(paper I) and unpublished data from tests performed after 2 years of wet-curing are shown in Figure 27.

On the left hand side in Fig. 27 the development of the compressive strength with time for the PC-mortars with different *w*/*b* are shown. As expected an increase in *w*/*b* results in a decreased compressive strength. A rapid-hardening cement (CEM I 52.5 R) was used in this study, and, as Fig. 27 shows, no significant change can be observed after 28 days for most of the PC-mortars. However, one exception is the mortar with *w*/*b* = 0.4 where an increase of 11 MPa was measured after 2 years of wet-curing compared to the 28 days strength. A possible explanation is a progressing hydration for the PC-mortar with the *w*/*b* = 0.4. Due to a greater densification of the cement matrix for lower *w*/*b* it is more difficult for the water in the pores to reach unreacted cement grains, which slows the rate of hydration [125] and thus extends the time to reach maximum strength.

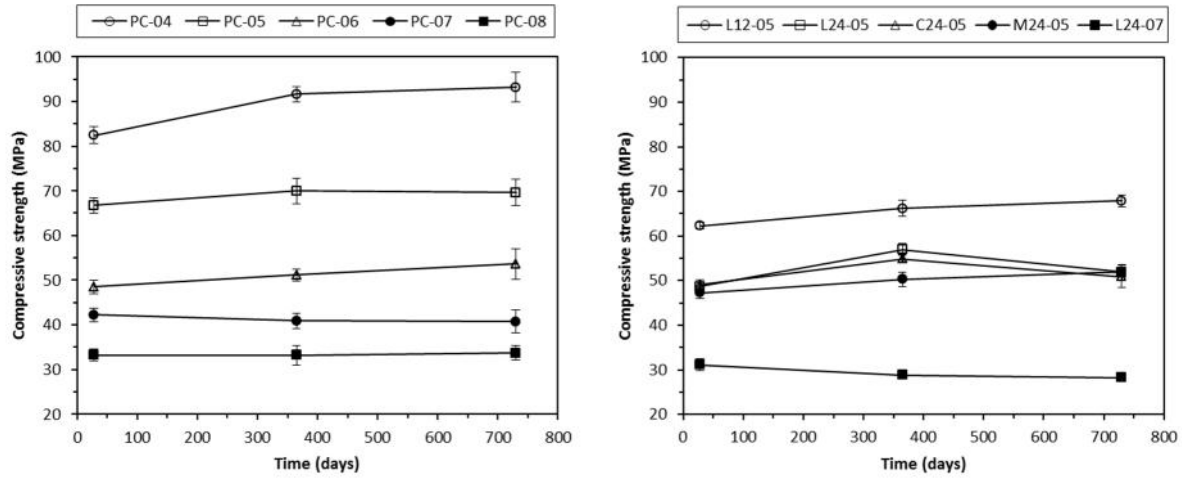

Figure 27. The development of the compressive strength with time for PC- and PLC-mortars with different w/b.

On the right hand side in Fig. 27 the compressive strength as a function of time for the PLC-mortars are shown. The *w*/*b* is 0.50 for all PLC-mortars except for one mortar with a *w*/*b* = 0.7 (L24-07). As for the PC-mortars an increase of the *w*/*b* will also reduce the compressive strength. Further, the amount of replacement of Portland cement with limestone also influences the compressive strength, and it is evident that that the replacement of Portland cement with limestone leads to a dilution effect similar to that of an increase of the water-cement ratio.

Some deviating results can be observed on the compressive strength results for the PLC-mortars L24-05 and C24-05. These mortars show a maximum after one year which is difficult to explain other than as an artefact in the casting of the samples, e.g. such as different degree of compaction.

In Fig. 28, the compressive strength results for both PC and PLC-mortars after one year of wet-curing are plotted against *c*/*w*. It is evident that some enhancing effect by the limestone on compressive strength must exist, otherwise the results of the PLC-mortars would have been on the same line as the PC-mortars. As illustrated in Fig. 28 with red arrows, the compressive strength for the PLC-mortars is higher compared to the corresponding PC-mortars with the same *w*/*c*. This implies that a certain amount of limestone filler has a cementitious effect regarding compressive strength, and that this cementitious effect is more pronounced for the lower replacement ratio.

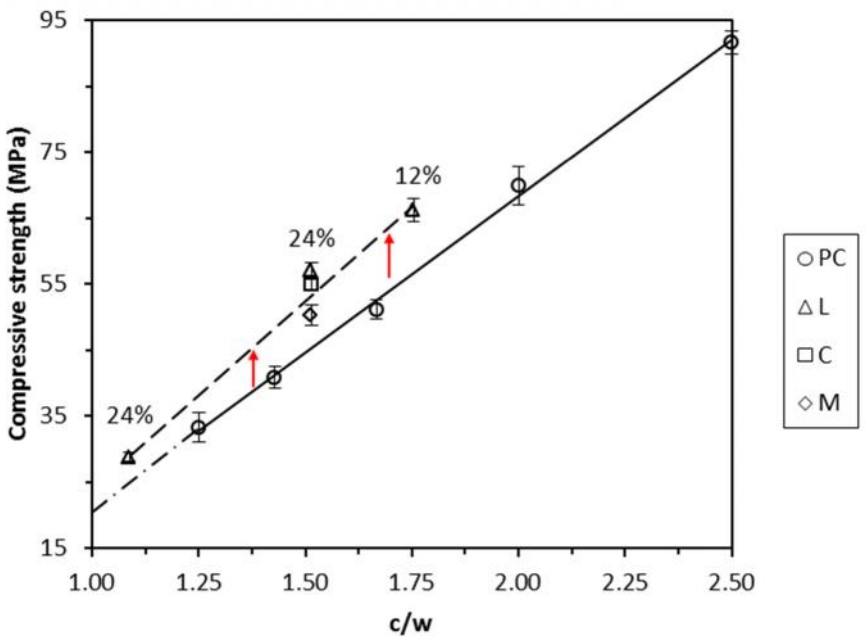

Figure 28. The compressive strength (1 year wet-cured specimens) as a function of the inverse of w/c.

In Table 4, by following the concept for evaluating the coefficients of efficiency (*k*-values) described in section 2.5.1, the cementitious effect of limestone filler was determined for the different PLC-mortars after different curing times. Each value in Table 4 is the mean value of six specimens, coming from three prismatic mortar specimens broken into two halves by flexure.

The *k*-value for the limestone fillers tested in this study depends foremost on the replacement ratio; no significant differences are evident when comparing different limestone types or *w*/*b*. The mean *k*-value in Table 4, when the binder consisted of 12% limestone filler is 0.9 and when the binder consisted of 24% limestone filler the same *k*-value is 0.3. If limestone filler did not have any cementitious effect the *k*-values would have been zero. With the knowledge that limestone does not possess any hydraulic or pozzolanic ability this cementitious effect must be attributed to some other mechanism.

Table 4. Calculated k-values for limestone filler with regard to compressive strength.

Mortar mix	*k*-values for compressive strength		
	28 days	1 year	2 years
L12-0.5	0.9 ± 0.1	0.8 ± 0.2	0.9 ± 0.1
L24-0.5	0.2 ± 0	0.5 ± 0.1	0.3 ± 0.1
L24-0.7	0.2 ± 0.1	0.2 ± 0	0.1 ± 0.1
M24-0.5	0.2 ± 0.1	0.2 ± 0.1	0.3 ± 0.1
C24-0.5	0.3 ± 0.1	0.4 ± 0	0.2 ± 0.1

As mentioned previously besides the dilution effect when an 'inert' mineral addition replaces Portland cement two additional effects are present, the filler effect and the heterogeneous nucleation. These two effects can contribute to the cementitious effect of limestone filler. The filler effect appears to be a mechanism more pronounced when very fine mineral additions (finer than cement) in combination with a plasticizer are used in concrete, levelling out particle size differences and creating a more homogeneous concrete.

For mortars Lawrence et al. [78] identified, in their extensive experimental program, heterogeneous nucleation to be the mechanism contributing to strength increments for inert mineral additions such as quarts and limestone filler. Heterogeneous nucleation is foremost coupled with an enhancement of the degree of hydration, but as can be seen in Table 3 the cementitious effect remains even after two years. This implies that the introduction of a large number of nucleation sites could also result in a more homogeneous distribution of C-S-H altering the pore size distribution in a beneficial way. The total porosity can be considered to be the major factor influencing the strength of cement-based materials. Additionally, it has been suggested that pores of different sizes (and shapes) affects strength in a varying degree [20]. Lawrence et al. [78] also found, when comparing mortars with quartz and limestone filler with the same replacement ratios and for equivalent fineness, higher compressive strengths for mortars containing limestone filler.

4.1.2 Chloride transport

In papers I to III the efficiency of limestone concerning chloride ingress was also studied, both by laboratory tests and field exposure. Initially, a brief description of the involved mechanisms regarding chloride binding will be given which will be helpful in the discussion of some of the observations made in the chloride ingress studies.

As previously mentioned the mechanism of chloride binding includes both physical binding and chemical reactions [45][126]. Chemical binding is attributed foremost as the result of reaction of chlorides with hydrated and unhydrated clinker phases of C_3A and C_4AF to form calcium-chloro-aluminate (Friedel's salt). Different reaction mechanisms have been proposed [45][126]. One is an ion-exchange between chlorides and hydroxyl or sulphate ions occurring foremost with hydrated phases of C_3A and C_4AF (AFm phases), which is a relative slow reaction. The other is a direct reaction between unhydrated C_3A or C_4AF and chloride ions, which can be considered as a faster reaction.

Physical binding, or more correctly physical adsorption, of chlorides is the results of electrostatic and/or van der Waals' forces attracting chloride ions. This takes place at the interface between the pore solution and solids [126]. These attracting forces are expected to decrease with the distance from the solid surface. The physical adsorption of chlorides is influenced by the temperature and the presence of competitive anions [126]. An increased temperature increases the ion's energy and hence mobility, which will give less physically bound chlorides. The presence of competitive anions, such as hydroxyl and sulphates, will depend on the binder type and on the exposure environment. Hydroxyl and sulphates will 'compete' with chloride ions to occupy sites on the surface of the solids to maintain electro-neutrality.

Non-steady state migration

Due to chloride ingress being a slow process, a number of accelerated methods have been developed to speed up the procedure when it comes to the assessment of resistance to chloride ingress for different binders. In this work the Rapid Chloride Migration test (NT-BUILD 492) [117] was used. Results after 28 days [124], 1 year (paper I) and unpublished data from tests performed after 2 years of wet-curing (saturated lime solution) are shown in Figure 29.

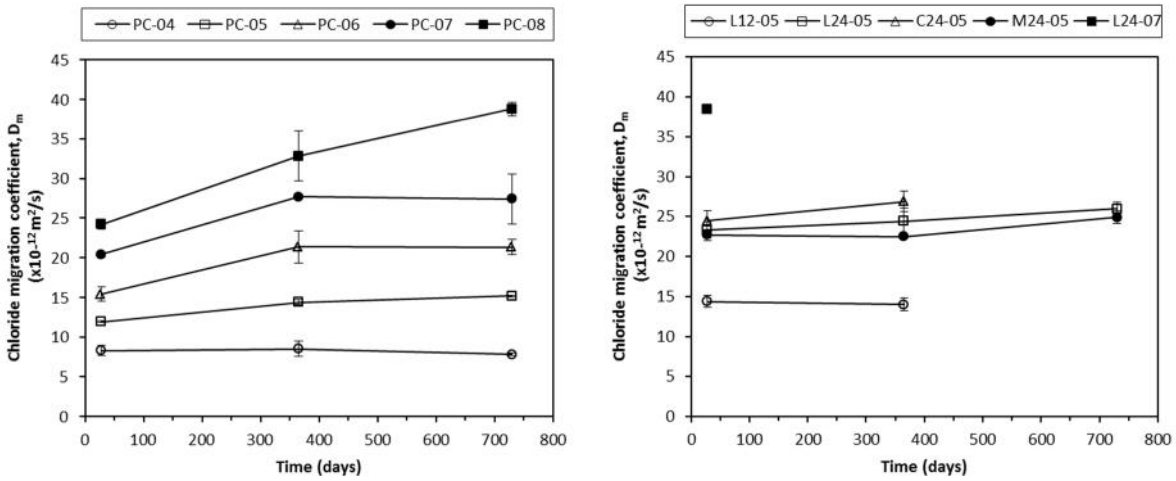

Figure 29. The development of the chloride migration coefficient (D_m) with time for PC-mortars (left hand side) and PLC-mortars (right hand side) with different w/b.

On the left hand side in Fig. 29 the development of the chloride migration coefficient (D_m) with time for the PC-mortars with different *w*/*b* are shown. The relationship seen between D_m and *w*/*b* is quite expected; an increased *w*/*b* and consequently an increased capillary porosity, results in an increased D_m at all tested ages. However, the evolution of the migration coefficient with time for most of the PC-mortars is quite unexpected, and especially the evolution of the D_m measured at 28 days compared with the results after one year (except mortar PC-04). Often the resistance to chloride ingress is reported to increase (decrease of D_m) with time as the capillary porosity will diminish with the increased degree of hydration. The magnitude of this decrease depends on the *w*/*b* and the type of binder [40]. However, the results from this study give another picture. These somewhat deviating results seem to get more pronounced as the *w*/*b* increases. Additional D_m measurements where performed at 28 days, giving the same results.

The changes over time of the resistance to chloride ingress will depend both on microstructural changes such as reduced capillary porosity but also changes in the chloride binding capacity [40]. If the development of the compressive strength in Fig. 27 is seen to reflect the development of the capillary porosity, no significant changes are observed after 28 days (except for mortar PC-04). So, the development of D_m from age 1 to 2 years is quite consistent with the assumed microstructural changes, except for mortar PC-08. Similar development with time of the D_m has been reported in [40]. However, the observation of a lower migration coefficient at 28 day compared with later ages is not consistent with the assumed microstructural changes; the only identifiable material parameter increasing the D_m is a time dependent chloride binding capacity. Sumranwanich and Tangtermsirikul [127] presented some evidence of higher chloride binding capacity for pastes with shorter curing time. They attributed that to a higher unhydrated fraction of C_3A and C_4AF. Direct comparisons with the results in Fig. 29 (left hand side) are not straightforward as the studied curing times were shorter in [127]. However, an assumption is

that the applied voltage in the migration tests will force the chloride ions to move fast through the pores. This would cause a limited chemical binding through the ion-exchange reaction because as previously mentioned this is expected to be a slow reaction. The possible chemical binding reactions will under such circumstances be a direct reaction with unhydrated aluminate phases, which will be more accessible at an earlier age. This can be manifested as a lower D_m at an early age, especially for mortars whose microstructure does not change markedly with time. In the case of PC-04 this was not apparent because an increased densification of the microstructure (Fig. 27) probably compensated for a decreased chemical binding with time.

Some support for the above assumption can also be found in the results from the PLC-mortars in Fig. 29 right hand side. As limestone is suggested to react with C_3A to form calcium carboaluminates, this will consume part of the amount of the unhydrated C_3A available for the chemical binding. Also the replacement of Portland cement itself will reduce the available calciumaluminates. In Fig. 29 (right hand side) this appears as a constant D_m with time, corresponding fairly well with the development of the compressive strength, which indicates the structural evolution, in Fig. 27 (right hand side).

Microstructural changes due to leaching explaining the unexpected development with time of the D_m is not likely, as the mortars were stored in lime saturated solution, which should prevent dissolution and leaching of calcium hydroxide.

A difference in the time-dependency of D_m between PC-mortars and PLC-mortars was evident when comparing the results of their interrelation after 28 days [124] with those after one year (paper I). Due to this difference, negative *k*-values were reported for the shorter curing time for the higher limestone replacement ratio while the corresponding *k*-values after one year of curing were about zero, see Table 5.

Non-steady state diffusion (field exposure)

The non-steady state chloride diffusion coefficient or apparent diffusion coefficient (D_a) for the PC-mortars and for the PLC-mortars was also determined. This was done by measuring chloride and calcium profiles after one and three years of submersion in the sea (papers I and II). The chloride ingress was evaluated and described by curve-fitting the measured chloride profiles with the analytical solution to Fick´s second law (complementary error function), with the assumptions as described in section 3.2.2.

Figure 30 shows measured chloride and calcium profiles after three years of exposure in the sea for mortar PC-06. The calcium profiles were measured simultaneously because chlorides are only diffusing through (and bound to) the cement paste, which means that the chloride content should be proportional to the amount of cement. As no calcium containing aggregates were used the cement amount for each powder sample could be determined from the calcium content. Figure 30(c) shows the chloride profiles expressed as total chloride as weight per cent of cement, based on the results in Figs. 30(a) and 30(b).

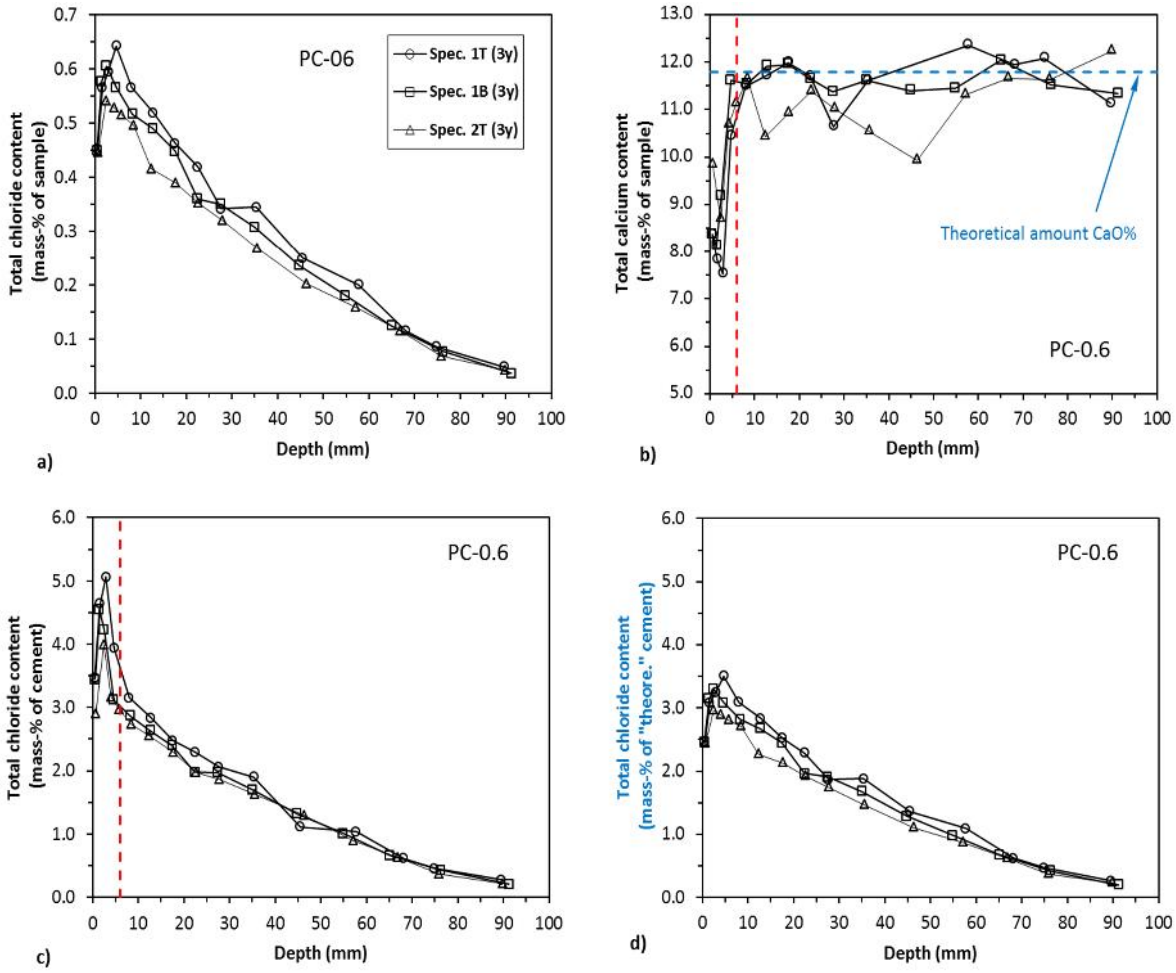

Figure 30. Examples of measured chloride and calcium profiles after 3 years of exposure in the sea.

In this work the surfaces were exposed to seawater. They were cut prior to submersion (20 mm slices were removed). This made it possible to observe the actually changes also in the calcium content (Fig. 30(b)), which otherwise often is overshadowed by the "concrete skin layer" (which often is richer in calcium than the bulk). As can be seen in Fig. 30(b) a much lower calcium content was measured close to the exposed surfaces, meaning that calcium has leached during the exposure in the sea water. In Fig. 30(b) the theoretical amount of calcium is marked with a dashed blue line. The theoretical amount of calcium is in this case 11.7% by weight of sample according to the proportions in Table 3 (PC-06) and the calcium oxide content of the cement (64.1% by weight). The actual measured mean value of calcium for the non-leached zones for the PC-06 mortar is 11.5%. The mean value of the standard deviations between the theoretical and measured calcium content for the PC-mortars is ± 0.3% and for the PLC-mortars is ± 0.4%. How the binder content is calculated for both PC and PLC-mortars is further described in paper I. For comparison Fig. 30(d) shows the chloride profiles expressed as weight per cent of the theoretical amount of cement, calculated assuming that the calcium content is 11.7 per cent by weight throughout the whole specimen.

No pronounced difference, if the leached zone (marked with red dashed line) is excluded, can be observed when comparing the chloride profiles in Fig. 30(a) and (d). This is because, besides that a cut exposed surface was used, the mortar specimens had a maximum aggregate size of 2 mm. However, in a concrete specimen with a cast surface (richer in calcium than the bulk) and with larger aggregate size, the measured chloride profile can be misleading if it is expressed as

weight per cent of sample or as a theoretical amount of binder. Figure 31 shows the chloride and calcium profiles from a concrete specimen submerged for 20 years in the same marine field site as the mortars [121]. This concrete was one of the specimens that were used to estimate the CTV in paper VIII. The concrete in Fig. 31 has a *w/c* = 0.35 and a sulphate resistant Portland cement as binder. As for the mortar specimens in Fig. 30, when the chlorides are expressed as weight per cent of sample (Fig. 31(a)) or weight per cent of theoretical amount of binder (Fig. 31(d)), the appearance characteristics of the profiles do not deviate in another way than in the scale of the chloride content. However, when the chloride profile is expressed as weight per cent of binder (Fig. 31(c)), based on the actual measured calcium content (Fig. 31(b)), the appearance characteristics of the chloride profile differ markedly. The main reason for this difference is as previously mentioned that the chloride content is proportional to the amount of cement (which in turn is proportional to the calcium content (Fig. 31(b)).

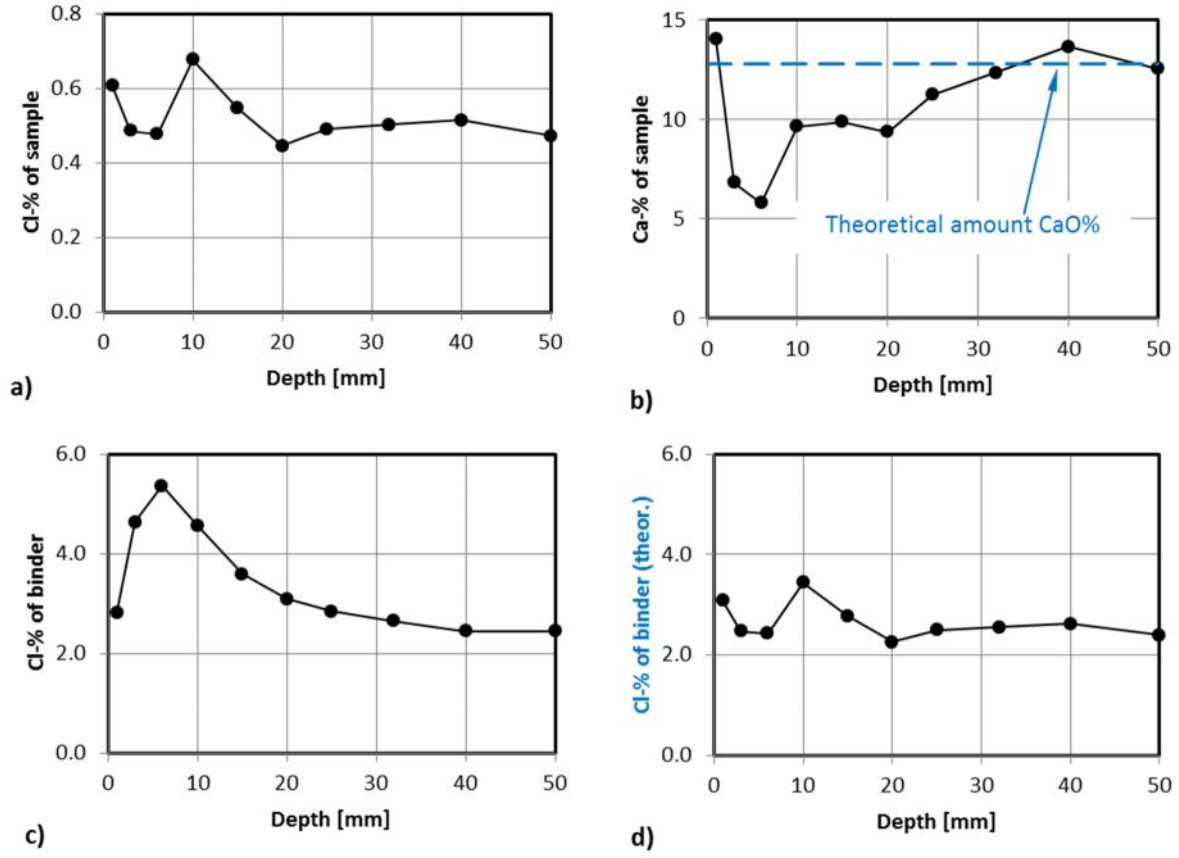

Figure 31. Results from a concrete specimen submerged in sea water for 20 years [121].

The scatter in the calcium profile for the concrete sample (Fig. 31(b)) is mainly evident at the near-surface region (0 to 20 mm). Because the exposed concrete surface in this case is the bottom side of the mould (with respect to casting direction), the main reason for the scatter in calcium content is likely the “wall effect”. This means that the difference in size between the aggregate particles will result in smaller aggregate particles in the vicinity of the mould surface and larger aggregate grains further in. The average aggregate content will be larger with depth up to a depth corresponding to half the size of the maximum aggregate size. A larger aggregate content will give a smaller binder content with depth. In Fig. 31(b) it seems as if the concrete is more homogeneous further in (> 20 mm) from the surface.

Even though no pronounced differences in the chloride profiles can be observed in Fig. 30 a slightly smaller scatter in the results can be observed in Fig. 30(c) between the individual profiles in the unleached zone. The condition is the opposite in the leached zone. However, as the leached zone was omitted in the curve fitting procedure the results are not affected by the higher scatter in this zone.

The curve-fitting procedure is to some extent quite a subjective matter. One of the reasons for this is, if it is correct to ignore the leached zone. Further, how the chloride profile is expressed can also lead to misconceptions concerning the curve fitting procedure.

The results from a slightly modified curve-fitting procedure from that in papers I and II are discussed in this section. The final results, however, did not differ significantly from those presented in papers I and II. The modification was done because of the two reasons presented below.

Firstly, because the chloride from the seawater could penetrate the specimens from both sides after three years of exposure, for some mortar qualities chloride ions had penetrated through the centre of specimens. When the results in paper II were evaluated the author was unaware that the chloride profile from one side is adequate for curve-fitting if the solution to Fick´s second law for double sided penetration (Eq. 25) is used. As three chloride profiles were measured for most mortar qualities (two profiles for mortars M24-0.5, C24-05 and L24-L), two from the same specimen (opposite sides) and one from a separate specimen, the scatter could be quantified. An overview of the scatter (standard deviations) in the curve-fitting results from field-exposed specimens is also included in Figs. 32 and 33; something that is quite rare in the literature.

Secondly, the point from where the curve fitting is started can have a huge influence on the regression parameters D_a (apparent diffusion coefficient) and C_{as} (apparent chloride surface content). For most of the measured chloride profiles in this work, the shape of the profiles deviated from the shape of the complementary error function (Eq. 24) at the same depth as the corresponding measured calcium content decreased from the bulk quantity (Fig. 30). The majority (but not all) of the regression analyses in paper I and II were therefore made with this certain depth as starting point. However, all the regression parameters (D_a and C_{as}), presented in this section are based on a curve-fitting procedure where the curve-fitting of the chloride profiles is started at the depth (x_L) where the calcium content is equal to the bulk content. By this approach the regression analyses gets less subjective and is coupled to a phenomenon actual happening in the material that most likely affects the deviation from the shape of the error function solution (Eq. 24). Leaching of calcium increases the porosity [128], which consequently can alter the chloride ingress. However, it cannot be claimed that leaching of calcium is the only reason for the deviation in the near-surface region. Other species also leach out of and diffuse into the sample affecting the chloride transport, as e.g. sulphate ions and hydroxide ions [129][130]. The exact mechanism behind the non-conformity between the measured chloride profiles and the modelled ones in the near-surface region cannot be explained with current knowledge [40].

The apparent diffusion coefficient (D_a) for the different PC-mortars is shown in the left hand side in Fig. 32 and for the PLC-mortars in right hand side. Further, Fig. 32 shows also the depth, x_L (the position of the red dashed line in Fig. 30), where the calcium content becomes equal to the bulk content for the PC and PLC mortars. This depth can be seen as a measure of the leached zone.

For the PC-mortars (upper left hand side in Fig. 32), an expected relationship of increasing D_a with increased w/c can be observed. However, the trend of the development of D_a with time is not unitary. For three out of five mortar qualities no change or a small reduction of D_a can be noticed between one and three years of exposure. The results for mortars PC-0.5 and PC-0.7 deviated from this observation. In the case of PC-0.5 one possible explanation can be the exposure arrangement (see Fig. 18), the submerging was done in open plastic boxes (baskets) immersed down to the seabed. At the end of the exposure times it was noted that some specimens were covered with mud. As the specimens were systematically arranged in the boxes the result for some mortar qualities as for PC-05 and L24-05 can have been affected by this condition. Further, when retrieving the specimen various degrees of marine fouling organisms were attached to the exposed surfaces. For PC-07 the deviating result can also be due to the large scatter in D_a that can be observed with increased w/c.

Also for the PLC-mortars (Fig. 32 upper right hand side) the expected relationship of an increasing D_a with increased w/c was observed. However, contrary to the PC-mortars, a quite clear tendency for D_a to increase with exposure time can be seen. The tendency of an increased D_a with time is more pronounced for the PLC-mortars with the higher w/c. The D_a is often assumed to decrease with exposure time [40], this is attributed to a reduction and refinement of the porosity with time. The improved characteristics of porosity with time are due to an increased degree of hydration. This would have been evident for lower w/c (≤ 0.45), that is common in marine structures and/or for binders incorporating pozzolanic material, which usually has a slower reaction rate and prolonged reaction time. As none of this is the case for the PLC-mortars, no significant changes of D_a would have been expected between one and three years of exposure, similar as for the PC-mortars.

One observation made, that can be related to the different development of D_a with time between PC- and PLC-mortars, is the progression of x_L (i.e. the depth to sound concrete) with time (lower left and right hand side in Fig. 32). It can be seen that despite a large scatter in some cases (PC-mortars with $w/c \geq 0.7$), there is generally a higher increase of x_L between one and three years of exposure for the PLC-mortars, compared to the PC-mortars. This means that the zone with increased porosity and consequently higher permeability due to leaching increases faster for the PLC-mortars. This is more pronounced for the higher w/c, which to some extent coincides with the results of D_a for the PLC-mortars (Fig. 32, upper right hand side).

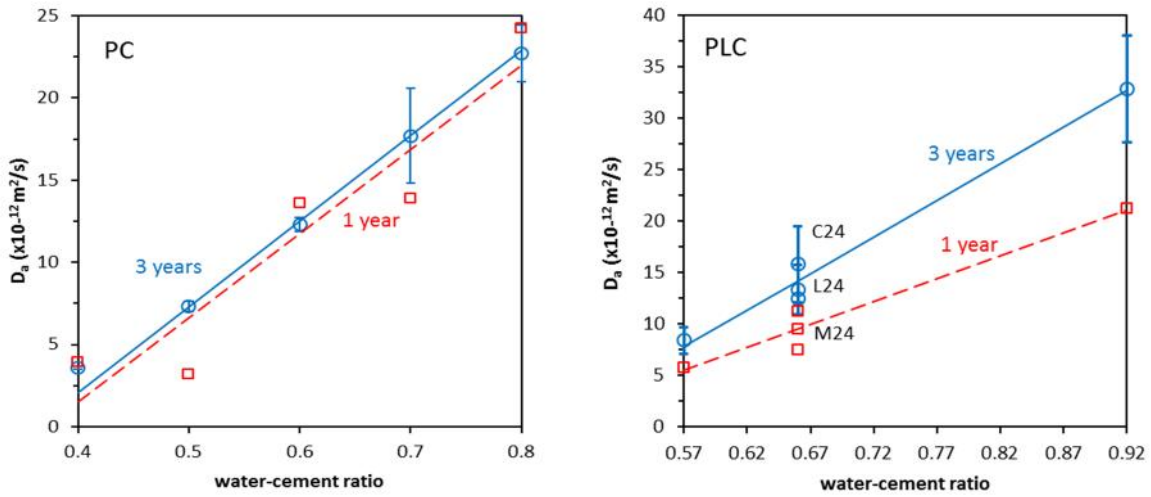

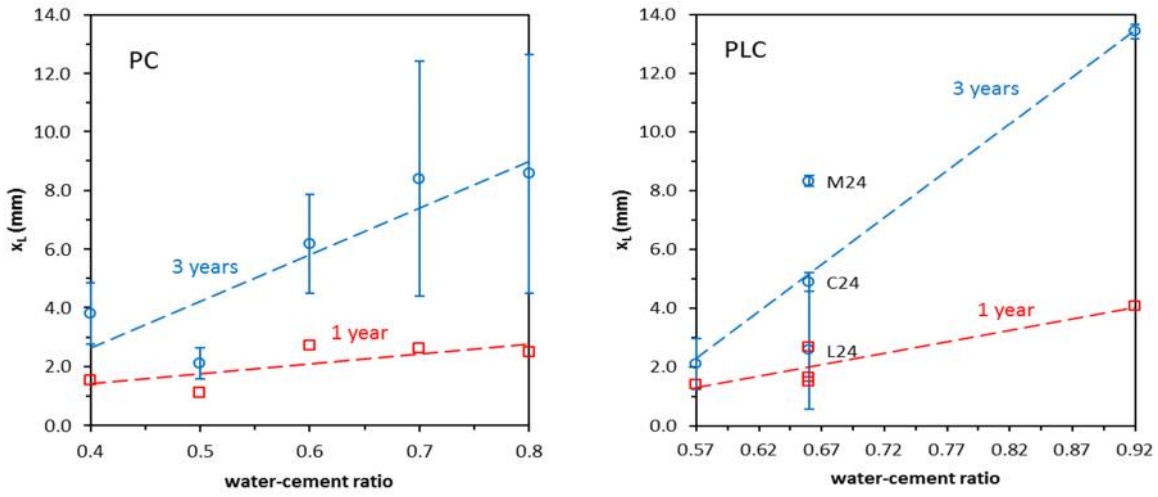

Figure 32. Apparent chloride diffusion coefficient (D_a) and the depth (x_L) where the calcium content is equal to the bulk content as a function of w/c for PC-mortars (left) and PLC-mortars (right), after one and three years of exposure.

As previously mentioned, mass transport of other species in and out of the submerged mortar specimens can affect porosity and the chloride ingress. In particular, sulphate attack on cementitious materials containing limestone filler has been discussed in the literature [98]. There are two possible factors for the sulphate ingress to have a more detrimental effect on the D_a for the PLC-mortars than for the PC-mortar. One is that cementitious materials containing limestone filler can under certain circumstances be more susceptible to sulphate attacks, in particular thaumasite sulphate attack [98]. This attack causes a gradual softening of the surface as well as a gradual inwards progression. In this work no specific investigation was carried for the identification of external sulphate attack. However, during the chloride profiling procedure no softening of the mortars or other visible sulphate attacks, such as cracks, were detected. The other factor is that an already lower chemical binding capacity of PLC-mortars can be further reduced, by the fact that sulphates can be stronger bound than chlorides by C_3A [45].

The second regression parameter, the apparent surface chloride concentration (C_{as}), obtained by the curve-fitting procedure is shown in Fig. 33 (left hand side for the PC-mortars and right hand side for the PLC-mortars). The C_{as} has been suggested to give an indication of the chloride binding capacity, but its value will also depend on the concentration of the exposure solution and on the porosity [131]. It must be kept in mind that C_{as} is an apparent value, often not the real chloride value at the exposed surface, but a value describing the boundary conditions at the exposed surface obtained from the regression analysis. However, often a higher C_{as} is a result of a steeper and shorter chloride profile shape (see, Fig. 8), which is attributed to a higher chloride binding capacity.

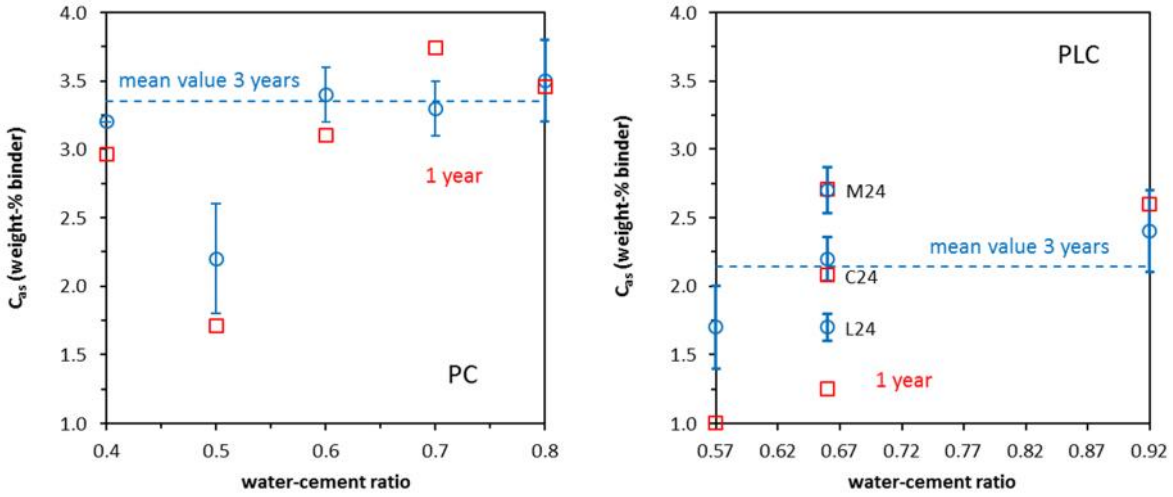

Figure 33. Apparent chloride surface content (C_{as}) as a function of w/c for PC-mortars (left) and PLC-mortars (right) at two different ages, expressed as weight of binder.

Figure 33 (left hand side) shows that for the PC-mortars the C_{as} appears to converge after three years of field exposure; one exception is mortar PC-05. For the rest of the mortars the mean value of C_{as} after three years is about 3.4% by weight of binder (dashed blue line). The deviating results for the PC-05 mortar may possibly be caused as previously mentioned by the exposure conditions. At the right hand side in Fig. 33, the C_{as} for the PLC-mortars shows to vary more irregularly compared to the PC-mortars. The mean value for all PLC-mortars is about 2.1% by weight of binder (dashed blue line) after three years.

The overall tendency for most of mortars is a slight increase of C_{as} with exposure time and that the values for PC-mortars are higher than for the PLC-mortars. This indicates that the PC-mortars have higher binding capacity than the PLC-mortars. If the C_{as} for the PLC-mortars is first recalculated to be expressed by weight of Portland cement then the mean value is 3.3 ± 0.3% by weight of Portland cement. This is almost the same value as for the PC-mortars. This implies that the limestone filler does not provide any chloride binding capacity.

Table 5 summarises the cementitious efficiency of limestone filler with respect to chloride ingress expressed as the coefficient of efficiency, the *k*-value. In the accelerated migration test, despite deviating *k*-values especially between the tests performed after 28 days (negative *k*-values) and one year, the actual measured migration coefficients for the PLC-mortars did not deviate markedly between the different test occasions (Fig. 29, right hand side). The apparent discrepancy of the *k*-values measured at 28 days is a result of a somewhat unexpected development of the migration coefficient for the PC-mortars with time (Fig. 29 left hand side).

Table 5. Calculated k-values for limestone filler with regard to chloride ingress.

	k-values for chloride ingress				
Method	Migration			Diffusion	
Age	28 days [123]	1 year (paper I)	2 years (not publ.)	1 year (paper I)	3 years (paper II)
L12-0.5	0.1	1.2	-	1.3	0.6
L24-0.5	-0.5	0	0	0.9	0.2
L24-0.7	-0.6	-	-	0.6	0
M24-0.5	-0.4	0.2	0.1	0.6	0.3
C24-05	-0.6	-0.2	-	0.4	0

From Table 5 it is difficult to draw any rigid conclusion about the cementitious efficiency of limestone filler with respect to chloride ingress. It can be observed that apart from the PLC-mortar with 12% replacement ratio, when comparing the 'one year *k*-values' from the migration test with the corresponding values from the natural diffusion test, it is quite clear that limestone filler seems to be less efficient when tested with the accelerated migration method. Possible reasons for this discrepancy are given in paper I, where it is shown that the ratio between the migration coefficient and the diffusion coefficient (D_m/D_a) for the PC-mortars is lower than for the PLC-mortars. This means that the measured cementitious efficiency depends on the test method. Further, an inconsistency between the *k*-values for chloride diffusion (D_a) measured after one and three years of field exposure can be observed in Table 5. The reason behind this decrease of the cementitious efficiency of the PLC-mortars is as previously mentioned the increasing tendency with time of D_a for the PLC-mortars as shown in the left hand side in Fig. 32.

Non-steady state and steady state diffusion (diffusion cell)

As can be concluded from the results in Table 5 the method of measuring the resistance to chloride ingress can have a major influence on the assessment of the effect of different binders. The two main parameters influencing the chloride ingress in cement-based materials, the porosity/pore structure and the chloride binding capacity were further investigated in paper III. An attempt to separate those two parameters was made in the effort to try to clarify how limestone filler influences chloride ingress. For this purpose the conventional diffusion cell test was used together with porosity and chloride binding measurements. The diffusion cell test was chosen because both the steady state diffusion coefficient (D_{ss}) and the non-steady-state diffusion coefficient (D_{nss}) can be measured in the same set-up. It is expected that D_{ss} does not take into account chloride binding because the binding capacity is exhausted when the steady state is reached. This means that D_{ss} is more a result of a material's microstructure, while for D_{nss} chloride binding is taking place, slowing down the chloride ion ingress. Theoretically D_{nss} is equal to D_a in the previous section, under the same exposure conditions. The results from the cell diffusion test are shown in Fig. 34(a) and (b), note that in Fig. 34(a) the D_{ss}/V_{paste} is plotted as a function of the *w*/*c*, where V_{paste} is the volume fraction of the cement paste. This was done to account for the different paste volumes of the mortars, the part of the mortars where the diffusion takes place. In principle mortars with the same mix proportions were used as in Table 3, with the same Portland cement and type L limestone filler.

In Fig. 34(a) for the PC mortars D_{ss}/V_{paste} is assumed to have a linear relationship with *w/c* in the studied interval; this assumption is supported in literature cited in paper III. It is clear from the results in Fig. 34(a) that the dilution effect of replacing Portland cement with limestone filler is not equivalent to a corresponding increment of the w/c. In Fig. 34(b) the effect of limestone filler replacement is somewhat different for the D_{nss} compared to D_{ss}. The D_{nss} for the PLC-mortars lies closer to the results of the corresponding PC mortars with the same w/c. This means that limestone filler shows a weaker cementitious effect on the D_{nss} compared to the D_{ss}.

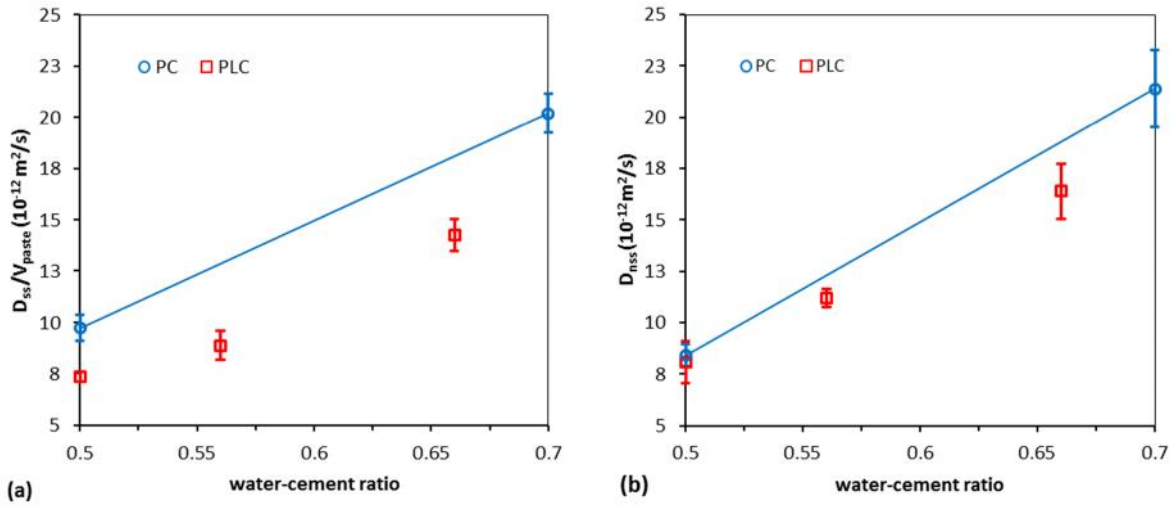

Figure 34. (a) D_{ss}/V_{paste} as a function of w/c. (b) D_{nss} as a function of w/c.

This somewhat different effect on chloride ingress by limestone filler when comparing D_{ss} with D_{nss} can be attributed to the different nature of the two measured chloride ion diffusion coefficients. As previous mentioned, D_{ss} reflects more a material's microstructure, while the D_{nss} also incorporates the chloride binding.

From the porosity measurements in paper III, it is clear that the replacement of Portland cement by limestone filler increases the porosity. So, the positive effect on D_{ss} by limestone must be due to some other microstructural improvement concerning chloride ingress. It has been suggested that despite a porosity increase due to limestone filler replacement, which is quite expected as limestone does not possess any hydraulic or pozzolanic ability, limestone contributes to an increase in the tortuosity of the pore structure, which can result in a lower permeability [93][95].

As have been discussed earlier, limestone filler can have a negative effect on the chloride binding, which can explain the differences in impact on the two chloride diffusion coefficients. Figure 35 shows the measured chloride binding isotherms. The results for C_b are recalculated and expressed as per gram Portland cement. In Fig. 35 two power functions (Freundlich isotherms, $C_b = \alpha c_f^{\beta}$) are also included, one representing the mean value of PC-05, PC-07 and L12-05, and the other representing the mean value of L19-04 and L24-05 (paper III).

The chloride binding data in Fig. 35 shows that a higher amount of limestone decreases the binding capacity; this gives some support to the results in Fig. 34. The positive effect of limestone on the microstructure and hence on D_{ss} is to some extent overshadowed by a lower binding capacity. The D_{nss} for the L24-07 would have been expected to be closer to the straight

line in Fig. 34(b); the results show, however, higher scatter for higher *w*/*c* which partly can explain this deviation.

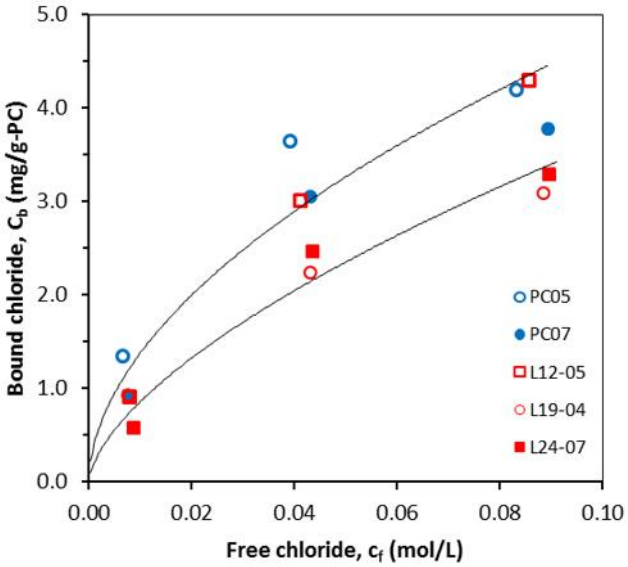

Figure 35. Chloride binding isotherms for the tested mortars (paper III).

Relationship between different chloride ingress coefficients

A discussion about some of the nonconformities between the results from different test methods for chloride ingress is given in this section.

Figure 36(a) shows the relationship of D_m obtained from the migration test on specimens that were wet-cured for a year (paper I) and the D_a from specimens that were wet-cured for 30 days and then submerged in the sea for three years (paper II). The results in Fig. 36(a) show that the D_m is higher for all tested mortars than the corresponding D_a. A potential regression curve for the PC-mortars with good correlation is also plotted in Fig. 36(a). It seems that the values for the PLC-mortars also fit this regression curve fairly well. Fig. 36(a) also shows that the interrelationship between D_m and D_a depends on the chloride ingress resistance, thus, the porosity. This is further clarified in Fig. 36(b) where D_m/D_a for the same set of data is plotted as a function of the water-cement ratio. In Fig. 36(b) it is obvious that D_m/D_a approaches 1 as the water-cement ratio increases. This means that as porosity increases, the D_a approaches the value of D_m.

An explanation to the result discussed above may be found in the nature of the test methods. For well-matured mortars, as in this case, the main part of chloride binding is attributed to physical binding. It is reasonable to believe that in the migration test where an applied voltage forces the ions to move forward, less chloride ions will be immobilised by electrostatic and/or van der Waals' forces associated with physical binding than in the case of natural diffusion. Consequently, D_m will be higher than D_a. The attraction of the physical binding forces is expected to decrease with the distance from the solid surface [126]. As *w*/*c* increases, so will also the pore sizes, which would lead to less interaction between chlorides and the pore walls. As the influence of physical binding on the chloride ion ingress is reduced with increased *w*/*c*, so will the difference between D_m and D_a.

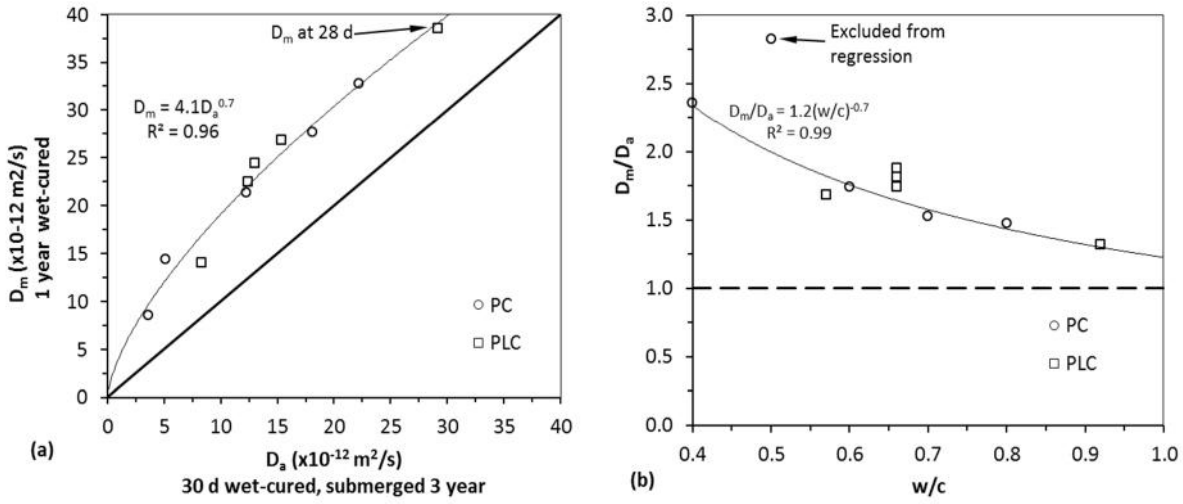

Figure 36. (a) Relationship between D_m (NT-Build 492 test after one year of wet-curing) and D_a (wet-cured 30 days and then submersion in the sea for three years. (b) The ratio of D_m and D_a plotted as a function water-cement ratio.

One other interesting observation is the relationship between the D_{nss} from the cell test (paper III) and D_a from the submerged specimens in the sea for three years (paper II). In this case both D_{nss} and D_a are non-steady state diffusion coefficients, so theoretically they are supposed to be equal under the same exposure conditions. However, except for the temperature variation at the field site, in the cell test, a sodium chloride solution with 18 g/L chlorides was used, while D_a was measured for specimens exposed to seawater (interaction with other ions), where the average chloride content was 14 g/L. . Though, a linear relationship can be observed in Fig. 37, the results from the laboratory tests are higher than the ones from the field exposure. However, it is well known that diffusivity increases with temperature [113][132] and the explanation for the difference between field and laboratory tests can be the effect of temperature. The annual average in the sea water (+11°C) at the field exposure site (southwest coast of Sweden) is much lower than the temperature of the exposure solution (+20°C) in the laboratory. Page et al. [113] measured in diffusion cell test the D_{ss} in temperatures ranging from 7 to 47°C for cement paste specimens, from their results the calculated mean ratio between D_{ss} at the temperatures +20 and +11°C is 1.6 ± 0.1. The mean value of $D_{nss(+20°C)}/D_{a(+11°C)}$ for the mortars in Fig. 37 is 1.4 ± 0.2.

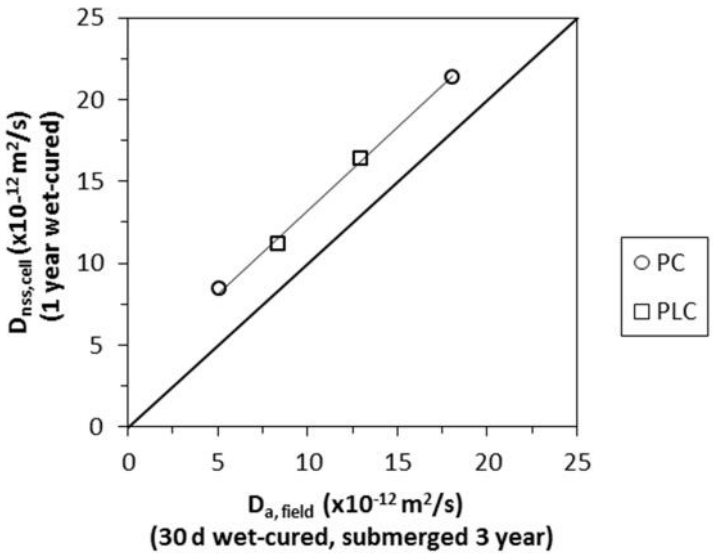

Figure 37. Relationship between the $D_{nss,\,cell}$ from cell diffusion test and D_a from submersion in the sea for three years.

4.2 Chloride threshold values

This chapter discuss the main results in the part of the project dealing with the development of a practice-related approach for determine chloride threshold values, based mainly on papers IV-VII. Further, the results from a field study reported in paper VIII are discussed. The approach to try to measure the chloride threshold values includes specimen shape, preconditioning, corrosion monitoring, and concepts to determine the chloride ion content at various times. The starting point for this approach is based on the work done by Nygaard and Geiker [120], with regard to specimen shape and the approach of introducing chloride ions. In short the shape of the specimens was chosen to prevent crevice corrosion and the precondition procedure to accelerate chloride penetration through capillary suction and diffusion.

4.2.1 Corrosion monitoring methods for assessment of corrosion initiation time

To measure the chloride threshold value (CTV) the time of onset of corrosion (t_{corr}) and the chloride content at the steel depth at this time must be identified. The starting point was to decide the most suitable corrosion monitoring method. Initially (paper IV) three electrochemical parameters were measured manually; corrosion rate, corrosion potential and macro-cell corrosion. Later (paper V and paper VI), corrosion potential and polarising current under a potentiostatically controlled condition were monitored with a data logger. The initiation of corrosion (the transition from passive to active corrosion) is accompanied by a sudden change in the electrochemical parameters, in particular, a decrease of the corrosion potential an increase of the corrosion rate of steel and an increase of the macro-cell current. The relationship between corrosion initiation and the sudden change in the electrochemical parameters is not clear-cut, which in turn can affect accuracy of the CTV. The choice of what “sudden change” identifies corrosion initiation is often based on experience, and introduces an element of subjectivity in the determination of CTVs [133].

When steel is in the passive state the corrosion rate is usually lower than 0.05-0.1 μA/cm^2 (~0.5-1.0 μm/year), while the active corrosion state is characterized by an average sustained corrosion rate > 0.1 μA/cm^2 (i.e. about > 1 μm/year) [61]. The values of the corrosion rate measurements (I_{corr}) in this study must primarily be seen as an indication of corrosion initiation and further as a relative value of the rate of degradation of the steel bars, and not as the actually loss of steel bars cross section. This is because as mentioned in section 3.3.2 the recalculation from corrosion current density (μA/cm^2) to I_{corr} (μm/year) assumes uniform corrosion. Chloride initiated corrosion will cause localized corrosion (pitting), in the case of reinforced concrete structures and a ratio varying from 3 to 10 between uniform corrosion and maximum pit depth has been found [134]. Other sources of error can be the confinement of the polarised steel surface and the assumption of B = 26 mV in Eq. (30). Despite these shortcomings, the interpretation of the data was quite clear as mostly changes over time were observed, rather than the absolute values (paper IV and paper V).

Figure 38(a) shows some typical results from the corrosion rate measurements (paper IV). As can be seen in some cases and also reported elsewhere (e.g. reference [135]) corrosion rate measurements show fluctuations from one measuring occasion to another. This can make it difficult to clearly detect the corrosion initiation time and hence determine the chloride threshold value.

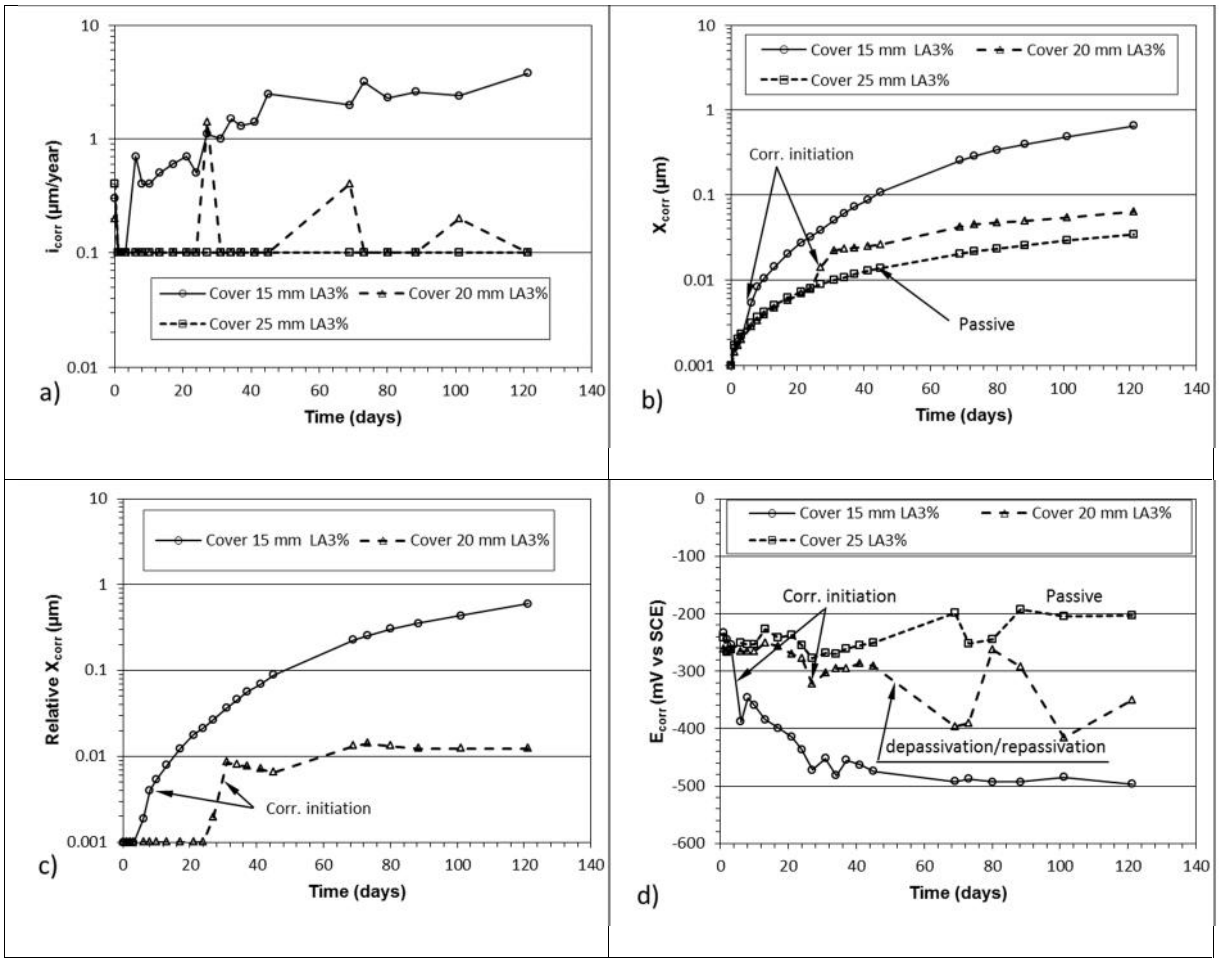

Figure 38(a) Corrosion rates (I_{corr}) vs. time. (b) Corrosion depth (X_{corr}, integral of corrosion rate with time) vs. time. (c) Relative corrosion depth vs. time. (d) Corrosion potential (E_{corr}) vs. time.

To try to improve the interpretation of the corrosion rate data it was suggested in paper IV to integrate the corrosion rate with time to gain an artificial "corrosion depth" (see Fig. 38(b)). This is done when comparisons are made with gravimetric loss test [61]. Further, this "corrosion depth" should be reduced by the "corrosion depth" from a passive steel bar, in this case the bar with a concrete cover of 25 mm (see Fig. 38(c)). In Fig. 38(d) the corresponding corrosion potential (E_{corr}) measurements are shown, which confirms quite well with the I_{corr} measurements in Fig. 38(a).

With regard to potential monitoring no exact potential change (drop) is generally established to characterize corrosion initiation. However, it have been reported from potential mapping in field structures that a change of 150-200 mV shows a change in the corrosion condition of bars, moving from passive to more active areas where the values are more negative [61]. This can be interpreted as that a sharp decrease of the corrosion potential (E_{corr}) with about 200 mV can be an indicator of depassivation. Previously it was often referred to the fixed value of ≤ -350 mV vs CSE (copper-copper sulphate electrode, approx. -280 mV vs SCE) recommended in ASTM C876-91 as value that indicates high corrosion risk. This fixed boundary limit of potential to distinguish between active and passive state has been proven to be misleading, because the absolute value of the corrosion potential can be affected by various parameters [136]. As mentioned above, Fig. 38(d) shows the development of E_{corr} that corresponds quite well to the I_{corr} measurements, a sudden increase of I_{corr} is accompanied with a sudden drop of E_{corr}. One important issue that Fig. 38 clearly shows is the difficulty that sometimes occurs in defining t_{corr}. For the bar with a cover depth of 15 mm the t_{corr} is quite clear, while for the bar with 20 mm cover depth the passivation/repassivation processes makes the determination of the t_{corr} more difficult. If the definition showed in Fig. 38(c) is adopted (as was the case in paper IV) then the t_{corr} is quite clear after about 30 days. However, this implies that the CTV is defined as the chloride content at the very first sign of depassivation. This will always yield a lower CTV compared with other common definitions, such as the chloride content associated with stable pit growth (no repassivation) or visible corrosion.

Figure 39 shows measured E_{corr} on the left hand side and polarising current under a potentiostatically controlled condition (I_{pc}) on the right hand side (papers V and VI). Once again the difficulty of determining the time to corrosion initiation is highlighted. The I_{pc} measurements gives a clear t_{corr}, but natural phenomena like repassivation as noted in the E_{corr} measurement would not be apparent. Once corrosion has been initiated the current will continue to increase until the bar in the specimen is disconnected. In the literature [62][63] it is generally reported lower CTVs when monitoring I_{pc} rather than E_{corr}, but this was not the case in this study. It must be pointed out that in this study the CTVs when monitoring E_{corr} were determined at the first sign of depassivation and repassivasion was not considered. This can be one of the reasons that the CTVs are equivalent for both monitoring methods. The other reason can be the applied potential (in this study set at 0 mV vs. SCE), which has been found to influence the CTVs [137].

The E_{corr} measurements in Fig. 39 reveal that for bars 1 and 2 the determination of t_{corr} is quite clear. However, for bar 3 it is more questionable when t_{corr} occurs, as repassivation occurs after an initial drop about 200 mV and continuously (> 10 days) very negative E_{corr}. After he E_{corr} goes back to the initial passive potential, it drops and rise again, this means that no stable pit growth has been established two months after the first sign of depassivation. However, Fig. 40 shows bar 3 and the steel concrete interface after removing the bar, where clear signs of corrosion initiation can be observed. So, the question is how long the corrosion shall proceed before t_{corr} can be established.

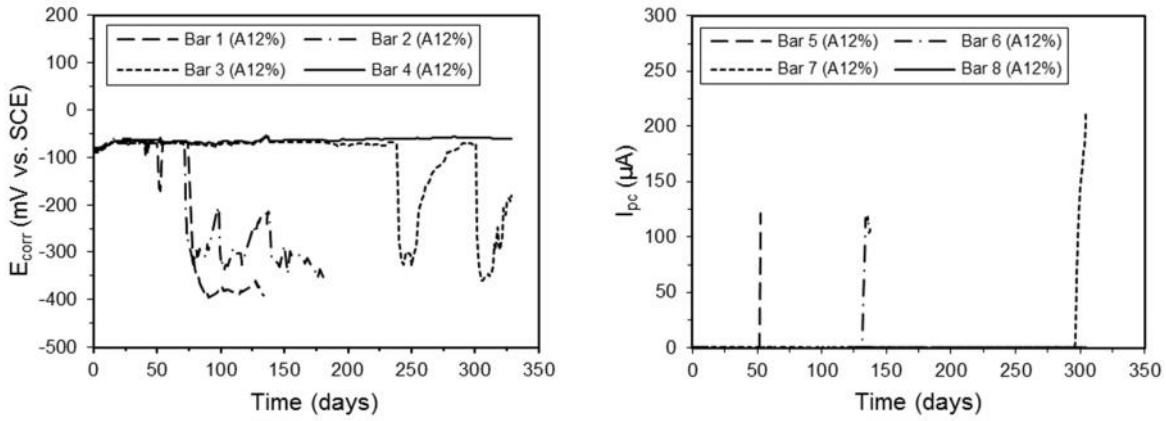

Figure 39. Corrosion potential (E_{corr}) and polarising current under a potentiostatic controlled condition (I_{pc}) vs. time (Paper V).

Figure 40. Picture showing corrosion locations at the steel/concrete interface after removing bar 3-A12% (Fig. 37).

In paper IV the macro-cell current was also monitored for assessment of corrosion initiation time. Figure 41(a) shows the results for the reference concrete (Ref) and Fig. 41(b) shows the results for the low alkali concrete (LA). Both concretes were exposed to 3% by weight sodium chloride solution. In Fig 41 the left vertical axis show the macro-cell current flowing between bars with 15 mm and 20 mm cover (see, Fig. 21) when connected. The right vertical axis in Fig. 41 shows the corrosion rate (I_{corr}) measured with the galvanostatic pulse method for the bars with 15 mm cover.

Figure 40 shows the macro-cell current flowing between bars with 15 mm and 20 mm cover (see, Fig. 21) when connectedand the corrosion rate (I_{corr}) measured with the galvanostatic pulse method for the bars with 15 mm cover.

The macro-cell measurements for the bars in the LA concrete after 45 day of exposure are not plotted because the bar with 20 mm cover depth also started to corrode at that time. Two main features can be observed when comparing Fig. 41(a) and (b). The first is the more than five times higher macro-cell current was measured for the bars in the Ref. concrete, and the second is the steeper gradient of I_{corr} with time for the bars in the Ref. concrete. This difference can be attributed to the large difference in resistivity, which for the LA concrete was one order of magnitude larger. The exact influence of concrete resistivity on the corrosion process is not well known but a clear tendency exists where an increasing concrete resistivity leads to decreasing corrosion rate [138]. Because macro-cell current can be very small and easy to

overlook for high resistivity concretes, care must be taken using this current as an indicator for corrosion initiation.

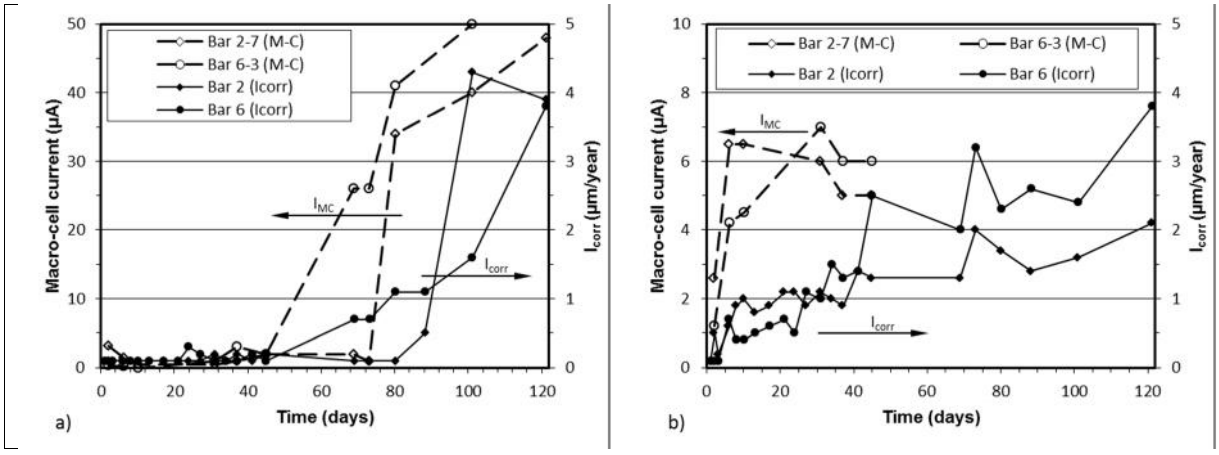

Figure 41. The corrosion rate (I_{corr}) measured with the galvanostatic puls method for the bars with 15 mm cover and the macro-cell current flowing between bars with 15 and 20 mm cover when connected. (a) bars in Ref and (b) bars in LA.

From destructive visual examinations it can be concluded that all corrosion monitoring methods gave reliable results in identifying corrosion initiation, though the destructive visual examinations were mostly performed some time after the indication of corrosion initiation. For the bars that did not show any signs of corrosion initiation in the electrochemical measurements no corrosion evidence was observed in the visual examinations.

4.2.2 Determination of chloride threshold values

As mentioned in section 3.3.4, the chloride content in the determination of CTVs was measured by chloride profiling at different occasions and using a simple model of chloride diffusion. This was done because this entails certain practical advantages compared with the determination of the chloride content at a thin layer at the depth of the steel bars. Because realistic concrete mixes (low *w*/*b*) are desirable for testing, the concrete cover depth has to be compromised. This causes a more difficult precision in sawing to the proper depth and complicates the sampling of concrete at the depth of the steel bar, as experienced in paper IV.

Further, it is well known that studies of corrosion initiation time always give a wide scatter, even for constant test parameters. For example, if ten bars are tested in the same series it is possible to get ten different t_{corr} occasions with a span of several months. To skip laborious sampling at ten different occasions, three different chloride profiles can be determined. Chloride profiles can be determined when the first and the last bars show corrosion initiation and one at a time in between. Another situation when it is advantageous to use chloride profiles are if multi-bars in a concrete specimen are used as in paper IV, paper V and paper VI, as frequent destructive sampling of individual corroding bars may interrupt the test of the remaining passive bars. Also, in the case where the determination of t_{corr} can be difficult as shown in Fig. 39 (Bar 3, left hand side) it is good to have the possibility to model the chloride content at different times.

Before a brief summary of CTVs determined in this work a correction must be made. In Fig. 5 in paper IV the plotted chloride profiles for Ref. 1 after 121 days of exposure are erroneous. In

Fig. 42 the correct profiles are plotted. The correct CTV for this concrete is given in Table 5 together with the rest of the determined CTVs. A correction must also be made in Table 1 in paper IV showing the concrete mix propositions, the limestone filler amount should be 369 kg/m^3 for the LA concrete.

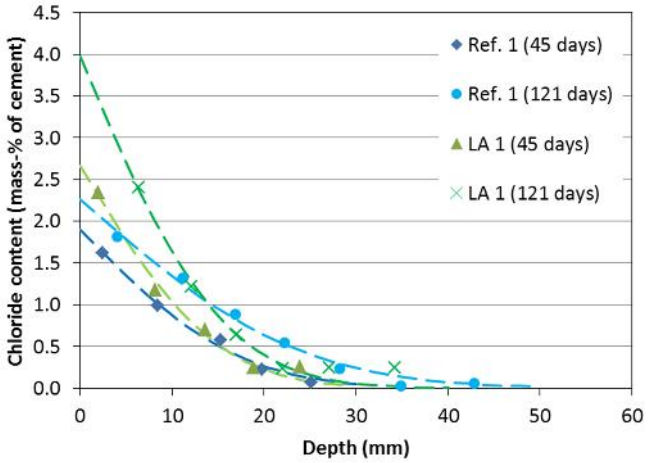

Figure 42. Chloride profiles for the different concrete qualities exposed to 3% NaCl solution, measured at two different occasions.

Because during the course of this work it was discovered that the steel bar surface condition played a very important role for the susceptibility to corrosion initiation, different surface conditions were investigated, those were:

I. Smooth bars "as-received" with the mill-scale visually intact.
II. Smooth bars delivered protected direct from the plant (paper V).
III. Smooth bars "as-received" with thin continuous rust layer (paper V).
IV. Smooth bars as in (II) and acid-pickled (paper V).
V. Ribbed bars "as-received" with the mill-scale visually intact (paper VIII).
VI. Ribbed bars acid-pickled and pre-rusted (paper VII).
VII. Ribbed bars "as-received" with the mill-scale and surface corrosion (paper VII).

The term "as-received" aims to the mode of delivery (for example, as received from the local steel supplier) and not to any specific surface condition. The surface condition of the "as received" steel bars could vary a lot as will be discussed in the text and can be seen in Fig. 42.

Table 6 summarises all the determined chloride threshold values and the investigated parameters. In the next section the influence of each of the investigated parameters will be discussed in detail. Because the corrosion conditions were not continually monitored during exposure in the field study (paper VIII), it is unknown when corrosion was actually initiated. Therefore, it is not possible to estimate the exact CTVs defined as in the laboratory tests. However, the CTVs were roughly estimated from analysis of chloride profiles and corrosion conditions after 10 years [139] 13 years [140] and 20 years [121]. The methodology is explained in more detail in paper VIII.

Table 6.Chloride threshold values and investigated parameters.

	Binder (w/b)	Steel surface	Cover [mm]	Pre-drying (weeks)	Conc. NaCl mass-%	Method	t_{corr}[4] [days]	CTV [mass-% cem]
Paper IV[1]	CEM I (0.46)	I	10-15	T = 20 °C RH = 50% (2)	3 %	X_{corr}/E_{corr}	13	0.7 ± 0.1
	60%CEM I +40%SF (0.81)	I	10-20		3 %	X_{corr}/E_{corr}	2	0.4 ± 0.2
Paper V[2]	CEM I (0.5)	II	10-20	T = 20 °C RH = 50% (2)	6 %	E_{corr}	77	1.3 ± 0.2
			15-20			I_{pc}	-	1.2 ± 0.1
		III	10-15			I_{corr}/E_{corr}	187	1.7 ± 0.4
		IV	10				-	> 2.0
Paper VI	CEM I (0.5)	II	10-20	T = 20 °C RH = 50% (2)	12 %	E_{corr}	77	1.2 ± 0.4
			10-20			I_{pc}	52	1.3 ± 0.1
	CEM II/A-LL (0.5)	II	10-15		6 %	E_{corr}	77	1.4 ± 0.1
			10-20			I_{pc}	71	1.3 ± 0.2
			10-20		12 %	E_{corr}	57	1.8 ± 0.3
			10-15			I_{pc}	60	1.9 ± 0.5
Paper VII	CEM I (0.45)	VII	9-14	T = 20 °C RH = 25% (5)	6.6 %	E_{corr}	36	0.9 ± 0.2
Paper VIII	Several	V	10-35	-	Sea water	I_{corr}/E_{corr}	-	~1[3]
Appendix I	CEM I (0.45)	VI	10	T = 20 °C RH = 45% (7)	3.3 %	E_{corr}/ I_{pc}	-	> 2.0

[1] Missing result for Ref. 2 and LA 2 due to failure in chloride analysis
[2] None of the chemical cleaned (acid-pickled) bars started to corrode
[3]Chloride content at the cover depth to cause a corrosion rate > 10 μm/yr
[4]The time to corrosion initiation.

4.2.3 Investigating parameters influencing chloride threshold values

Surface condition of steel bars

Among the three different surface conditions investigated in paper V, the bars with chemically cleaned surface gave the lowest susceptibility to corrosion initiation and mill-scaled bars gave the highest susceptibility to corrosion initiation (i.e. lowest CTVs), whilst the bars with the as-received rusty surface had a corrosion initiation susceptibility between the above two conditions. It was concluded in paper V that the steel surface condition has a strong effect on the corrosion initiation of reinforcement in concrete, and can likely be one of the most decisive parameters attributing to the variability in the reported chloride threshold values obtained in laboratory experiments. Further, support for this conclusion can be found from the result in Appendix 1 (RILEM TC 235-CTC, Report of Round-Robin Test), where rebars with pre-treated surface did not show corrosion initiation after more than 21 months of exposure and a chloride content up to 2% by mass of cement.

As previously mentioned the half-cell reactions in corrosion are accompanied by the passage of an electric current. For this to happen a potential difference must exist between one part of the structure and another. A large number of factors can give rise to variations in potential on a structure. These variations may be due to differences either on the metal or on the electrolyte (concrete). Even if a metal surface appears to be perfect there will always exist imperfections

(heterogeneities) on it; such heterogeneities may vary in size from the atomic scale to the macroscopic scale [51]. At the macro-scale, typical heterogeneities on the metal surface are the mill-scale that originates from the manufacturing process and atmospheric surface corrosion often occurring during transport and storage. In what is called “as-received” condition both of these heterogeneities can more or less be present (see Fig. 43).

Figure 43. Photo of surface condition for an “as-received” steel bar.

The mill-scale is formed on the outer surface of the steel bars and is composed of iron oxides mostly ferric, and is bluish black in colour. As long as no breaks occur in it the mill-scale provides protection against corrosion. However, the handling of the steel bars brings breaks in the mill-scale continuity. Ghods et al [141] investigated mill-scale properties of steel bars and showed that even apparently uniform layer of mill-scales contained localized cracks, crevices and voids (see Fig. 44). These imperfections in the mill-scale were shown to provide sites for pitting corrosion on the underlying steel. The mill-scale is cathodic to steel (i.e. has a more noble potential) and this difference in potential promotes corrosion where disruptions occurs in this coating. In neutral solutions this difference of potential between bare steel and mill-scale can amount to 200-300 mV, this couple is almost as powerful generator of corrosion current as the copper-steel couple [142]. The formation and maintenance of a passive film requires an outward transport of cations (Fe^{2+}) and its combination with O^{2-} and OH^{-} ions at the film/solution interface. In this case the mill-scale can work as a barrier, prohibiting the O^{2-} and OH^{-} ions from reaching the Fe^{2+}, and hence weakening or hindering the formation of the passive film. Evidence for this has been reported by Mahallati and Saremi [143]. The increased corrosion susceptibility from this “barrier effect” will be pronounced at breaks in the mill-scale, where neither the mill-scale nor a proper passive film will be present (see Fig. 44).

So, the increased susceptibility to corrosion initiation for reinforcing steel bars covered with mill-scale can be twofold, it increases the driving force (potential difference) for corrosion and likely weakening the prohibiting effect of the passive film.

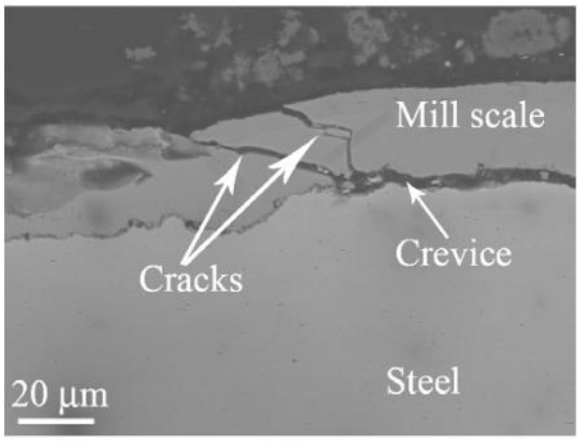

Figure 44. SEM cross-section image of as-received steel bar surface with mill-scale [141].

If the original surface of the steel is covered with a rust-scale, this will reduce the physical contact between the alkaline environment and the steel surface which can decrease the passivation efficiency, in the same way as the above mentioned "barrier effect". However, the formation of a rust-scale can also level out differences in potential on the steel surface by "peeling of" the mill-scale, which can lead to a reduced susceptibility to corrosion initiation. Further, in the same manner as physical contact between the alkaline environment and the steel surface can be shielded, the corrosion process can also be hindered: the cathodic reaction may be affected by a low diffusion rate of oxygen, whereas the anodic reaction may be retarded by limiting the supply of water and chloride ions. This is the same as the principle behind the so-called "weathering" steel [144]. For the positive effects of the rust-scale to be benefited the rust-layer must be continuous and stable with time (compare the results in paper VII and Appendix 1).

The implication is that if the aim of a test method is to determine CTVs that will be representative for service-life design then surface modifications such as pickling, polishing and so on must be avoided, or thoroughly considered. However, if the aim of a test method is to distinguish between for example the suitability of different binders concerning corrosion, than surface modifications can be an alternative for repeatability and reproducibility purposes.

Exposure conditions

The prerequisites of the test set-up are that the test conditions should be reasonably comparable with those in service and the test method should be reproducible and as rapid as possible concerning the slow diffusion nature of the investigated phenomenon. The method to accelerate corrosion by adding chlorides direct into the mix ("admixed chlorides") was not an option due to the fact that it has no time for steel to become passive, which means that the initial formation of passive layer becomes questionable [145]. Admixed chlorides can also lead to extraneous effects on the concrete itself. The way to accelerate the testing was to introduce chlorides in the concrete by a combination of capillary suction (accomplished by drying before exposure) and diffusion. Further, elevated NaCl concentrations and reduced concrete covers compared with structures in service were also used (see Table 6). Moreover, in an attempt to provide corrosion initiation within a reasonable time the concrete specimen were not fully immersed, this gives a constant source of chlorides and simultaneously allowing access of oxygen. All the laboratory tests were performed in a controlled temperature of 20°C.

As expected, when chlorides are introduced from an external source into concrete the most decisive parameter determining the time to corrosion initiation was the thickness of concrete cover. However, the cover thickness did not show to be a consistent influencing factor of CTV. It should be mentioned that the CTVs have been estimated on specimens with shallow concrete cover, whilst in the reality the cover thickness of infrastructural concrete is normally larger than 45 mm. Some theoretical considerations of the effect of cover thickness on the chloride threshold value were made by Fagerlund [146], who proposed a hypothesis that the chloride threshold value exponentially increases with the cover thickness and there is a critical cover thickness beyond which corrosion is impossible. However, this hypothesis has not been verified.

An increased concentration of the salt solution from 6 to 12% by mass did not shorten the initiation time significantly as can be seen in Table 6. Apart from the surface condition of steel bars it is the pre-drying that shows significant influence on the corrosion initiation time.

In Table 6 the results from Paper IV deviates somehow with regard to the influence of the pre-drying and the concentration of the exposure solution on corrosion initiation time. Further, also in the same study the lowest CTVs were determined. The special case where the binder consisted of 60% CEM I and 40% silica fume will be discussed in the subsequent paragraph. However, also the concrete with 100% CEM I showed comparatively short corrosion initiation time. This can be due to the fact that this concrete contained a large amount of fine aggregates (0-8 mm) which made the mixture stiff, as indicated by the slump value (30 mm) indicates, and hard to compact. This resulted in a large amount of entrapped air which was very evident on cut surfaces of the concrete and on steel concrete interface at the visual examination. Another indication of pore compaction is the compressive strength at 28 days which was 54.5 MPa for this concrete with *w*/*c* 0.46 compared to 58 MPa for the concrete in paper V and VI with *w*/*c* 0.5. Defects on the steel concrete interface such as entrapped air bubbles are recognized to have a detrimental effect on the CTVs [66]. Further, owing to the thin concrete cover, entrapped air bubbles will significantly reduce the chloride ion path, increasing quickly the chloride ion concentration and developing differential concentration cells, which increases the susceptibility to corrosion.

Binders

In this work four different binders were used in the laboratory tests (Table 7), and about seven different binders were available to investigate from the field site (paper VIII). Generally three important parameters are identified affecting corrosion initiation depending on the binder type; those are: chloride binding, the pH of the pore solution and the electrical resistivity of the concrete [62].

The chloride binding controls the amount of chloride available in the pore solution (free chlorides). Two main mechanisms are general accepted to be responsible, physical adsorption to C-S-H surfaces and chemical reaction mainly with the C_3A [45]. The physical adsorption depends on the amount of C-S-H, which in turn is dependent on the amount of cement. Further, for binders with reactive mineral admixtures more C-S-H can be formed due to the pozzolanic reaction. The amount of C_3A is determined by the type of binder used, sulphate resistant cement (SRC), such as Anl. in Table 7, will have a lower chloride binding, due to lower amount of C_3A. This will result in higher available free chloride in the pore solution. A hypothesis exist that only free chlorides participate in the corrosion process, implying a lower CTV for SRC compared with a binder with higher binding capacity. As Table 7 shows, this could not be

confirmed in this work, because the steel surface condition seems to overshadow any such effect. Moreover, the hypothesis that only the free chlorides present a corrosion risk has been questioned [68].

The pH of the pore solution affects the formation of the passive layer on the steel bars in such a way that a higher pH leads to a greater inhibiting effect to chloride-induced corrosion. The pH in the pore solution depends mainly on the alkali content of the cement [3]. Cements with greater Na_2O-eq (content of alkalis, Na^+ and K^+) than 0.6% are regarded as high alkali cements. Table 7 shows a rough estimation of pH with respect to Na_2O-eq. of the cements from data reported in [147], and the actually measured pH for the silica blended binder [148]. Some support can be found in Table 7 for the beneficial effect of a higher pH on the CTV, when comparing the silica blended binder (60% Anl.+40% SF) with the rest of the binders. However, no clear distinction can be made on the CTV between the rest of the binders with respect to the pH, it must be kept in mind the pH in this case was a rough estimation. A comparison is also difficult due to the different steel surface conditions.

Table 7. Properties of binders (according to suppliers) used in the laboratory tests and CTVs.

Binder type	C_3A (%)	Na_2O-eq. (%)	pH of pore solution	Steel surface I/II/III/IV/V/VII
100% Anl.[1]	2	0.6	13.5-13.8[5]	0.7/1.3/1.7/>2.0/-/0.9
60% Anl.[1] + 40% SF[2]			11.2 [148]	0.4 (I)
100% Bygg.[3]	6	0.9	≥13.8[5]	1.3-1.9 (II)
100% FB[4]	7	1.0	≥13.8[5]	> 2.0 (VI)

[1]CEM I 42.5 N/SR/LA (CEMENTA, Sweden)
[2]Silica fume (ELKEM, Norway)
[3]CEM II 42.5 R/A-LL (CEMENTA, Sweden)
[4]CEM I 42.5 R (AKMENÉS CEMENTAS, Lithuania)
[5]Estimation of pH with respect to Na_2O-eq. from data reported in [147]

The electrical resistivity determines the ion mobility in the pores and hence the corrosion rate [59]. The degree of saturation of the pores is identified to be the most influencing factor for concrete resistivity, also temperature is considered to be important. In the following discussion – when comparing the influence of binders on CTV – these environmental factors will not be considered as only concretes with equivalent exposure conditions will be compared. The choice of binder (for concretes with the same *w*/*b*) can influence the electrical resistivity in concrete by modifying the microstructure properties and the pore solution characteristics [138].

A direct theoretical link between CTV and concrete resistivity has not been found. From a phenomenological point of view the following has been suggested by Polder [149]. Keeping in mind Fig. 12, which illustrates the propagation stage of pitting corrosion, the following sequence of events are possible. After breakdown of the passive film a minimum concentration of chloride ions in the pore solution is necessary to get the process running in the beginning. Both the availability of chloride ions and the ion mobility (depending on the resistivity) will be important parameters to sustain a corrosion pit in this initial stage and to develop a high corrosion rate so that repassivation is no longer possible. This means that a higher resistivity can suppress the corrosion rate despite having the same availability of chlorides, thus

postponing or completely preventing the development of stable pits. However, it was concluded that this hypothesis needs further confirmation.

As previous mentioned in connection with the laboratory tests (paper IV) the concrete resistivity was shown to be one order of magnitude higher for the concrete with the silica fume blended binder (60% Anl. +40% SF) compared to the reference concrete with only CEM I (100% Anl.) as binder. The effect of the resistivity on the corrosion rate is showed in Fig. 41, where a higher acceleration of the corrosion rate of the bars embedded in the reference concrete can be observed. However, the corrosion initiation occurs earlier and the CTV is lower for the concrete with silica fume. This is likely due to the lower pH of the pore solution (Table 7) and to initially faster chloride ingress (Fig. 42). Though, if the definition of corrosion initiation is set as a certain corrosion rate limit (from a practical engineering point of view > 2 µm/year [134]), then the CTVs would have been in the same range, as it takes longer for the concrete with silica fume to reach this corrosion rate.

Because the corrosion conditions were not continuously monitored during the field exposure (paper VIII), it was not possible to determine the CTVs in the same way as in the laboratory tests. So, the definition of active corrosion was set as a corrosion rate > 10 µm/year, based on non-destructive corrosion rate measurements and on destructive visual examinations, and the CTV was defined as the chloride content required to maintain active corrosion. This made it possible to roughly estimate the CTVs from evaluation of the corrosion conditions after a certain time and the chloride contents at the cover depth at that time. With this definition of corrosion initiation it was concluded reasonable to assume a CTV of about 1% by weight of binder for marine concrete structures in an environment similar of that in the south west coast of Sweden. This threshold value of 1% by weight of binder was valid for various unitary and binary binders including ordinary Portland cement, sulphate resistance Portland with 5% silica fume, and also with different water-binder ratios in a range of 0.3 to 0.5. However, for the ternary binder, blended with 5% silica fume and 10% fly ash with water binder ratio 0.35, the CTV can be as high as 2% by weight of binder content, with the same definition of the CTV.

4.2.3 Expression of chloride threshold values

It must be pointed out that when the water-binder ratio (w/b) is calculated for concretes including certain mineral additions blended with Portland cement, different efficiency factors (k-values) are used; for silica fume (SF) the k-value can be 1 or 2 and for fly ash (FA) 0.2 or 0.4 according to EN-206-1.

In paper VIII, $k = 1$ for SF and $k = 0.3$ for FA was used for calculating the w/b, these k-values were chosen to be consistent with previously reported work from the field site. However, when the chloride content was expressed as total chloride relative to the weight of binder, the k-value concept was not adopted. Figure 45 shows a chloride profile for a concrete with a binder consisting of 85% Portland cement, 10% FA and 5% SF (mix 12-35 in paper VIII). The chloride content is expressed in two ways; alternative 1, without taken into consideration the k-value concept and alternative 2, adopting the k-value concept ($k = 1$ for SF and $k = 0.3$ for FA). Alternative 2 means a reduction of the binder by 7%, which in turn means a corresponding increase of the chloride content with 7%, when expressed as per cent by weight of the effective binder.

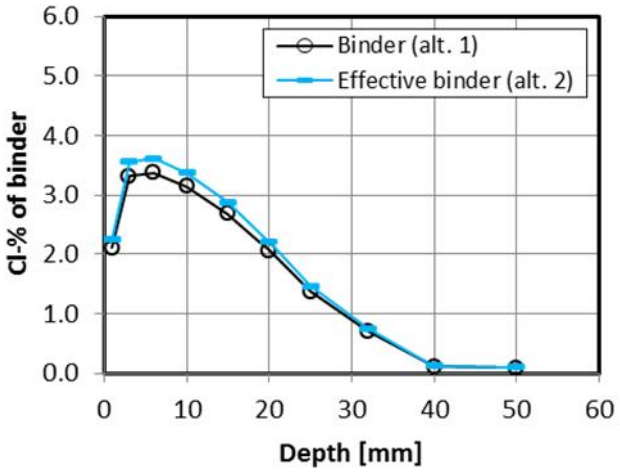

Figure 45. Chloride as weight per-cent of binder, alt. 1, without taken in consideration the k-value concept and alt. 2, adopting the k-value concept.

5 CONCLUSIONS

The aim was to study the effect on chloride induced reinforcement corrosion when a certain amount of cement is replaced by limestone filler. The first part of the work is concentrated on the efficiency of limestone filler as part replacement of cement in the binder concerning chloride ingress. The concept of equivalent water-cement ratio was adopted introducing the *k*-value as a parameter to evaluate the efficiency of limestone filler. In this part the compressive strength was also measured for all mortar mixes, mostly as an indicator for the overall quality and also as a measure of microstructure development. In the second part of the work the idea was initially to determine the chloride threshold values for the mixtures investigated in the first part. However, during the work the need for the development of a practice-related method for determining the chloride threshold values was identified and the focus of the research was somewhat redirected.

Chloride transport

The efficiency of limestone filler as replacement for cement in mortars with respect to compressive strength was shown to depend on the replacement ratio. Independent of testing age when 12% of the binder consisted of limestone filler the *k*-value was 0.9 ± 0.1. The corresponding *k*-value for the binder with a replacement rate of 24% by limestone filler was found to be 0.3 ± 0.1; the influence of different water-binder ratios and the use of limestone fillers from different sources were included.

The efficiency of limestone filler concerning chloride ingress did not show the same consistency as for compressive strength. Besides being dependent on replacement ratio it was also shown to depend both on time and on the type of diffusion coefficient (the test method) that was measured. It was not possible to draw any rigid conclusion of the limestone filler's efficiency regarding chloride ingress. For the moderate replacement ratio (12%) the *k*-values varied from 0.1 to 1.3 depending on age and testing method. This means that the *k*-value ranges from almost no cementitious efficiency to be able to fully replace Portland cement. For the higher replacement ratio (24%) the *k*-value spans from being negative, this means that it had a detrimental effect, to be up to 0.9, meaning that Portland cement could almost be fully replaced.

Some reason for the inconsistency in the results became apparent when the chloride ingress was divided into two parts, i.e. in chloride ion transport with and without chloride binding. When the chloride ingress was studied under steady state conditions, meaning no influence of chloride binding, an improvement of the microstructure concerning chloride ingress was identified with limestone filler, resulting in a lower steady-state diffusion coefficient. However, when the chloride ingress was studied under non-steady a state conditions (which includes chloride binding) the microstructural improvement was overshadowed by a decrease in chloride binding capacity. This highlights that the method of measuring the resistance to chloride ingress can have a major influence on the assessment of the effect of different binders.

Chloride induced corrosion

The steel surface condition was shown to have a strong effect on the corrosion initiation, and can likely be one of the most decisive parameters attributing to the variability in the reported chloride threshold values obtained in laboratory experiments.

From the experience of this work the most promising experimental procedure and setup to measure the chloride threshold values is the one used in paper VII. In short:

- ribbed bars in as-received condition
- embedded in "real structural concrete" (low *w*/*b*)
- external ingress of chloride by capillary suction and diffusion
- monitoring the corrosion state continually
- measuring chloride profiles to determine the chloride threshold value

However, some obstacles must be overcome in order to fully achieve the objective of the development of a practice-related standard method.

There are two advantages of using rebars in as-received condition. One is the shortening of the duration of the test, as a steel surface combination of discontinuous mill-scale and surface corrosion was found to be most susceptible to corrosion. And another is that this steel surface is what is used in "real life"; this can likely make a calibration of the results against real structures easier in the future. However, in addition to different transportation and storage conditions which can alter the steel surface condition of as-received rebars, there exists a large variability in physical and chemical properties on the surfaces of rebars from different manufactures, which can make it difficult to compare results from different investigations.

Embedded rebars in "real structural concrete" (low *w*/*b*) and external ingress of chlorides must be taken as prerequisites for a practice-related method. Testing embedded rebars is due to the fact that except the pH of the pore solution, the corrosion progression is also strongly dependent on transport processes in the concrete, which are difficult to simulate in any other way. The second prerequisite is linked to the fact that a certain period of time is required for the passive film to form on the rebars, before being reached by chloride ions. Both these prerequisites will extend the test duration time. To obtain results in a reasonable time span the following measures are recommended:

- A controlled pre-conditioning (desiccation) to facilitate chloride ingress by capillary suction to some distance (about 5 mm) from the rebar, and from there the chloride ingress is facilitated by diffusion. Note, that the desiccation shall be performed without elevating the temperature, but only through decreasing the relative humidity.
- Reducing the concrete cover (to about 10-20 mm), depending on concrete quality. The thickness of concrete covers investigated in this work (which were quite thin) did not show a consistent influence on the chloride threshold value.
- An enhanced concentration of the exposure salt solution, approximately twice as that of sea water (about 6% NaCl by weight).

The determination of the corrosion initiation time was found not to be straightforward. From the experience of this work it is recommended to monitor the corrosion potential continually with a data logger for continuous traceability and for being less laborious. Further, for a more accurate assessment of the influence of different binders on chloride induced corrosion, after the potential measurement indicates corrosion initiation, the corrosion rate development is suggested to be followed up with the non-destructive method for a certain period of time. A binder's influence on the corrosion propagation is at least as important as its influence on the corrosion initiation.

For the concrete with limestone blended cement (CEM II/A-LL 42.5R) tested in this work the measured chloride threshold value was at the same level as for the sulphate resistant Portland cement (CEM I 42.5 N MH/SR/LA), which is a common binder in Sweden for structural concrete. This sulphate resistant Portland cement was used throughout the experimental work as a reference. For practice-related steel surface condition the chloride threshold value for the sulphate resistant Portland cement from the laboratory experiments could be estimated to be about 1% by weight of binder. Unfortunately, this result could not be correlated to the measurements from the field specimens. This was due to the fact that already at the first occasion when corrosion rate measurements were performed, the corrosion rates for the rebars embedded in slabs with the sulphate resistant Portland cement were already above the corrosion criterion. The chloride contents at the cover depth at that time varied from 1.5 to 3%, depending mainly on the cover depth and the w/b.

The results from the field test showed that from a practical engineering point of view the chloride threshold value can be estimated to be of at least 1% by weight of binder, for binders including ordinary Portland cement, sulphate resistance Portland with 5% silica fume. And as high as 2% by weight of binder for the tested slag cement (CEM III/B) and for the ternary binder, blended with 85% Portland cement, 10% fly ash and 5% silica fume.

6 FUTURE WORK

On the basis of the work undertaken in the present thesis, the following recommendations for future research work are given.

Chloride transport

Two main tasks were identified concerning chloride ingress in cement-based materials that needs to be clarified.

The first is in what way chloride binding is linked to a cement-based materials maturity (degrees of reactions) and to what extent this can influence chloride ingress. This can be decisive in the assessment of the influence of different binders on chloride ingress, especially when accelerated methods are used.

The second is to identify the exact mechanisms occurring in the near-surface region causing the non-conformity with an expected chloride profile, i.e. a gradually decreasing chloride content from the surface and inward with the depth of penetration. A clarification of these mechanisms will improve the modelling of chloride ingress and provide more accurate service life design.

Chloride threshold values

Concerning the development of a laboratory tests method to measure chloride threshold values for embedded reinforcement steel, this work has identified the necessity of agreement upon a “standard” metal surface condition that can provide a low scatter and at the same time a short test duration time.

One other parameter not studied in this work, which has been identified to have a decisive influence on the chloride threshold, value is the steel/concrete interface. This also became evident during the course of this work, together with the need of a method to quantify it.

In this study it has repeatedly been highlighted a strong effect of the steel surface condition on the chloride threshold value in the laboratory work. It would be interesting to follow up this finding by testing acid pickled reinforcement steel in the field test. As acid pickling of carbon steels to remove impurities and mill-scales is a common procedure in an industrial scale, this can be found to be an economical justified method to improve the durability of reinforced concrete structures if it is possible to give the whole rebar structure a clear steel surface.

7 REFERENCES

[1] D. W. Hobbs, Concrete deterioration: causes, diagnosis, and minimising risk, Int. Materials Reviews 46 (2001) 117-143.

[2] European standard EN 197, Cement – Part 1: Composition, specification and conformity criteria for common cements, second ed., European committee for standardization, 2011.

[3] H.F.W. Taylor, Cement Chemistry, second ed., Thomas Telford, London, 1997.

[4] C.D. Lawrence, The Constitution and Specification of Portland Cement, in: Hewlett P.C., (Eds.), Lea´s Chemistry of Cement and Concrete, Arnold, London, 1998.

[5] C. Műller, Blended cements the sustainable solution for the cement and concrete industry in Europe, ECOserrve NETWORK puplication, available at www.eco-serve.net, 2006.

[6] I. Odler, The Constitution and Specification of Portland Cement, in: Hewlett P.C., (Eds.), Lea´s Chemistry of Cement and Concrete, Arnold, London, 1998.

[7] P.K. Mehta, P. J. M. Monteiro, Concrete , Microstructure, Properties and Materials, third ed., McGraw-Hill, New York, 2006.

[8] K.L. Scrivener, The Microstructure of Concrete, in: J. Skalny (Eds.), Material Science of Concrete I, USA, 1989.

[9] M.J. Angus F.P. Glasser, The critical environment in cement matrices, in: Proc. L.O. Werme (Ed.), Int. Symp. on scientific basis for nuclear waste management IX, Mat. Res. Soc. Symp. Proc. Vol. 50, Pittsburg, 1985, pp. 547-556.

[10] T.C. Powers, T.L. Brownyard, Studies of the Physical Properties of Hardened Portland Cement Paste, Bulletin 22, Research Laboratories ot the Portland Cement Association, Chicago, 1948.

[11] T.C. Powers, Physical properties of cement paste, in : Proc. Fourth Int. Symp. on the Chemistry of Cement, 1960, U.S. Department of Commerce, National Bureau of Standards, Washington D. C., 1962, Vol. 2, pp. 577-613.

[12] T.C. Hansen, Physical structure of hardened cement paste. A classical approach, Mater. and Struct. 19 (1986), 423-436.

[13] G. Fagerlund, in: Ljungkrantz C., Möller G., Peterson N., (Eds.), Handbook of concrete (in Swedish), AB Svensk Byggtjänst, Solna, 1994.

[14] K. Scrivener, Characterization of the ITZ and its quantification by test methods, in: M.G. Alexander, Arliguie, G. Ballivy, A. Bentur, J. Marchand (Eds.), Engineering and Transport Properties of the Interfacial Transition Zone in Cementitious Composites, RILEM Report 20, RILEM Publications, Cachan, 1999, pp 3-15.

[15] K. Scrivener, A.K. Crumbie, P. Laugesen, The Interfacial Transition Zone (ITZ) Between Cement Paste and Aggregate in Concrete, Interface Sci. 12, (2004) 411-421.

[16] J.P. Ollivier, J.C. Maso, B. Bourdette, Interfacial Transition Zone in Concrete, Advn. Cem. Based Mater. 2, (1995) 30-38.

[17] I. Odler, Strength of cement (final report), Mater. and Struc. 24, (1991) 143-157.

[18] A.M. Neville, Properties of Concrete, fourth ed., Longman Group Ld, Harlow Essex, 1995.

[19] S. Diamond, J. Huang, The ITZ in concrete - a different viewbased on image analysis and SEM observations, Cem. Con. Comp., 23 (2001), 179-188.

[20] G. Fagerlund, Relations between porosity and materials mechanical properties, (in Swedish), Report 26, Inst. Building Technology, Lund Univ., Sweden, 1972.

[21] M. Röβler, I. Odler; Investigation on the relationship between porosity structure and strength of hydrated Portland cement pastes I. effect of porosity, Cem. Conc. Res. 15 (1985), 320-330.

[22] H.J. Gilkey, Water-Cement Ratio Versus Strength-Another Look, Proc. ACI-J. 57 (1961), 1287-1312.

[23] S.P. Shah, S. Chandra, Critical Strength, Volume Change, and Microcracking of Concrete, Proc. ACI-J. 65 (1968), 770-781.

[24] S. Popovics, Strength and related properties of concrete a quantitative approach, J. Wiley & Sons, Inc., USA, 1998.
[25] G. Möller, N. Peterson, L. Elfgren, Strength, in: Ljungkrantz C., Möller G., Peterson N., (Eds.), Handbook of concrete (in Swedish), AB Svensk Byggtjänst, Solna, 1994.
[26] H.K. Hilsdorf, Introduction and problem statement, in: J. Kropp, H.K. Hilsdorf (Eds.), Performance Criteria for Concrete Durability, RILEM Report 12, E & SPON, London, 1995, pp 1-3.
[27] J. Kropp, H.K. Hilsdorf, H. Grube, C. Andrade, L-O. Nilsson, Transport mechanisms and definitions, in: J. Kropp, H.K. Hilsdorf (Eds.), Performance Criteria for Concrete Durability, RILEM Report 12, E & SPON, London, 1995, pp 4-13.
[28] L-O. Nilsson, J.P. Ollivier, Fundamentals of transport properties of cement-based materials and general methods to study transport properties, in: M.G. Alexander, Arliguie, G. Ballivy, A. Bentur, J. Marchand (Eds.), Engineering and Transport Properties of the Interfacial Transition Zone in Cementitious Composites, RILEM Report 20, RILEM Publications, Cachan, 1999, pp 113-147.
[29] R.E Oberholster, Pore structure, permeability and diffusivity of hardened cement paste and concrete in relation to durability, in: Proc. 8th Int. Congr. Chem. Cem., Rio de Janeiro, 1986, Vol. I, pp. 323-335.
[30] L-O. Nilsson, L. Tang, Relations between different transport parameters, in: J. Kropp, H.K. Hilsdorf (Eds.), Performance Criteria for Concrete Durability, RILEM Report 12, E & SPON, London, 1995, pp 15-32.
[31] J-P. Ollivier, M. Massat, L. Parrott, Parameters influencing transport characteristics, in: J. Kropp, H.K. Hilsdorf (Eds.), Performance Criteria for Concrete Durability, RILEM Report 12, E & SPON, London, 1995, pp 15-32.
[32] T.C. Powers, L.E. Copeland, J.C. Hayes, H.M. Mann, Permeability of Portland cement paste, Research and Development Laboratories of the Portland Cement Association, Bulletin 53, Chicago, 1955.
[33] T.C. Powers, Structure and physical properties of hardened Portland cement paste, Jour. Amer. Ceramic Soc. 41 (1958) 1-6.
[34] P.K. Mehta, D. Manmohan, Pore size distribution and permeability of Portland cement pastes, in: Proc. 7th Int. Congr. Chem. Cem., Paris, 1980, Vol. VII, pp. 83-87.
[35] B.K. Nyame, J.M. Illston, Relationship between permeability and pore structure of hardened cement paste, Mag. Conc. Res. 33 (1981) 139-146.
[36] C.D. Lawrence, Transport oxygen through concrete, in: F.P. Glasser (Eds.), Chemistry and Chemical Related Properties of Concrete, British Ceramic Soc. Meeting, London, 1984.
[37] R.K. Dhir, P.C. Hewlett, Y.N. Chang, Near surface characteristics of concrete: intrinsic permeability, Mag Conc. Res. 41 (1987) 87-97.
[38] J. Marchand, A. Delagrave, Influens on ITZ on ionic diffusion and leaching, in: M.G. Alexander, Arliguie, G. Ballivy, A. Bentur, J. Marchand (Eds.), Engineering and Transport Properties of the Interfacial Transition Zone in Cementitious Composites, RILEM Report 20, RELEM Publications, Cachan, 1999, pp 157-171.
[39] H.S. Wong, M. Zobel, N.R. Buenfeld, R. W. Zimmerman, Influnce of the interfacial transition zone and microcraking on the diffusivity, permeability and sorptivity of cement-based materials after drying, Mag. Conc. Res. 61 (2009) 571-589.
[40] L. Tang, L-O. Nilsson, P.A.M. Basheer, Resistance of concrete to chloride ingress, Spon Press, Abingdon, 2012.
[41] J. Kropp, in: Chloride in concrete, in: J. Kropp, H.K. Hilsdorf (Eds.), Performance Criteria for Concrete Durability, RILEM Report 12, E & SPON, London, 1995, pp 138-164.
[42] L. Tang, Concentration dependence of diffusion and migration of ions Part 1. Theoretical considerations, Cem. Concr. Res. 29 (1999) 1463-1468.
[43] C. Andrade, Calculations of chloride diffusion coefficients in concrete from ionic migration measurements, Cem. Concr. Res. 23 (1993) 724-742.
[44] L-O. Nilsson, E. Poulsen, P. Sandberg, H.E. Sørensen, O. Klinghoffer, HETEK, Chloride penetration into concrete, State of the Art, Transport processes, corrosion initiation, test methods and prediction models, Report 53, Danish Road Directorate, 1996.

[45] Q. Yuan, C. Shi, G.D. Schutter, K. Audenart, D. Deng, Chloride binding in cement-based material subjected to external chloride environment – A review, Constru. Build. Mater. 23 (2009) 1-13.
[46] L. Tang, L-O. Nilsson, Chloride binding isotherms – An approach by applying the modified BET equation, in: Proc. Inter. RILEM workshop on Chloride Penetration into Concrete, St-Rémy-lès-Chevreuse, 1995, pp. 36-42.
[47] E.L. Cussler, Diffusion, mass transfer in fluid systems, Cambridge University Press, New York, 2005.
[48] M. Massat, L.-O. Nilsson, J.-P. Ollivier, J.-P., A clarification of fundamental relationship concerning ion diffusion in porous materials, 3rd International Colloquium on material science and restoration, Technische Akademi Esslingen, Germany, 1992.
[49] K.R Trethewey, J. Chamberlain, Corrosion for science and engineering, second ed., Longman, Burnt Mill, 1995.
[50] E. McCafferty, Introduction to corrosion science, Springer, New York, 2010.
[51] G. Butler, H.C.K. Ison, Corrosion and its prevention in waters, Leonard Hill, London, 1966.
[52] M. Pourbaix, Atlas of electrical equilibrium in aqueous solution, National Association of Corrosion Engineers, Houston, 1974.
[53] C.M. Hansson, Comments on electrochemical measurements of the rate of corrosion of steel in concrete, Cem. Concr. Res. 18 (1984) 574-584.
[54] A. Benture, S. Diamond, N.S. Berke, Steel corrosion in concrete – fundamentals and civil engineering practice, Taylor & Francis, London, 1997.
[55] H. Arup, The mechanism of protection of steel in concrete, in: A.P. Crane (Eds.), Corrosion of reinforcement in concrete construction, Ellis Horwood Limited, Chichester, 1983, pp. 151-157.
[56] H. Böhni, Localized corrosion of passive metals, in: R.W. Revie (Eds.), Uhlig´s Corrosion Handbook, second ed., John Wiley & Sons, USA, 2000, pp. 173-187.
[57] G.S. Frankel, Pitting corrosion of metals a review of the critical factors, Journal of the Electrochemical Society 145 (1998) 2186-2198.
[58] H.-H. Strehblow, Breakdown of passivity and localized corrosion, theoretical concepts and fundamental experimental results, in: Int. congress on metallic corrosion, Toronto, 1984, pp. 99-111.
[59] L. Bertolini, B. Elsener, P. Pedeferri, R. Polder, Corrosion of steel in Concrete – Prevention, Diagnosis, Repair, Wiley-VCH, Weinheim, 2004.
[60] K. Tuutti, Corrosion of steel in concrete, Ph.D Thesis, Cement and Concrete Research Institute, Stockholm, 1982.
[61] C. Andrade, Corrosion State Monitoring, in: R. Cigna, C. Andrade, U. Nürnberger, R. Polder, R. Weydert, E. Seitz (Eds.), Corrosion of steel in reinforced concrete structure, COST Action 521, European Commision, Luxembourg, 2003, pp. 101-111.
[62] U. Angst, B. Elsener, C.K. Larsen, C.K., Ø. Vennesland, Critical chloride content in reinforced concrete – A review, Cem. and Concr. Res. 39 (2009) 1122-1138.
[63] M.C. Alonso, M. Sanchez, Analysis of the variability of chloride threshold values in the literature, Mater. Corros. 60 (2009) 631-637.
[64] D.A. Hausman, Steel corrosion in concrete, Materials Protection. How does it occur? 6 (1967) 19-23.
[65] S. Diamond, Chloride concentrations in concrete pore solutions resulting from calcium and sodium chloride admixture, Cement Concrete and Aggregates 8 (1986) 97-102.
[66] G.K. Glass, N.R. Buenfeld, Chloride threshold levels for corrosion induced deterioration of steel in concrete, in: L.O. Nilsson, J.P. Ollivier (Eds.), Chloride Penetration into Concrete, RILEM, St-Remy-les-Chevreuse, 1995, pp. 429-440.
[67] C.L. Page, Initiation of chloride-induced corrosion of steel in concrete: role of the interfacial zone, Mater. Corros. 2009, 60, 586-592.
[68] G.K. Glass, N.R. Buenfeld, The presentation of the chloride threshold level for corrosion of steel in concrete, Corr. Sci. 39 (1997) 1001-1013.

[69] Tang, L., "Estimation of cement/binder profile parallel to the determination of chloride profile in concrete". SP Report 2003:07, SP Swedish National Testing and Research Institute, Borås, (2003), pp. 30.
[70] P.K. Mehta, Pozzolanic and Cementitious Byproducts as Mineral Admixtures for Concrete-A Critical Review, in: Proc. First Int. Conf. on The use of fly ash, silica fume, slag and other mineral by-products in concrete, Montebello, 1983, Vol. I, ACI publ. SP-79; pp. 1-46.
[71] F.P. Glasser, S. Diamond, D.M. Roy, Hydration reaction of cement pastes incorporating fly ash and other pozzolanic materials, in: G.J. McCarthy, F.P. Glasser, D.M. Roy, S. Diamond (Eds.), Fly ash coal conversion by-products:characterization, utilization and disposal III, Mat. Res. Soc. Symp. Proc. Vol. 86, Pittsburg, 1987, pp. 139-158.
[72] P.K. Mehta, Pozzolanic and Cementitious Byproducts in Concrete-Another Look, in: Proc. Third Int. Conf., Fly ash, silica fume, slag and natural pozzolans in concrete, Trondheim, 1989, Vol. I, ACI publ. SP-114; pp. 1-43.
[73] R.F. Feldman, Pore structure, permeability and diffusivity as related to durability, in : Proc. 8th Int. Congr. Chem. Cem., Rio de Janeiro, 1986, Vol. I, pp. 336-356.
[74] J.A. Larbi, J.M. Bijen, Effect of mineral admixtures on the cement paste-aggregate interface, in: Proc. Fourth Int. Conf., Fly ash, silica fume, slag and natural pozzolans in concrete, Instanbul, 1992, Vol. I, ACI publ. SP-132; pp. 655-661.
[75] A. Bentur, I. Odler, Development and nature of interfacial microstructure, in: J.C Maso (Eds.), Interfacial Transition Zone in Concrete, RILEM Report 11, RELEM Publications, E & FN Spon, London, 1996, pp 18-44.
[76] A. Leemann, R. Loser, B. Műnch, Influence of cement type on ITZ porosity and chloride resistance of self-compacting concrete, Cem. Conc. Comp. 32 (2010) 116-120.
[77] H. Moosberg-Bustness, B. Lagerblad, E. Forssberg, The function of fillers in concrete, Mater. Struct. 36 (2004) 74-81.
[78] P. Lawrence, M. Cyr, E. Ringot, Mineral admixtures in mortars Effect of inert materials on short-term hydration, Cem. Conc. Res. 33 (2003) 1939-1947.
[79] W. Stumm, Chemistry of the solid-water interface, Wiley, New York, 1992.
[80] M. Cyr, P. Lawrence, E. Ringot, Efiiciency of mineral admixtures in mortars: Quantification of the physical and chemical effect of fine admixtures in relation with compressive strength, Cem. Conc. Res. 36 (2006) 264-277.
[81] B. Lothenback, K. Scrivener, R.D. Hooten, Supplementary cementitious materials, Cem. Conc. Res. 41 (2011) 1244-1256.
[82] I.A. Smith, The design of fly ash concrete, in: Proc. Inst. Civ. Eng., London, Vol. 36, 1967, pp. 769-790.
[83] EN 206-1, Concrete-Part 1: Specification, performance, production and conformity, European standard, 2000.
[84] Concrete – Application of EN 206-1 in Sweden, 2008.
[85] Cements for a low-carbon Europe, Published by CEMBUREAU, The European Cement Association, 2012.
[86] R.D. Hooton, M. Nokken, M.D.A Thomas, Portland–limestone cement: State-of-the-art report and gap analysis for CSA A 3000, Cement Association of Canada, Ottawa, 2007.
[87] A.P. Barker, H.P. Cory, The early hydration of limestone-filled cements, in: R. N. Swamy (Ed), Proc. Inter. Conf. on Blended Cements in Construction, Sheffield, 1991, pp. 107-124.
[88] G. Kakali, S. Tsivilis, E. Aggeli, M. Bati, Hydration products of C_3A, C_3S and Portland cement in the presence of $CaCO_3$, Cem. Conc. Res. 30 (2000) 1073-1070.
[89] V.L. Bonavetti, V.F. Rahhal, E.F. Irassar, Studies of the carboaluminate formation in limestone filler-blended cements", Cem. Conc. Res. 31 (2001) 853-859.
[90] S. Husson, B. Gullhot, J. Pera, Influence of Different Fillers on the Hydration of C_3S, in: (Eds.), Proc. of the 9th International Congress on the Chemistry of Cement, New Delhi, 1992, Vol. IV, pp. 83-89.
[91] V.S. Ramachandran, Z. Chun-Mei, Dependence of Fineness of Calcium Carbonate on the Hydration behaviour of Tricalcium Silicate, Durability Building Materials 4 (1986) 45-66.
[92] R.L. Sharma, S.P. Pandey, Influence of mineral additives on the hydration characteristics of ordinary Portland cement, Cem. Concr. Res. 29 (1999) 1525-1529.

[93] P. Pipilikaki, M. Beazi-Katsioti, The assessment of porosity and pore size distribution of limestone Portland cement pastes, Constr. Build. Mater. 23 (2009) 1966-1970.
[94] K.K. Aligizaki, Pore structure of cement-based materials, Taylor & Francis, Abingdon, 2006.
[95] E.J. Sellevold, D.H. Bager, E Klintgaard-Jensen, T. Knudsen, Silica fume-cement pastes: Hydration and pore structure, in O.E. Gjorv, K.E. Loland (Eds.) Condensed Silica Fume in Concrete, Trondheim, 1982, pp. 19-50.
[96] R. Ranc, M. Moranville-Regourd, G. Cochet, G. Chaudouard, Durability of Cements with Fillers, in: (Eds.), Proc. of the 2nd Int. Conf. on Durability of Concrete, Montreal, (YEAR), Vol. II, pp. 1239-1257
[97] P.D. Tennis, M.D.A Thomas, W.J. Weiss, State-of-the art-report on use of limestone in cement at levels of up to 15%, Portland Cement Association, Skokie, 2011.
[98] E.F. Irassar, Sulfate attack on cementitious materials containing limestone filler – A review, Cem. Concr. Res. 39 (2009) 241-254.
[99] I. Soroka, N. Stern, Calcareous fillers and the compressive strenth of portland cement, Cem. Concr. Res. 6 (1976) 367-376.
[100] G. Menendez, V. Bonavetti, E.F. Irassar, Strength development on ternary blend cement with limestone filler and blast-furnace slag, Cem. Concr. Composites 25 (2003) 61-67.
[101] T. Vuk, V. Tinta, R. Gabrovsek, V. Kaucic, The effect of limestone addition, clinker type and fineness on properties of Portland cement, Cem. Concr. Res. 31 (2001), 135-139.
[102] S. Kenai, W. Soboyejo, A. Soboyejo, Some Engineering Properties of Limestone Concrete, Materials and Manufacturing Properties 19 (2004) 949-961.
[103] P. Lawrence, M. Cyr, E. Ringot, Mineral admixture in mortars effect of type, amount and fineness of fine constituents on compressive strength, Cem Concr. Res. 35 (2005) 1092-1105.
[104] H. Hornain, J. Marchand, V. Duhot, M. Moranville-Regourd, Diffusion of Chloride Ions in Limestone Filler Blended Cement Pastes and Mortars, Cem. Concr. Res. 25 (1995), 1667-1678.
[105] Y. Tezuka, D. Gomes, J.M. Martins, J.G. Djanikian, Durability Aspects with High Limestone Filler Content, Proceedings, 9th International Congress on the Chemistry of Cement, New Delhi, Vol. 5, 1992, pp. 53-59.
[106] R.K. Dhir, M.C. Limbachiya, M.J. McCarthy, A. Chaipanich, Evolution of Portland limestone cements for use in concrete construction, Mater. Struct. 40 (2007) 459-473.
[107] C. Muller, E. Lang, Durability of concrete made with Portland-limestone and Portland-composite cement CEM II-M (S-LL), Concrete Technology Reports 2004-2006, VDZ, Deutsche Zementindustrie, pp.29-53.
[108] M. Ghrici, S. Kenai, M. Said-Mansour, Mechanical properties and durability of mortar and concrete containing natural pozzolana and limestone blended cements, Cem. Concr. Comp. 29 (2007) 542-549.
[109] M. Moukwa, Penetration of chloride ions from sea water into mortars under different exposure conditions, Cem. Concr. Res. 19 (1989) 894-904.
[110] V. Bonavetti, H. Donza, V. Rahhal, E. Irassar, Influence of initial curing on the properties of concrete containing limestone blended cement, Cem. Concr. Res. 30 (2000) 703-708.
[111] J.D. Matthews, Performance of Limestone Filler Cement Concrete, Proceedings, Euro-Cement: Impact of ENV-197 on Concrete Constructions, 1994, pp. 113-146.
[112] C.L. Page, Steady-state diffusion characteristics of cementitious materials, in: L.O. Nilsson, J.P. Ollivier (Eds.), Chloride penetration in concrete, RILEM, St-Rémy-lès-Chevreuse, 1995, pp. 77-84.
[113] C.L. Page, N.R. Short, A. El-Tarras, Diffusion of chloride ions in hardened cement pastes, Cem. Concr. Res. 11 (1981) 395-406.
[114] J. Crank, The Mathematics of Diffusion, 2nd ed., Oxford Science Publication, 1975.
[115] J. Arsenault, J.-P. Bigas, J.-P. Ollivier, Determination of chloride diffusion coefficient using two different steady-state methods: Influence of concentration gradient, in: L.O. Nilsson, J.P. Ollivier (Eds.), Chloride penetration in concrete, RILEM, St-Rémy-lès-Chevreuse, 1995, pp. 150-160.

[116] L. Tang, Chloride ingress in concrete exposed to marine environment – Field data up to 10 years exposure, SP Swedish National Testing and Research Institute, Borås, 2003.
[117] NT BUILD 492, Concrete, Mortar, and Cement-based Repair Materials: Chloride Migration Coefficient from Non-steady-state Migration Experiments. *Nordtest methods,* 1999.
[118] L. Tang, L.-O. Nilsson, Rapid determination of chloride diffusivity of concrete by applying an electrical field, ACI Mater. Journ. 49 (1992) 49-53.
[119] L. Tang, Chloride transport in concrete – measurements and prediction, PhD. Thesis, Chalmers university of Technology, Gothenburg, 1996.
[120] Nygaard, P. V., and Geiker, M. R., A method for measuring the chloride threshold value level required to initiate reinforcement corrosion in concrete, Materials and Structures, 38, 2006, 489-494.
[121] D. Boubitsas, L. Tang, P. Utgenannt, Chloride ingress in concrete exposed to marine environment - Field data up to 20 years' exposure", SBUF Report 12684, Borås, Sweden 2014.
[122] H. Arup, H.E. Sørensen, A proposed technique for determining chloride thresholds, in: L.O. Nilsson, J.P. Ollivier (Eds.), Chloride penetratration in concrete, RILEM, St-Rémy-lès-Chevreuse, France, 1995, pp. 460-469.
[123] L. Tang, Mapping corrosion of steel in reinforced concrete structures, SP Report 2002:32 (SP Swedish National Testing and Research Institute), 2002.
[124] D. Boubitsas, Replacement of cement by limestone filler: the effect on strength and chloride migration in cement mortars, Nordic Conc. Res. 32 (2004) 31-44.
[125] G. Fagerlund, Textbook in building materials (in Swedish), Lund university, Dep. of building materials, 2001.
[126] C.K. Larsen, Chloride binding in concrete-Effect of surrounding environment and concrete composition, Thesis, Norwegian Univerity of Science and Technology, Trondheim, 1998.
[127] T.Sumranwanich, S. Tangtermsirikul, A model for predicting time-dependent chloride binding capacity of cement-fly ash cementitious system, Mater. Struct. 37 (2004) 387-396.
[128] T. Ekström, Leaching of Concrete, Experiments and Modelling, PhD thesis, Division of Building Materials, Inst. Building Technology, Lund Univ., Sweden, 2003.
[129] G. Sergi, S.W. Yu, C.L. Page, Diffusion of chloride and hydroxyl ions in cementitious materials exposed to a saline environment, Mag. Concr. Res. 44 (1992), 63-69.
[130] K. De Weerdt, H. Justnes, M.R. Geiker, Changes in the phase assemblage of concrte exposed to sea water, Cem. Concr. Compo. 47 (2014), 53-63.
[131] J.M. Frederiksen, H.E. Sørensen, A. Andersen, O. Klinghoffer, HETEK The effect of the w/c ratio on chloride transport into concrete, Report 54, Danish Road Directorate, Copenhagen 1997.
[132] Y.-H. Li, S. Gregory, Diffusion of ions in sea water and in deep-sea sediments, Geochimica et Cosmochimica Acta 38 (1974) 703-714.
[133] L. Bertolini, E Redaelli, Depassivation of steel reinforcement in case of pitting corrosion: detection techniques for laboratory studies, Mater. Corros. 60 (2009) 608-616.
[134] C. Andrade, C. Alonso, R. Gulikers, R. Polder, Ø. Vennesland,., M. Salta, A. Raharinaivo, B. Elsener, Tets methods for on-site corrosion rate measurement of steel reinforcement in concrete by means of the polarization resistance method, Mater. Struct. 37 (2004), 623-643.
[135] C. Alonso, C. Andrade, M. Castellote, P. Castro, Chloride threshold values to depassivate reinforcing bars embedded in a standardized OPC mortar, Cem. Conc. Res. 30 (2000) 1047-1055.
[136] B. Elsener, C. Andrade, J. Gulikers, R. Polder, M. Raupach, Half-cell potential measurements – Potential mapping on reinforced concrete structures, Mater. Struct. 36 (2003), 461-471.
[137] M.C. Alonso, M. Castellote, C. Andrade, Chloride threshold dependence of pitting potential of reinforcement, Electrochimica Acta, 47 (2002) 3469-3481.
[138] K. Hornbostel, C.K. Larsen, M.R. Geiker, Relationship between concrete resistivity and corrosion rate – A literature review, Cem. Conc. Res. 39 (2013) 60-72.

[139] L. Tang, A collection of chloride and moisture profiles from Träslövsläge field site – From 0.5 up to 10 years investigations, Chalmers University of Technology, Building Materials, Pub. No. P-03:3, Gothenburg, Sweden, 2003.
[140] L.Tang, P. Utgenant, P. Fidjestøl, Evaluation of Chloride-Induced Corrosion of Steel in Concrete after Long-Time Exposure in a Marine Environment", SP Report 2005:54, Borås, Sweden, 2005.
[141] P. Ghods, O.B. Isgor, G.A. McRae, J. Li, G.P. Gu, Microscopic investigation of mill scale and its proposed effect on the variability of chloride-induced depassivation of carbon steel rebar, Corr. Sci. 53 (2011) 946-954.
[142] D.B. Berger, Fundamentals and prevention of metallic corrosion, in: P.A. Scheitzer (Ed.) Corrosion and corrosion protection Handbook, Marcel Dekker Inc., New York, 1988, pp. 1-22.
[143] E. Mahallati, M. Saremi, An assessment on the mill scale effect on the electrochemical characteristics of steel bars in concrete under DC-polarization, Cem. Concr. Res. 36 (2006) 1324-1329.
[144] P.A. Schweitzer, Fundamentals of corrosion: mechanism, causes and preventative methods, Taylor and Francis Group, USA, 2010.
[145] A. Poursaee, C.M. Hansson, Potential pitfalls in assessing chloride-induced corrosion in concrete, Cem. Concr. Res. 39 (2009) 391-400.
[146] G. Fagerlund, The threshold chloride level for initiation of reinforcement corrosion in concrete - Some theoretical considerations", Report TVBM-3159, Division of Building Materials, Lund Institute of Technology, 2011.
[147] F. Hunkeler, Corrosion in reinforced concrete: processes and mechanisms, Chapter in: Corrosion in reinforced concrete structures, (Ed) H. Böhni, Woodhead Publishing Ltd, England, 2005.
[148] M.C., Alonso, J.L. Garcia Calvo, C. Walker, M. Naito, S. Pettersson, I. Puigdomenech, M.A. Cunado, M. Vuorio, H. Weber, H. Ueda, K. Fujisaki, Development of an accurate pH measurement methodology for the pore fluids of low pH cementitious materials, Report R-12-02, Swedish Nuclear Fuel and Waste Management Co, 2012.
[149] R.B. Polder, Critical chloride content for reinforced concrete and its relationship to concrete resistivity, Mater. Corros. 60 (2009) 623-630.